04

SPACE SCIENCES LABORATORY

ANALYSIS OF RIVER MEANDERS FROM ERTS-1 IMAGERY

A report of work done by scientists at the Institute of Geophysics and Planetary Physics, University of California, Los Angeles Campus, under NASA Contract No. NAS 5-21827

1317D

Final Report
14 July 1973
Space Science Laboratory Series 16, Issue 52

UNIVERSITY OF CALIFORNIA, BERKELEY

Final Report

ANALYSIS OF RIVER MEANDERS FROM ERTS-1 IMAGERY

Co-Investigators: Gerald Schubert & Richard Lingenfelter

Institute of Geophysics and Planetary Physics
Los Angeles Campus

TECHNICAL REPORT STANDARD TITLE PAGE

1. Report No.	2. Government Accession No.	3. Recipient's Catalog No.

4. Title and Subtitle	5. Report Date
ANALYSIS OF RIVER MEANDERS FROM ERTS-1 IMAGERY	6. Performing Organization Code

7. Author(s)	8. Performing Organization Report No.
Gerald Schubert & Richard Lingenfelter	

9. Performing Organization Name and Address	10. Work Unit No.
Institute of Geophysics and Planetary Physics University of California Los Angeles, Calif. 90024	11. Contract or Grant No. NAS 5-21827, Task 4
	13. Type of Report and Period Covered 29 August 1972 - 14 July 1973 Type III
12. Sponsoring Agency Name and Address National Aeronautics and Space Administration Goddard Space Flight Center Greenbelt, Maryland 20071	14. Sponsoring Agency Code

15. Supplementary Notes Technical Monitor: Ed Crumpe
Originally prepared as Chapter 5 in "An Integrated Study of Earth Resources in the State of California Based on ERTS-1 and Supporting Aircraft Data" Robert N. Colwell, Principal Investigator, Space Sciences Laboratory, University of California, Berkeley, Calif.

16. Abstract

The purpose of this investigation was to try to develop a technique for the remote sensing of water resources by inferring river discharges from power spectral analyses of river meander patterns. We used ERTS-1 data to help determine whether a correlation between river meander power spectra and river discharge frequency exists. In the course of this study we developed techniques for analyzing remote sensing imagery of river channel patterns; we discovered an important new relationship between the discharge spectra of rivers and the time dependence of their flood recessions, which is important to hydrologic modeling of stream flow; and, within the uncertainty imposed by the data we were able to analyze, we showed that only a rough correlation exists between the meander power spectra and the discharge spectra of rivers, and that other variables must also influence this relationship preventing a simple inversion of the meander spectrum to obtain a discharge spectrum.

17. Key Words (Selected by Author(s))	18. Distribution Statement
hydrology spectral analysis pattern recognition hydrologic modeling	

19. Security Classif. (of this report)	20. Security Classif. (of this page)	21. No. of Pages	22. Price*
Unclassified	Unclassified	46 +	

ABSTRACT

The purpose of this investigation was to try to develop a technique for the remote sensing of water resources by inferring river discharges from power spectral analyses of river meander patterns. We used ERTS-1 data to help determine whether a correlation between river meander power spectra and river discharge frequency exists. In the course of this study we developed techniques for analysing remote sensing imagery of river channel patterns; we discovered an important new relationship between the discharge spectra of rivers and the time dependence of their flood recessions, which is important to hydrologic modeling of stream flow; and, within the uncertainty imposed by the data we were able to analyze, we showed that only a rough correlation exists between the meander power spectra and the discharge spectra of rivers, and that other variables must also influence this relationship preventing a simple inversion of the meander spectrum to obtain a discharge spectrum.

TABLE OF CONTENTS

LIST OF ILLUSTRATIONS

Page

LIST OF TABLES

1. Introduction

1.1 Background

A large number of correlations between some average meander wavelength and some characteristic discharge have been proposed [see for example Jefferson, 1902; Inglis, 1949; Leopold and Wolman, 1957; Dury, 1965; Carlston, 1965; Schumm, 1971]. These correlations clearly suggested that there was a relationship between meander wavelength and discharge but they failed to agree on its quantitative form. Some of this disagreement results from the oversimplification inherent in using a single meander wavelength and a single discharge to characterize the river rather than using the complete spectra of wavelengths and discharges.

Speight (1965, 1967) appreciated that the entire oscillatory pattern of a river must be important in characterizing its meandering and presented power spectra of the auto-correlations of the directions of flow measured at equally spaced points on the talwegs of several Australasian rivers. These meander power spectra showed structure which we interpreted as an indication that several characteristic length scales may be required to quantitatively describe a meander pattern. The idea of using a spectral analysis of the reach of a river as the basis of a correlation rather than a subjective estimate of an assumed single length scale is a necessary generalization in describing the connection between a river's meander

pattern and its discharge. However, he retained the idea that a single discharge could be correlated with the multiple length scales. Just as there is an essential difficulty in attempting to characterize a meander pattern by a single length scale, there is a fundamental problem in trying to choose the dominant discharge, i.e. that discharge most effective in establishing the system of meanders. We investigated the possibility that the further generalization of the correlation to include the time-behavior of the discharge might bring an order to the relationship between the total meander pattern and the complete record of the discharge. This more general correlation should be sufficiently reliable to quantitatively assess a river's flowrate from a spectrum of its meanders, thus making the knowledge of a region's water resources accessible from aerial or satellite imagery of the area.

1.2 Outline of Study

Our study of a possible correlation between the stream meander power spectrum and the stream discharge frequency distribution required the accomplishment of the following tasks:

1. Selection of appropriate rivers.
2. Collection of suitable photographic coverage.
3. Collection of historical streamflow data.
4. Digitization of streamflow data.
5. Digitization of stream meander patterns.

6. Matching of individually digitized portions of meander patterns to obtain a continuous record.
7. Construction of stream discharge frequency distribution from discharge data.
8. Construction of power spectra of local river meander directions.
9. Determination of relationship between meander power spectra and discharge frequency distributions.

The completion of the first eight tasks for the Feather River in California and a number of other rivers throughout the United States, established general procedures for generating the stream discharge probability density functions and meander power spectra for all rivers.

From these analyses we have shown that a rough relationship appears to exist between the discharge spectra and meander spectra of most of the rivers studied. From the data for this study we were not able, however, to determine a qualitative relationship suitable for uniquely determining the discharge spectrum of a river from remote sensing imagery of its meander pattern. But such a relationship may yet be realizable from a broader data base.

1.3 Data Acquisition

Prior to attempting to obtain the imagery and hydrologic data required for our study, we first had to develop selection criteria for defining rivers suitable

for study. These were

1. Uniformity of geology.
2. Length of reach with minimum spatial variation in discharge along the course.
3. Length of reach with minimum seasonal variation in discharge.
4. Resolvability of river on ERTS-1 imagery and/or availability of historical photographic coverage.
5. Availability of continuous historical hydrologic data.

Using these criteria we selected sixteen rivers which sampled a wide range of discharge rates and a broad geographical distribution.

TABLE 1

LIST OF RIVERS STUDIED

River	Imagery	Hydrologic Station	Median Q ft. 3/sec	Length of Reach (ft.)
Mississippi River	ERTS-1	7/0320,2890	350,000	4.1×10^6
Sacramento River	ERTS-1	11/3780,3890,3895	8,000	6.0×10^5
Feather River	ERTS-1 & Aerial	11/4070	3,000	1.2×10^5
Manistee River	Aerial	4/1235,1240,1260	200 - 1000	5.0×10^5
Chippewa River	Aerial	5/3565	1,000	1.8×10^5
Ontonagon River	Aerial	4/0400	900	7.5×10^5
Flambeau River	Aerial	5/3585	800	1.3×10^5
Muskegon River	Aerial	4/1215	700	1.2×10^5
Manistique River	Aerial	4/0495,0550	400 - 600	1.6×10^5
Homochitto River	Aerial	7/2910, 2925, 2945	400	2.6×10^5
Red River	Aerial	5/0540	300	3.9×10^5
Bad River	Aerial	4/0270	250	1.3×10^5
White River	Aerial	4/0275	200	1.1×10^5
Boise Brule River	Aerial	4/0255	150	1.3×10^5
Rifle River	Aerial	4/1395,1405,1420	80 - 200	1.7×10^5
Jump River	Aerial	5/3615,3620	70 - 140	1.8×10^5

1.3.1 ERTS-1 Imagery and Aerial Photography

Of these sixteen rivers (see Table 1) only three were of sufficient size that their meander patterns were clearly resolvable in the IR imagery from ERTS-1. These were the Feather and Sacramento Rivers in California, and the Mississippi River from Tennessee to New Orleans. These rivers also had largest mean discharges (see Table 1). Fourteen other rivers, which were needed to broaden the range of discharges but were not resolvable in the ERTS-1 imagery, had to be studied using aerial photography. Table 1 lists all of these rivers giving the type of imagery used, the hydrologic stations from which discharge data was available, the median discharge and the total length of the reach of river studied. Where a range of discharges is listed, corresponding to values at different stations, shorter reaches associated with each station were analyzed. We have obtained aerial photographs (both infrared and panchromatic) of rivers from the Agricultural Stabilization and Conservation Service of the U.S. Department of Agriculture, Department of Water Resources of the California State Resources Agency, the Topographical Division of the U.S. Geological Survey, and the Cartographic and Audiovisual Records Division of the National Archives and Records Service. Infrared satellite imagery from ERTS-1 has been provided by the NASA Data Processing Facility at Goddard Space Flight Center.

1.3.2 Hydrologic Data

The streamflow data for all of the rivers used in this study consisted of daily discharge measurements from gauging stations operated by the U.S. Geologic Survey. This data was obtained in machine measurable format from the Water Resources Division of the U.S. Department of the Interior. The discharge records for some of these rivers, such as the Sacramento, encompass as much as seventy five years of continuous measurement.

2. Accomplishments

As a basis for this study we have developed a fully automated system for obtaining both the discharge and meander wavelength spectra. Discharge spectra (probability of discharge per unit discharge vs. discharge) are constructed from historical records of daily stream discharge. Generation of meander power spectra involves three elements: digitization by photoelectric optical tracking of stream banks on each frame of photographic or television imagery; collation and matching of successive frames into a single data record for each stream; and a Fourier transform analysis of the data. This system has been developed to facilitate the analysis of the large number of rivers required to assure the statistical reliability of the correlation.

From the imagery of a selected river reach, we determine

the positions of the curve with respect to a cartesian coordinate system. This description of the river's course is transformed to a (θ,s) representation, where θ measures the angle that the curve makes with a reference direction as a function of distance travelled along the curve s. The (θ,s) description is preferred since the meander pattern of a river may be represented by a multivalued function of position in a cartesian representation. The meander power spectrum which we calculate is the power spectral density of $\theta(s)$.

2.1 Digitization

The digitization of river meander patterns from aerial imagery is most accurately and economically accomplished through photoelectric optical scanning. We have developed a program for digitizing river meanders, using commercially available machines employing this technique. An important condition on the digitization procedure is that data points be located at equal increments of distance along the meander curve. This condition follows from the fact that local meander direction, θ, is a function of distance along the meander and the algorithm used for constructing the power spectrum requires that we know this quantity at equal increments of distance.

The essence of the digitization procedure is as follows (see also Fig. 1): The initial point on the meander pattern is found by scanning along a horizontal or vertical line and

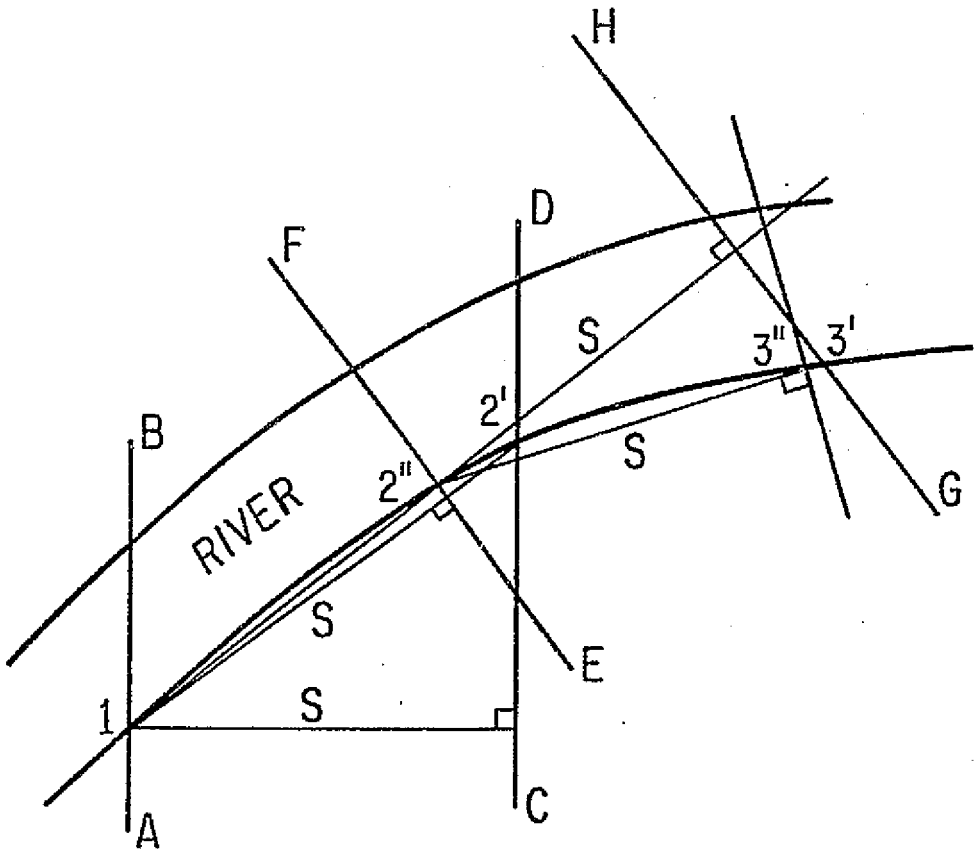

Figure 1. Digitization Procedure

measuring the optical density profile along the scan (line AG in Fig. 1). The river bank, i.e., the point digitized, is defined as the location of the point of maximum gradient in the density profile (point 1). The second point is determined by an iterative process starting with a scan (line CD) parallel to the initial scan but displaced by a distance, s, from point 1. The first estimate of this point (2′) is determined in the same manner as above. The distance between points 1 and 2′ is then calculated and if it is not equal to the required spacing, s, plus or minus some small Δ, another scan (line EF) is made alone a line perpendicular to that line connecting points 1 and 2′ at a distance s from point 1. Point 2″ is then determined along this scan. If the distance between it and point 1 is still not within $s \pm \Delta$, the iterative process is repeated until convergence is obtained. Once point 2 is located, the search for point 3 begins along a scan line (GH) perpendicular to the line connecting points 1 and 2 at a distance s from point 2. In this manner the machine proceeds along the meander curve digitizing points at equal distance increments along the curve.

As is generally the case, the imagery of the river consists of a number of overlapping frames, thus this digitization procedure is repeated for each frame. The data for adjacent frames must then be matched to give a continuous digitized record of the meander pattern. Because of the large overlap between frames (roughly one-third of the data on the end of

each frame overlaps with the data on the beginning of the next frame) the data sets can be uniquely matched for congruency in the overlap region. We have developed a computer program which finds the appropriate coordinate transformation, i.e., includes both translation and rotation of one frame with respect to the other. This is accomplished by considering a length of river roughly half the length of the overlap region on one frame and effectively sliding this portion of the data along the overlap portion of the adjacent frame, finding that transformation within the overlap region which minimizes the sum of the squares of the distances between matched points. Once the appropriate coordinate transformation is determined all of the data points on the second frame are transformed. The process is then repeated to match successive frames until the entire record is transformed into a single coordinate system.

For purposes of comparison a computer generated plot of the digitized meander pattern of a section of the Feather River is shown as a slightly displaced overlay in Figure 2 together with the infrared photograph from which the pattern was derived. As can be seen this technique provides an accurate reproduction of the meander pattern. A sample of the final product of this digitization and matching procedure is shown in Figure 3 for a 23 mile reach of the Feather River below the dredge tailings at Oroville to the Southern Pacific Railroad bridge north of

Figure 2. Infrared imagery of section of Feather River with slightly displaced overlay of digitized meander pattern

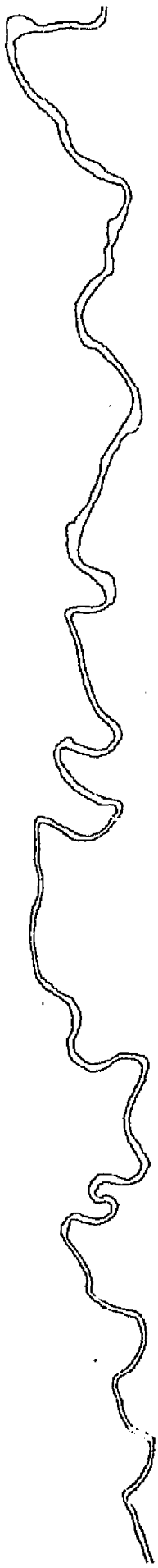

Figure 3. Calcomp plot of digitized meander pattern of Feather River.

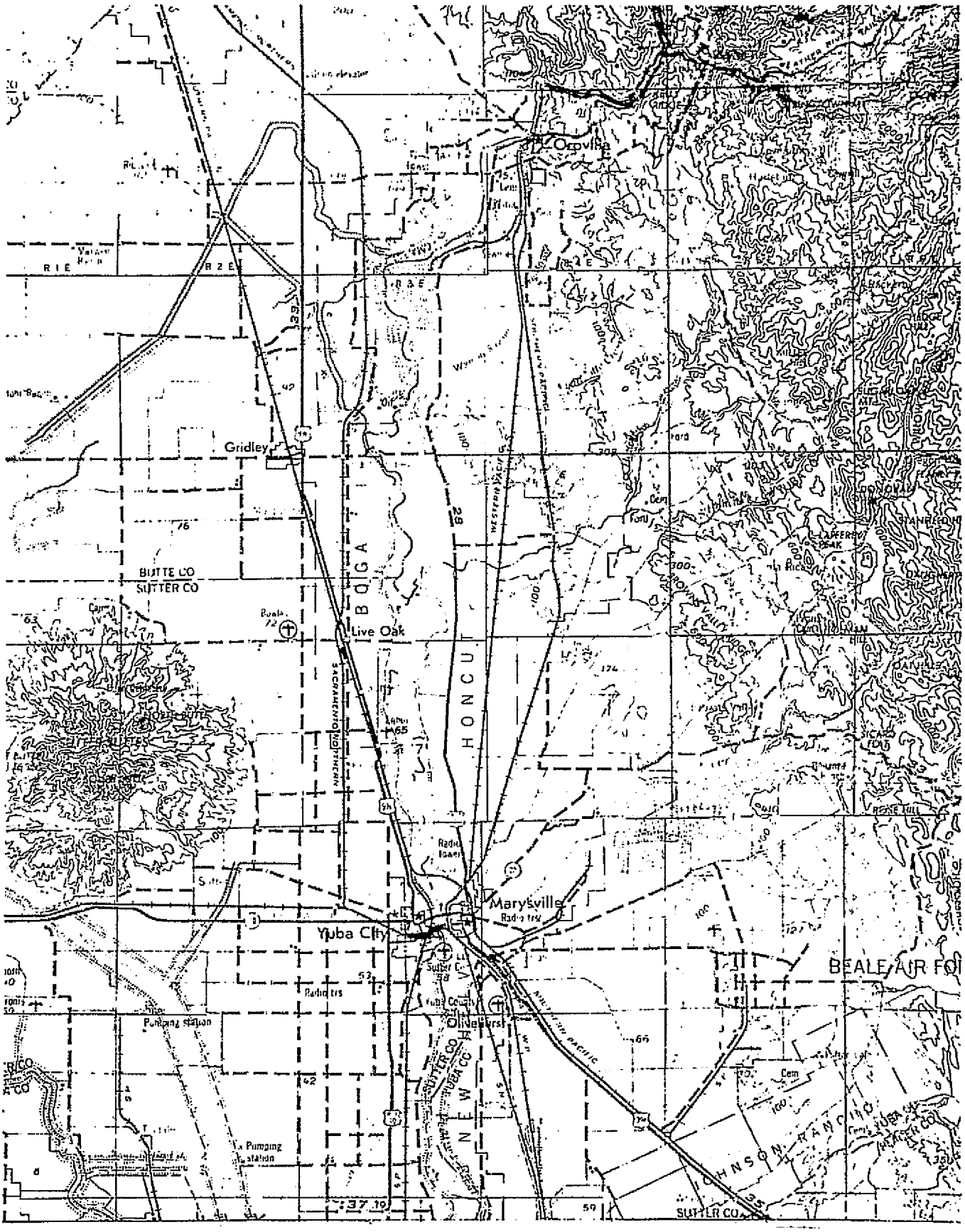

Figure 4: Topographic map of Feather River Reach studied indicated by sinuous.

Yuba City. A topographic map of this reach of river is shown in Figure 4.

2.2 River Meander Power Spectra

2.2.1 Technique

The digitization and matching procedures described above produce a set of data points (S,Y coordinates) which are equally spaced along the course of the river. A power spectral analysis of the river cannot be made directly from the X versus Y data since the river may double back upon itself making X a double valued function of Y. An equivalent representation of the river, which is single valued and thus amenable to power spectral analysis is its local direction, θ, as a function of the distance, s, along the river's course.

The power spectral density ($deg^2/10^3$ ft.) for the direction θ is computed using standard techniques for determining the autocorrelation function, smoothing, and taking the Fourier transform (e.g., J.S. Bendat and A.G. Piersol, Measurement and Analysis of Random Data, John Wiley, 1966).

These spectra are calculated as a function of wave number (per 10^3 ft.). The range of wave number is limited at the high end (short wavelength) by the interval between data points and at the low end (long wavelength) by the length of the reach Fourier analyzed and the number of degrees of freedom. The maximum wave number is given by the Nyquist criterion to be $N/2\ell$ where N is the number of data points

and ℓ is the length of the reach. The minimum wave number at which spectral information is obtained is $N/2\ell m$ where m is the number of spectral estimates, or alternatively $n/4\ell$ where $n = 2N/m$ is the number of degrees of freedom, a measure of the uncertainty in the power spectral density. The analyses are all for 6 or more degrees of freedom which gives us 80% or more confidence that the spectral value lies within 2.8 and 0.5 times the computed estimate.

2.2.2 Characteristics of Spectra

The meander spectra which we have calculated for the various rivers described above are all rather simple, broad spectra having significant power over a wave number range of more than a decade. All of these spectra are shown in Appendix I. Three examples are also shown in Figuure 5, together with scaled traces of the meander patterns which have been spectrally analyzed. The error bar on each spectrum indicates the 80% confidence interval for the power spectral density determined from the number of degrees of freedom (Blackman and Tukey, 1958).

At intermediate wave numbers each of these spectra have an apparent power-law dependence of the spectral density on wave number, as shown by the dashed line preliminary fit to the spectral estimates. The exponent of the power law is given by the indicated slope which is probably accurate to within ± 20%. At lower wave numbers the spectrum flattens,

suggesting a broad peak at a power density two to three orders of magnitude above the noise level. The wave numbers at which the power law dependences break to flatter dependences on the Ontonagon, Homochitto and White Rivers, correspond to wave lengths of $5x10^3$, 10^4 and $2.5x10^3$ ft., respectively and reflect recognizable scales in the meander patterns of each river shown in the figure. At high wave numbers the power law dependence is truncated at the relatively constant level of the noise which extends up to the Nyquist limit on the wave number. Though there are small scale fluctuations about the general spectral structure outlined above, they are not significant within even the 80% confidence interval.

Some streams, however, do show more complex structure as can be seen in Fig. 6. Clearly the off-set structure shown in the spectrum of the Manistee River is significant within the 80% confidence interval. There is also a suggestion of similar structure in the spectra of the Bad and Bois Brule Rivers though not at the same level of confidence.

Thus the spectra which we have investigated so far can be described by one or more linear power law segments of differing slopes and magnitude which break at characteristic wave numbers.

We have investigated the stationarity of meander power spectra by constructing spectra for a series of subreaches of the Manistee River to study the variation of its spectrum

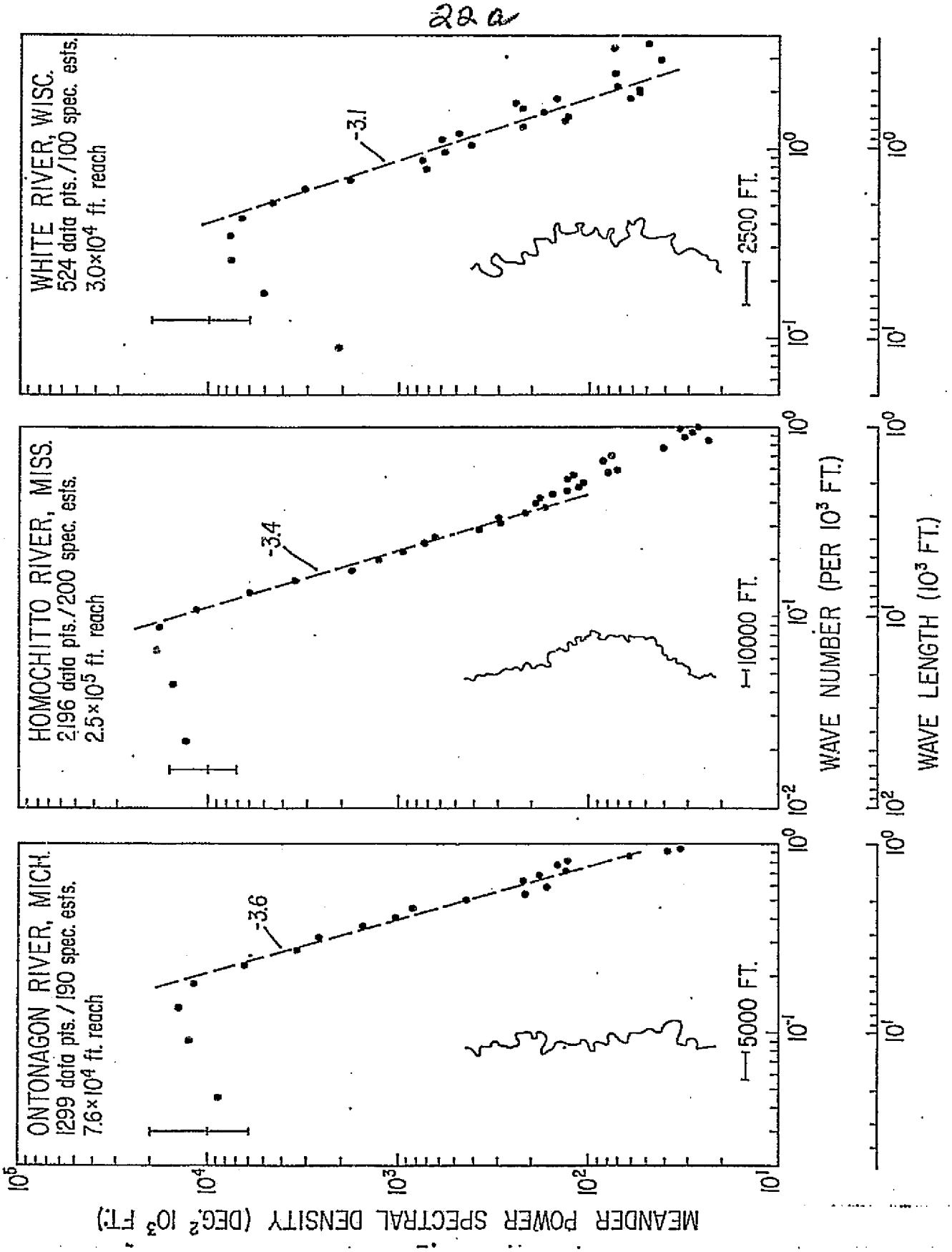

Figure 5. Power spectral density (deg^{2}10^{3}ft.) versus wave number (per 10^{3}ft.) and wave length (10^{3}ft.) for three river reaches showing rather simple, broad spectra with power law dependent segments approximately fitted by dashed lines with slopes indicated. A scaled trace of the meander pattern of each reach analyzed is also shown, together with data on the length of the reach, the number of data points, and the number of spectral estimates, and an error bar indicating the 80% confidence internal for the power spectral density estimate.

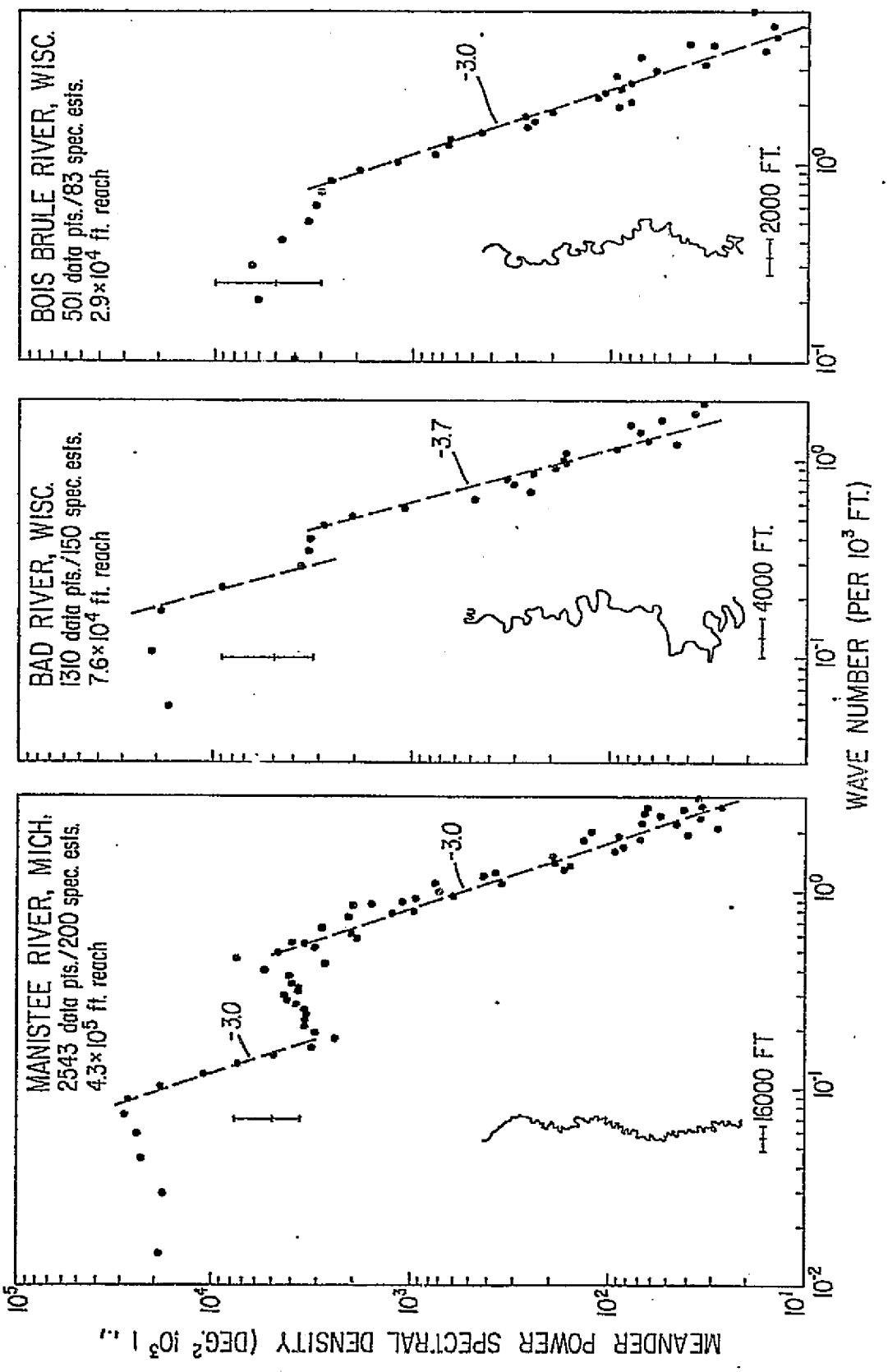

Figure 6. More complex meander power spectrum showing two offset power law dependent segments.

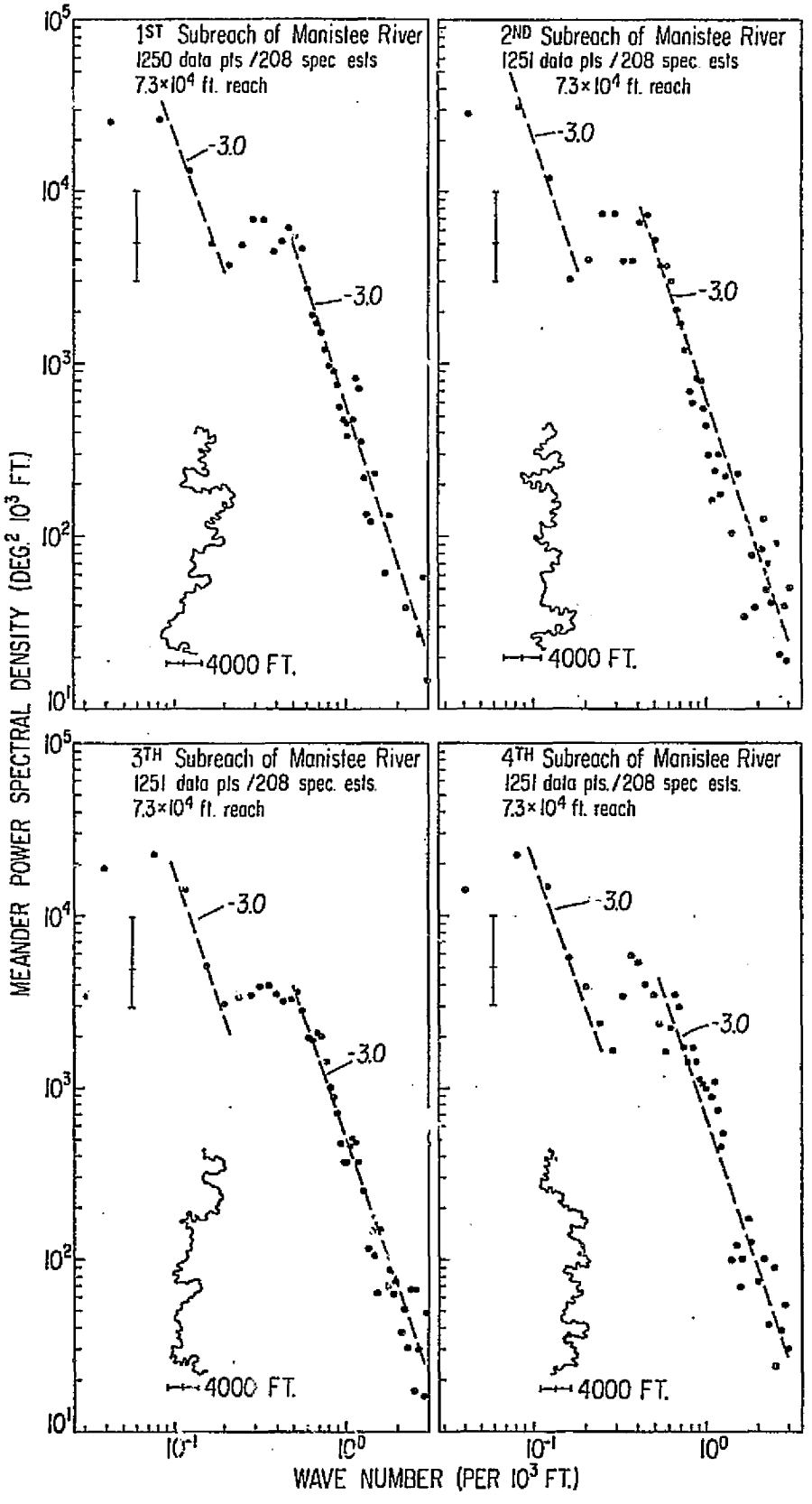

Figure 7. Stationarity of the offset structure in the power spectrum of the Manistee River shown by its persistence in the spectra of four separate readers spanning a total length of sixty miles.

along the course of the stream. Figure 7 shows spectra for four such consecutive subreaches, each of length 7.3×10^4 ft. at the downstream end of the larger reach of the Manistee River shown in Figure 6. Each subreach may be recognized in the larger reach of the Manistee River by the traces of their meander patterns. As can be seen in Figure 7 the spectra of the four subreaches are quite similar; the slopes and magnitudes of the power-law segments of the spectra and the wave numbers of breaks in the spectra at 10^{-1} and 5×10^{-1} are the same in all four spectra to well within the 80% confidence interval. Thus these characteristic features of the power spectrum of the Manistee River are stationary over a length of at least 60 miles along its course. We have also constructed the power spectrum of a 7.3×10^4 ft. subreach of the Manistee River located beyond the upstream end of the reach shown in Figure 6. This spectrum has only a single power law dependent segment, breaking at a wave number of 1 and differing significantly from those shown in Figure 7. This difference is not surprising, however, in view of the fact that the median discharge in this upper subreach also differs by a factor of 5 from that in the lower subreaches.

In comparing our meander power spectra with those of earlier investigators (Speight, 1965, 1967; Toebes and Chang, 1967) we note first that they used linear scales to plot the power spectral density estimates. Thus they did not observe

the power law segments of meander spectra identified in this paper. Speight (1965, 1967) appears to have placed an unwarranted credence in the physical significance of a great many "spectral peaks", nearly all of which we would classify as random fluctuations on the power law portions of the spectra. In fact none of Speight's "peaks" were resolvable on the basis of the number of degrees of freedom which he used in his spectral analysis, but he attributed significance to them on the basis of some stationarity over the reach. On the other hand, Toebes and Change (1967) have gone to the opposite extreme in suggesting that meander spectra are inherently nonstationary, reflecting only a randomness in the meander patterns. Neither of these investigators analyzed a large enough number of meander power spectra to justify their respective views.

Based on the rivers which we have studied so far (examples of which have been presented here) we believe that there is significant structure in a meander power spectrum, namely the slopes and magnitudes of the power law segments and the wave numbers at which breaks in these segments occur. It is these characteristic parameters of the meander spectra which we will attempt to correlate with such characteristics of the discharge spectra as the modal discharge and the exponent of the flood recession.

The cause of this simple power law relationship is not yet understood but because of the generality of the relationship

it may be fundamental for the process of meander formation.

2.3 Discharge Spectra

2.3.1 Technique

The discharge spectrum or frequency distribution of a river is the probability per unit discharge that its discharge, or flow rate, Q lies within the interval ΔQ at Q. The integral of this distribution over discharge is the flow duration curve commonly used in hydrologic studies (see, for example, Chow, 1964). From an historical discharge record of length T, the frequency distribution which we calculate is $\frac{1}{T} \cdot \frac{\Delta t}{\Delta Q}$ where Δt is the portion of the time the discharge lies within ΔQ at Q.

2.3.2 Power Law Dependence

From historical records of daily river discharge, we have constructed the frequency distributions from the fraction of time the discharge lies within a prescribed interval per unit interval. These are all shown in Appendix I. A remarkable property of most of these discharge frequency distributions is their nearly linear character on log-log plots for values of discharge larger than the mode (Schubert and Lingenfelter, 1974). Several examples of this are shown in Figure 8. The daily discharge data on which each distribution was based extends over the indicated time interval for the particular gauging station identified by number according to the convention adopted by the U.S.G.S. (1964). The slopes of the linear portions of these distributions vary from river to river and even from station to station on the same river

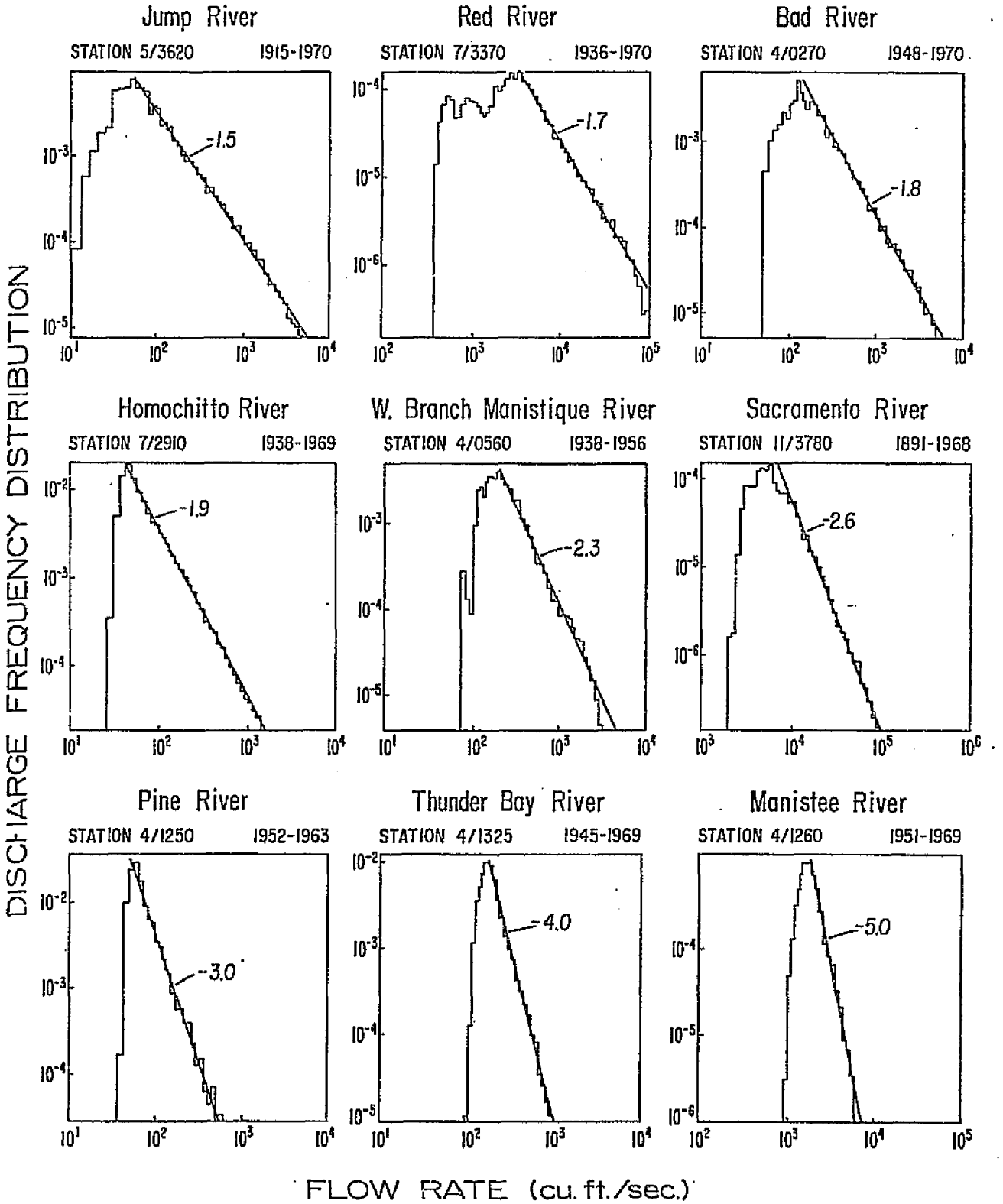

Figure 8. Log-log representations of discharge frequency distributions (probability per unit discharge that discharge Q lies within ΔQ at Q) for a number of rivers identified by name and U.S.G.S. gauging station number based on daily discharge data over the period noted. The straight lines with slopes indicated represent best fits to the linear parts of the distributions.

over the range from less than -1 to -5. Flow duration curves have previously been interpreted as representing a random process described, for example, by a log-normal distribution (Chow, 1964; Leopold et al., 1964). Our results, however, show that such an interpretation is not appropriate for a large number of rivers, since it is inconsistent with the clearly linear character of the log-log frequency distribution plots. Out interpretation of this relationship is discussed in section 2.4.

2.4 Relationship Between Discharge Spectra and River Flood Decay

We have shown (Schubert and Lingenfelter, 1974) that the distribution for discharges greater than the mode is not stochastic as previously suggested but is essentially deterministic in nature, reflecting the decay phase of the flood hydrograph. We have not found any previous suggestion of a direct relationship between the form of the flow duration curve and the flood hydrograph.

If s is the slope of the log-log frequency distribution, then

$$\frac{dt}{Dq} \propto Q^s \qquad (2.4.1)$$

Integrating eq. (1) we find

$$Q \propto t^{\frac{1}{s+1}} \qquad . \qquad ((2.4.2)$$

Since the observed values of s lie between about -1.5 and -5 the exponent $\frac{1}{s+1}$ would range from about -2.0 to -0.25. We suggest that equation (2.4.2) represents the decay phase of the flood hydrograph, where t is measured from a time t_0 near the flood peak. The time t_0 can be uniquely determined from any two discharge measurements Q_1, Q_2 at times t_1, t_2 during the flood recession by

$$t_0 = \left\{t_2 \left(\frac{Q_1}{Q_2}\right)^{s+1} - t_1\right\} / \left\{\left(\frac{Q_1}{Q_2}\right)^{s+1} - 1\right\} \qquad . \qquad (2.4.3)$$

The inverse power law dependence of the discharge on time, which we find here, differs from the superposition of several exponential decay curves, which have previously been used (Chow, 1964) to empirically fit the flood recession.

To test our suggestion that the linear nature of many of the log-log frequency distributions represents the recession portion of the flood hydrograph, we have compared the time dependence of the discharge predicted by equations (2.4.2) and (2.4.3) with the measured decay of discharge following individual flood peaks on the various rivers studied. We find that the predicted decay at each station does indeed describe the measured discharge following all flood peaks at that station. A typical example of the agreement between predicted

and measured flood recession is shown in Figure 9 for the Sacramento River near Red Bluff, California, in 1936. As can be seen, the curves of the theoretical flood decay are an excellent fit to the data points which indicate the measured values of the daily discharge. The theoretical curves are based on a value of s equal to -2.6 (see Figure 8) and values of t_0 equal to 16 January, 22 February and 4 April for the respective floods shown in Figure 10. At this station on the Sacramento River floods decay according to the rule $t^{-0.625}$, which allows the recession to be determined for as long as a month following the flood peak. From the hydrograph of Figure 10 it can be seen that the deterministic flood decay extends down to discharges of about 10^4 c.f.s. at this station. Below this discharge level the flow rate variations appear to be stochastic in nature. This also is consistent with the fact that the linear relationship in the log-log frequency distribution (Figure 9) ceases at discharges below about 10^4 c.f.s. at this station.

Additional examples of the agreement between predicted power law flood decays and measured flood recessions are shown in Figure 10 and 11 for 3 consecutive flood decays on the Homochitto River (7/2910) and the Bad River (4/0270), respectively. The power law decays are excellent fits to the observed values of daily discharge during the flood recessions. Values of s equal to -1.9 and -1.8 (from Figure 8) for the

Homochitto and Bad Rivers, respectively, were used to construct the power law decays shown in Figures 10 and 11. The floods at this station on the Homochitto River decay according to $t^{-1.11}$, while on the Bad River station the recession follows the law $t^{-1.25}$.

It is noteworthy that the flood decays on the Sacramento River (Figure 9) extend from discharges of about 10^5 c.f.s. down to 10^4 c.f.s., while on the Bad River (Figure 11) the recessions extend from 10^4 c.f.s. down to below 10^3 c.f.s. and on the Homochitto River the transients cover the discharge range from more than 10^3 c.f.s. to below 10^2 c.f.s. The power law flood decays are thus seen to be excellent representations of the measured discharges for recessions which extend over 3 orders of magnitude in discharge. Moreover these rivers are from widely separated regions and represent widely differing hydrologic systems. From Figure 8 it can be seen that the Red River (5/0540) is similar to the Sacramento in that power law flood decays range from 10^5 c.f.s. down to below 10^4 c.f.s. Also from Figure 8 we note that the Manistee River (4/1260) like the Bad River (4/0270) has power law flood decays in the discharge range 10^4 - 10^3 c.f.s. and the Pine (4/1250), Thunder Bay (4/1325) and West Branch Manistique (4/0550) Rivers, like the Homochitto River (7/2910), have power law flood recessions in the discharge range 10^3 - 10^2 c.f.s. The Jump River (5/3620) has power law transients over a two order of magnitude discharge

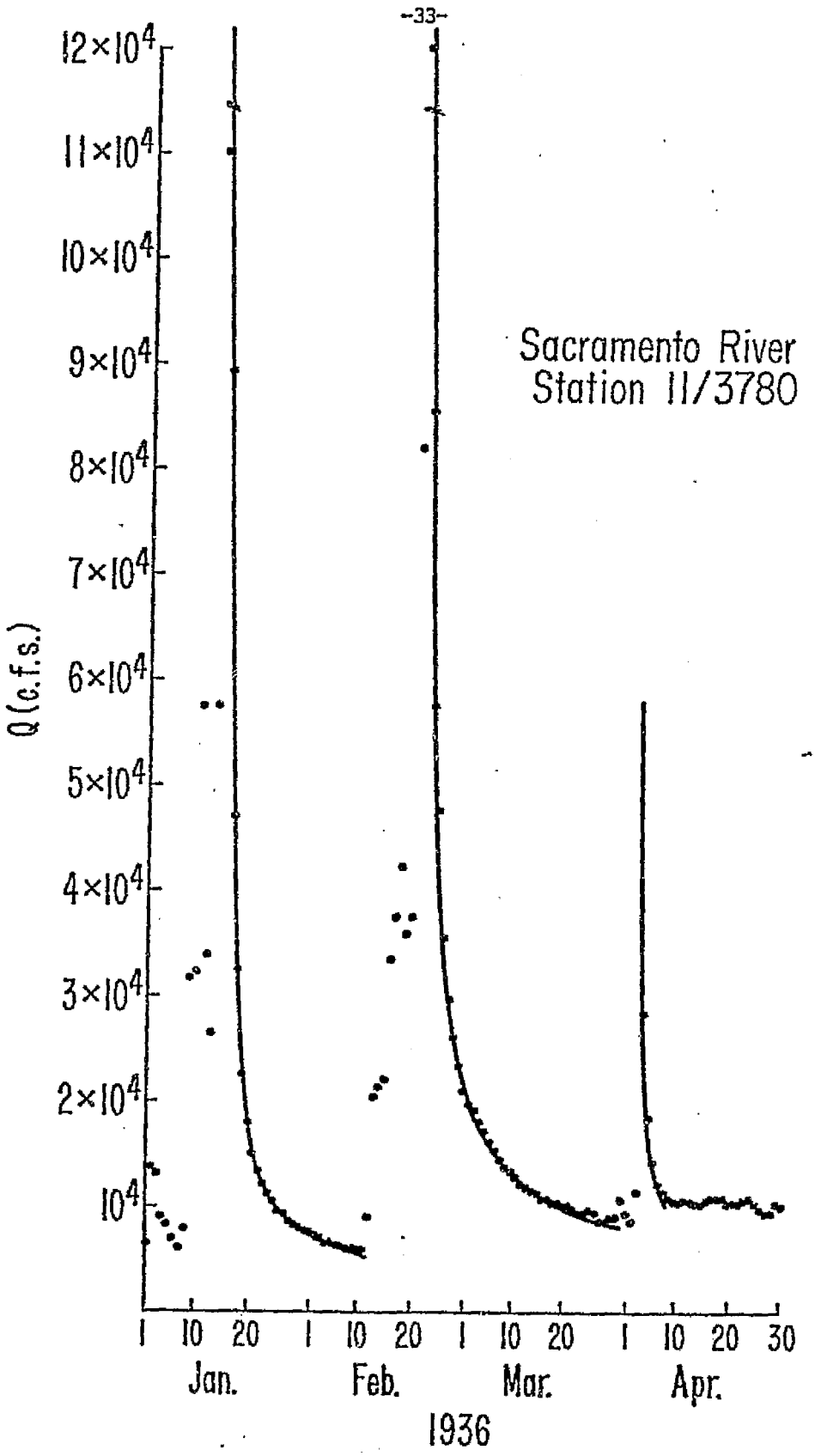

Figure 9. Typical daily discharge data (circles) showing the recessions of three floods on the Sacramento River near Red Bluff in 1936. The theoretical curves of the form $t^{1/(s+1)}$ are based on the $s = 2.6$ power law dependence of the discharge frequency distribution on discharge at this station shown in Fig. 8. The good agreement between the theoretical curves and data shows that the flood recessions follow an inverse power law dependence on time which in turn is reflected in the power law dependence of the discharge frequency distribution.

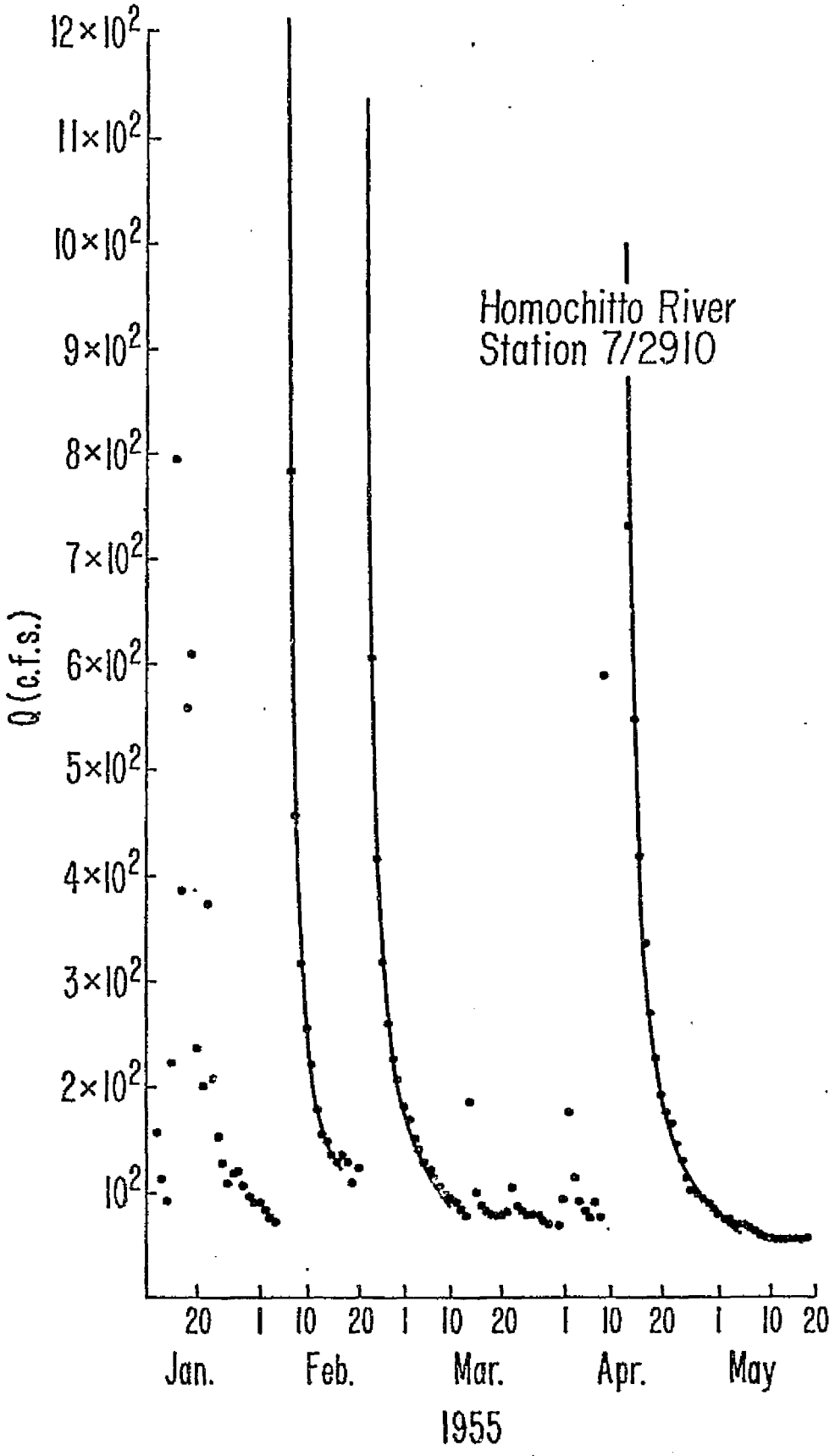

Figure 10. Power law fits to daily discharge data (circles) of 3 flood recessions on the Homochitto River (7/2910) in 1955. The floods decay according to $t^{-1.11}$ ($t^{\frac{s}{s+1}}$ with s = -1.9 from Figure 8).

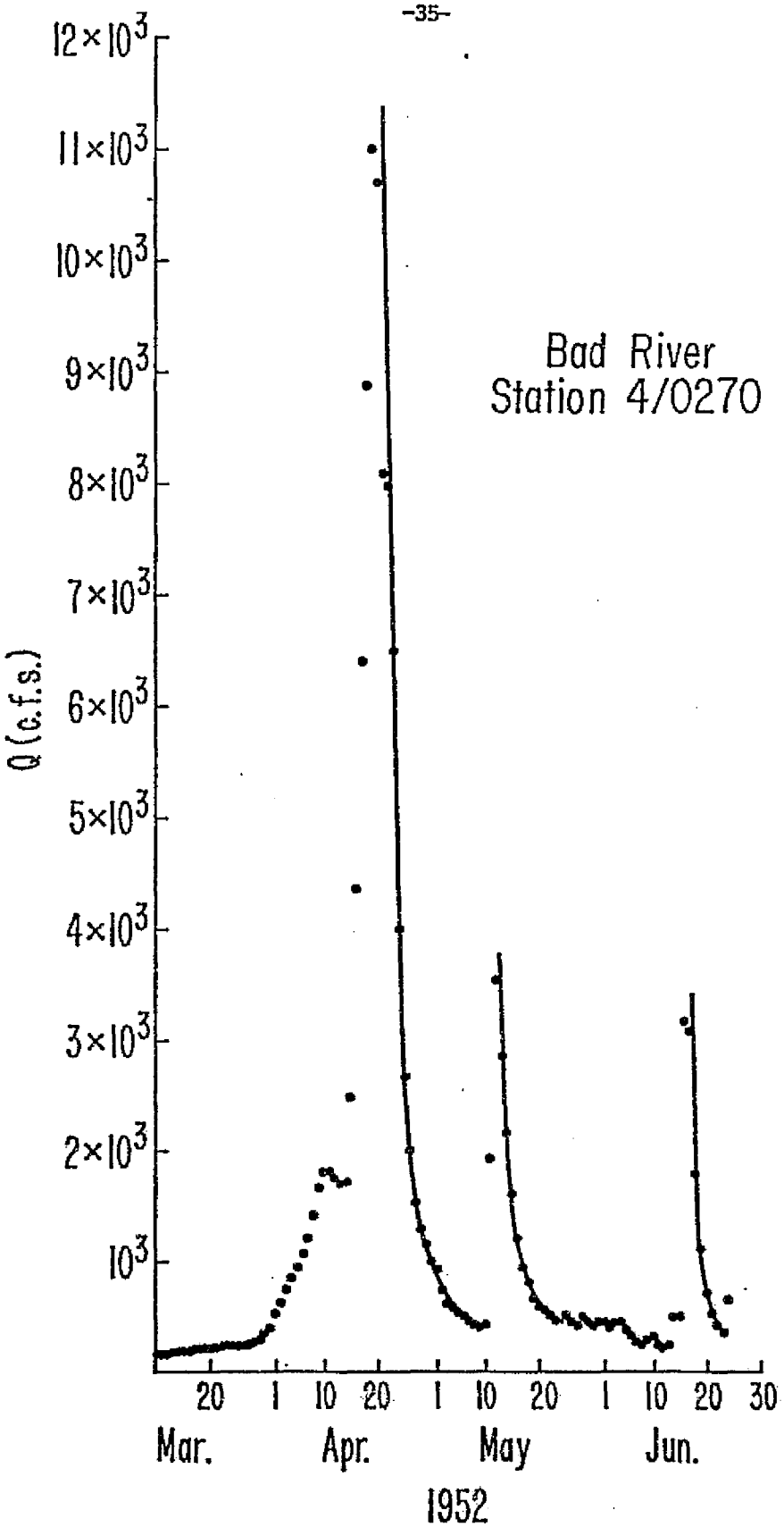

Figure 11. Power law fits of the form $t^{-1.25}$ to daily discharge data (circles) for 3 flood decays on the Bad River (4/0270) in 1952. Individual floods at this station indeed follow a power law decay, as implied by the long term discharge frequency distribution shown in Figure 8.

range, from nearly 10^4 c.f.s. to below 10^2 c.f.s.

To firmly establish the validity of our suggestion that the slope s of long term discharge frequency distributions reflects the short term decay of individual river floods according to $t^{\frac{1}{s+1}}$ we have used the power law decays with the appropriate value of s, to fit ten sample flood recessions at each of the gauging stations of Figure 8. The results are summarized in Table 2 which lists, for each river in Figure 8, the inclusive dates of the sample flood recessions, the root mean square (rms) errors in the power law fits of the recessions, and the average rms error of fit for the 10 cases. The flood recessions listed in Table 2 were selected by scanning the available hydrologic data in the Water Supply Papers to find the longest uninterrupted flood decays for each river. Each recession was terminated when the flood had decayed to the stochastic level of discharge as indicated by the data. The rms errors of the power law fits of the 90 flood recessions listed in Table 2 are remarkably small, averaging only about 5%, a value comparable to the uncertainties in the measured daily discharges themselves. The smallness of these rms errors clearly establishes that floods decay with an inverse power law time dependence.

In conclusion, we have found that floods decay with an inverse power law dependence on time. The exponent of this dependence varies from river to river and even from station to

TABLE 2. POWER LAW FITS TO RIVER FLOOD DECAYS

RIVER	INCLUSIVE DATES OF FLOOD DECAYS	RMS ERROR OF FIT	MEAN RMS ERROR
MANISTEE RIVER 4/1260 $s = -5.0$ $Q \propto t^{-.25}$	4/11-4/14/59, 7/26-7/30/52, 11/21-11/24/58 4/7-4/10/56, 10/8-10/11/54, 4/11-4/14/58 6/5-6/8/54, 7/14-7/18/57, 4/22-4/25/60 5/30-6/2/53	1.7%, 7.1%, 1.6% 1.7%, 5.2%, 1.4% 0.4%, 1.1%, 2.4% 3.3%	2.6%
THUNDER BAY RIVER NEAR HILLMAN, MICHIGAN 4/1325 $s = -4.0$ $Q \propto t^{-0.33}$	5/23-5/30/59, 4/7-4/13/59, 4/9-4/26/56 4/27-5/9/57, 3/25-4/3/53, 3/23-3/30/48 10/18-10/26/54, 4/13-4/22/47, 4/9-4/15/54 3/15-3/21/46	1.3%, 3.3%, 5.5% 8.7%, 2.4%, 3.8% 3.8%, 8.6%, 4.0% 6.0%	4.7%
PINE RIVER NEAR LEROY, MICHIGAN 4/1250 $s = -3.0$ $Q \propto t^{-0.5}$	5/21-5/30/60, 7/10-7/20/57, 10/18-10/26/54 6/27-7/6/54, 5/7-5/14/54, 3/24-4/2/53 5/4-5/16/53, 4/8-4/21/58, 4/9-4/15/59 11/19-11/25/58	6.7%, 4.3%, 5.8% 5.4%, 1.7%, 3.9% 1.9%, 4.7%, 3.9% 6.7%	4.5%
SACRAMENTO, NEAR RED BLUFF 11/3780 $s = -2.6$ $Q \propto t^{-0.625}$	1/17-2/10/36, 2/24-3/23/36, 3/31-4/15/05 2/6-2/16/07, 4/9-5/9/07, 2/27-3/13/10 2/15-2/28/11, 3/22-4/1/32, 4/18-4/30/20 2/21-3/8/26	3.6%, 2.9%, 3.0% 5.2%, 8.0%, 3.2% 6.6%, 6.2%, 2.7% 5.5%	4.7%
WEST BRANCH OF MANISTIQUE RIVER NEAR MANISTIQUE, MICHIGAN 4/0560 $s = -2.3$ $Q \propto t^{-0.769}$	4/14-4/25/53, 4/16-4/27/51, 5/6-5/21/47 5/5-5/14/40, 4/21-5/13/42, 4/13-4/23/56 3/22-4/15/46, 4/30-5/20/54, 4/23-5/10/55 4/26-5/9/52	5.8%, 4.5%, 4.1% 2.7%, 3.3%, 5.4% 6.1%, 6.9%, 8.5% 3.5%	5.1%

TABLE 2. (continued)

RIVER	INCLUSIVE DATES OF FLOOD DECAYS	RMS ERROR OF FIT	MEAN RMS ERROR
HOMOCHITTO RIVER 7/2910 $s = -1.9$ $Q \propto t^{-1.11}$	2/16-2/29/56, 5/20-6/4/53, 4/14-4/29/55 2/7-2/14/55, 3/28-4/5/42, 2/27-3/9/53 2/23-3/9/55, 4/18-4/27/57, 4/10-4/20/51 4/24-5/4/51	5.9%, 7.2%, 4.2% 5/6%, 3.3%, 1.8% 5.5%, 6.7%, 3.8% 7.4%	5.1%
BAD RIVER 4/0270 $s = -1.8$ $Q \propto t^{-1.25}$	5/15-5/28/56, 6/2-6/13/59, 10/31-11/8/55 7/6-7/15/53, 6/4-6/13/51, 7/6-7/15/51 5/11-5/23/50, 5/14-5/23/52, 4/23-5/5/52 5/7-5/18/49	4.7%, 9.9%, 6.7% 4.4%, 5.7%, 6.7% 3.2%, 4.0%, 4.3% 4.2%	5.4%
RED RIVER 7/3370 $s = -1.7$ $Q \propto t^{-1.429}$	7/19-7/26/48, 2/21-3/2/56, 2/24-3/7/51 3/1-3/9/39, 2/7-2/15/41, 10/3-10/10/36 4/4-4/14/45, 2/26-3/8/38, 4/28-5/8/52 11/7-11/17/41	5.7%, 8.0%, 8.9% 7.7%, 8.9%, 8.1% 3.4%, 7.2%, 4.8% 8.2%	7.1%
JUMP RIVER NEAR SHELDON, WISCONSIN 5/3620 $s = -1.5$ $Q \propto t^{-2}$	7/16-8/5/58, 5/7-5/18/58, 5/12-5/21/50 6/11-6/21/40, 11/6-11/17/34, 11/24-12/15/34 4/25-5/10/20, 11/13-11/24/19, 12/24-1/11/19 11/18-11/27/26	10.5%, 5.4%, 7.9% 5.8%, 3.3%, 10.5% 8.6%, 4.8%, 8.1% 8.3%	7.3%

station along the same river. Nonetheless, despite the complex interactions of the large number of factors which undoubtedly affect the flow at any point on a stream, the resultant time dependence of flood decays can be described by a single parameter, which can be uniquely determined from long term records of the discharge. This power law time dependence makes possible the forecasting of river discharge with an uncertainty of about 5% for as long as a month following the flood peak. Finally we should note that an inverse power law dependence of the flow rate on time is characteristic of diffusive and random walk processes, suggesting a direction for future hydrologic modeling of the flood recession.

2.5 Relationship Between Meander Spectra and Discharge Spectra

The primary objective of this investigation was to try to determine whether significant information on stream flow rates could be obtained from aerial and satellite imagery of river meander patterns based on a possible correlation between the meander and discharge spectra of rivers. Such a correlation could provide the basis for a simple and inexpensive technique for remote sensing of the water resources of large geographical areas, eliminating the need for much hydrologic recording.

The test of the existence of such a correlation can be seen in Figure 12 where we plot the median discharge Q determined from the discharge spectra versus the characteristic

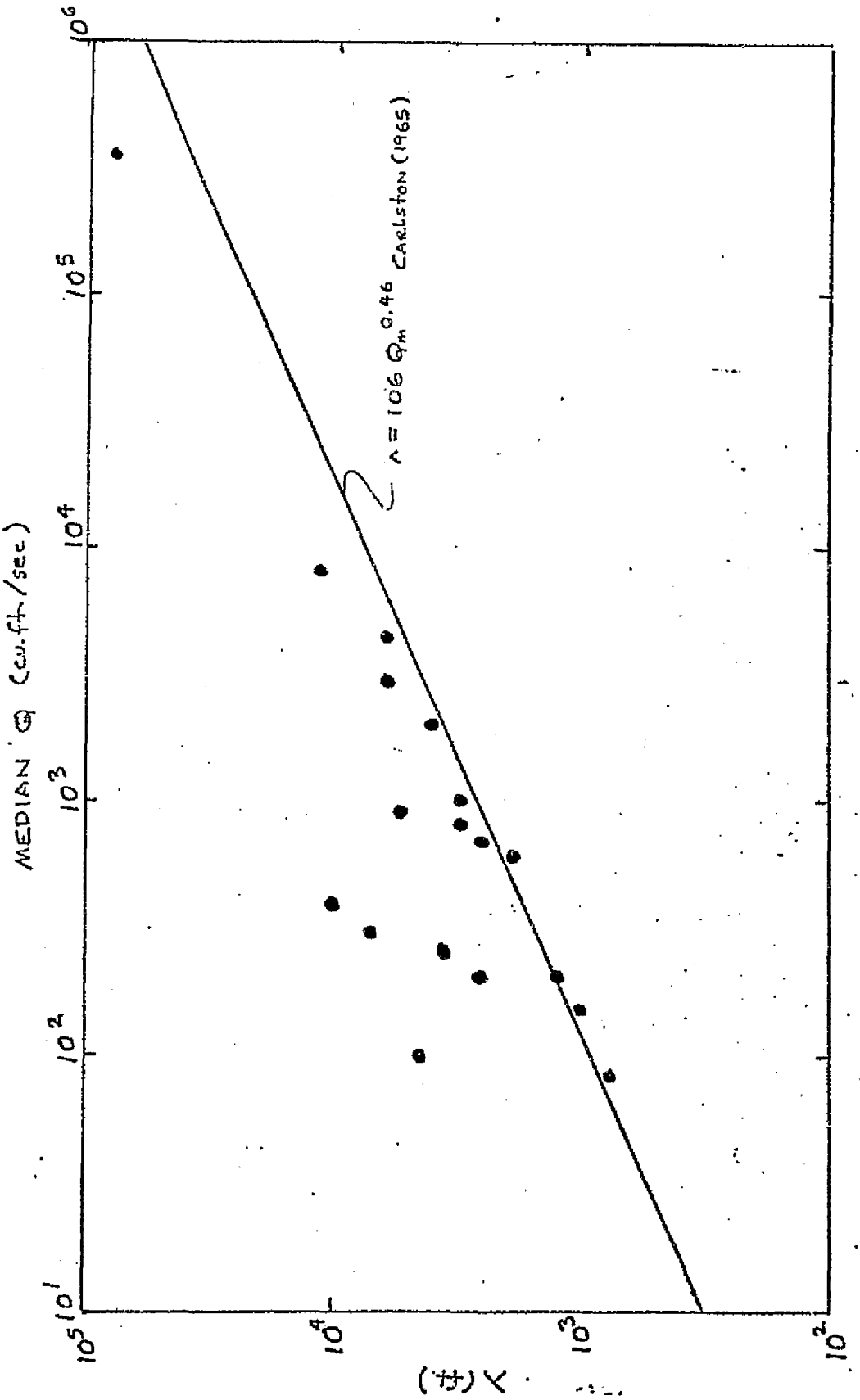

Figure 12. Median discharge versus wavelength of break in meander power spectrum.

wave length λ associated with the break in the meander power spectra for the rivers studied. As can be seen there is only a crude correlation between these two quantities, confirming that additional factors (see e.g. Schumm, 1968) also govern this relationship. This prevents a simple inversion of the meander power spectrum of a stream to obtain its discharge spectrum. The general trend of the correlation between median discharge and the characteristic wavelength is nonetheless qualitatively consistent with earlier studies using less quantitative methods of analysis as can been seen by comparison of the relationship determined by Carlston (1965).

3. Summary

Although NASA no longer supports this research we are continuing our efforts to understand the individual discharge and meander spectra and their correlations. We have been impressed with the uniformity in the slopes of meander power spectra over the small wavelength portions of the spectra. As λ (wavelength) $\to 0$, we have found that the meander power spectral density estimates behave as λ^{α}, where α has a value between 3 and 4 for all the rivers we have investigated. The value of α appears to be independent of discharge and other variables such as local geology, etc. The slope of meander power spectra for short wavelengths must, in some way, be characteristic of the fundamental

meander forming processes.

In an attempt to understand the significance of the essentially constant α, we are computing the power spectra of artificially generated meanders to see if the slopes of the spectra of these mathematical meanders bear any relationship to the values of α determined for rivers. In particular, we are testing the validity of the theory of meander formation proposed by Langbein and Leopold (1966). The theory asserts that meander formation is a random or stochastic phenomenon in which the meander planform is a most probable path defined by a random-walk model. The probability p that a river deviates by an angle $d\theta$ from its previous direction in a distance ds along the river is described by a distribution which is assumed to be Gaussian

$$dp = c\, e^{\frac{1}{2}\left(\frac{d\theta}{\sigma}\right)} ,$$

where σ is the standard deviation and c is such that $\int dp = 1$. The solution for the most probable path, or meander form, between given points is the elliptic integral

$$s = \frac{1}{\sigma} \int \frac{d\theta}{\sqrt{2(\cos\omega - \cos\theta)}} ,$$

where s is the arc length along the river whose local direction θ is measured from the line joining the end points and ω is the

maximum value taken by θ.

We have computed $s(\theta)$ for various values of ω and have numerically inverted the function to obtain $\theta(s)$. $\theta(s)$ is exactly what we measure in computing the meander spectra of rivers. We are presently computing the power spectra of $\theta(s)$ for various ω. Should the mathematical $\theta(s)$ yield spectra whose slopes are in agreement with the river value, then we have found an empirical verification of the minimum variance theory of river formation. If not, then one must question the relevance of the model of Langbein and Leopold to actual rivermeander formation.

REFERENCES

Bendat, J.S., and A.G. Piersol, 1966, Measurement and Analysis of Random Data, New York, John Wiley.

Blackman, R.B., and J.W. Tukey, 1958, The Measurement of Power Spectra, New York, Dover.

Carlston, C.W., 1965, The relation of free meander geometry to stream discharge and its geomorphic implications, Am. J. of Sci., 263, 864-885.

Chow, V.T., 1964, editor, Handbook of Applied Hydrology, A Compendium of Water-Resources Technology, New York, McGraw-Hill.

Dury, G.H., 1965, General theory of meandering valleys, U.S. Geological Survey Prof. Paper 452-C, 43 pp.

Inglis, C.C., 1949, The behavior and control of rivers and canals, Poona, India, Central Waterpower Irriq, Navigation Research Sta., Research Pub. 13, pt. 1, 298 pp.

Jefferson, M.S.W., 1902, Limiting width of meander belts, Nat. Geog. Mag., 13, 373-384.

Leopold, L.B., and Wolman, M.G., 1957, River channel patterns: braided, meandering, and straight, U.S. Geological Survey Prof. Paper 282-B, 85 pp.

Leopold, L.B., M.G. Wolman and J.P. Miller, 1964, Fluvial Processes in Geomorphology (Freeman, San Francisco) pp. 67-69.

Schubert, G., and R.E. Lingenfelter, 1974, Power Law Dependence on Time of River Flood Decay and its Relationship to Long-Term Discharge Frequency Distribution, Water Resources Research, 10, 98-102.

Schumm, S.A., 1968, River Adjustment to Altered Hydrologic Regimen USGS Prof. Paper 598 (Washington GPO).

Schumm, S.A., 1971, Fluvial geomorphology: the historical perspective, in River Mechanics, H.W. Shen ed. (Fort Collins, Colo.).

Speight, J.G., 1965, Meander Spectra of the Angabunga River, Journal of Hydrology, 3, 1-15.

Speight, J.F., 1967, Spectral Analyses of Meanders of Some Australasian Rivers, in Landform Studies from Australia and New Guinea, pp. 48-63, Jennings, J.N. and Mabbitt, J.A. editors.

Toebes, G.H. and T.P. Chang, 1967, Planform Analysis of Meandering Rivers, International Association of Hydraulic Research Proceedings, Vol. 1, 362-369.

APPENDIX I

Individual River Discharge and Power Spectra

MISSISSIPPI RIVER

ST. 7/320 AT MEMPHIS, TENN. 1933-1970

IN TAPE AAH154 F1 RCDS. 1225 -1677

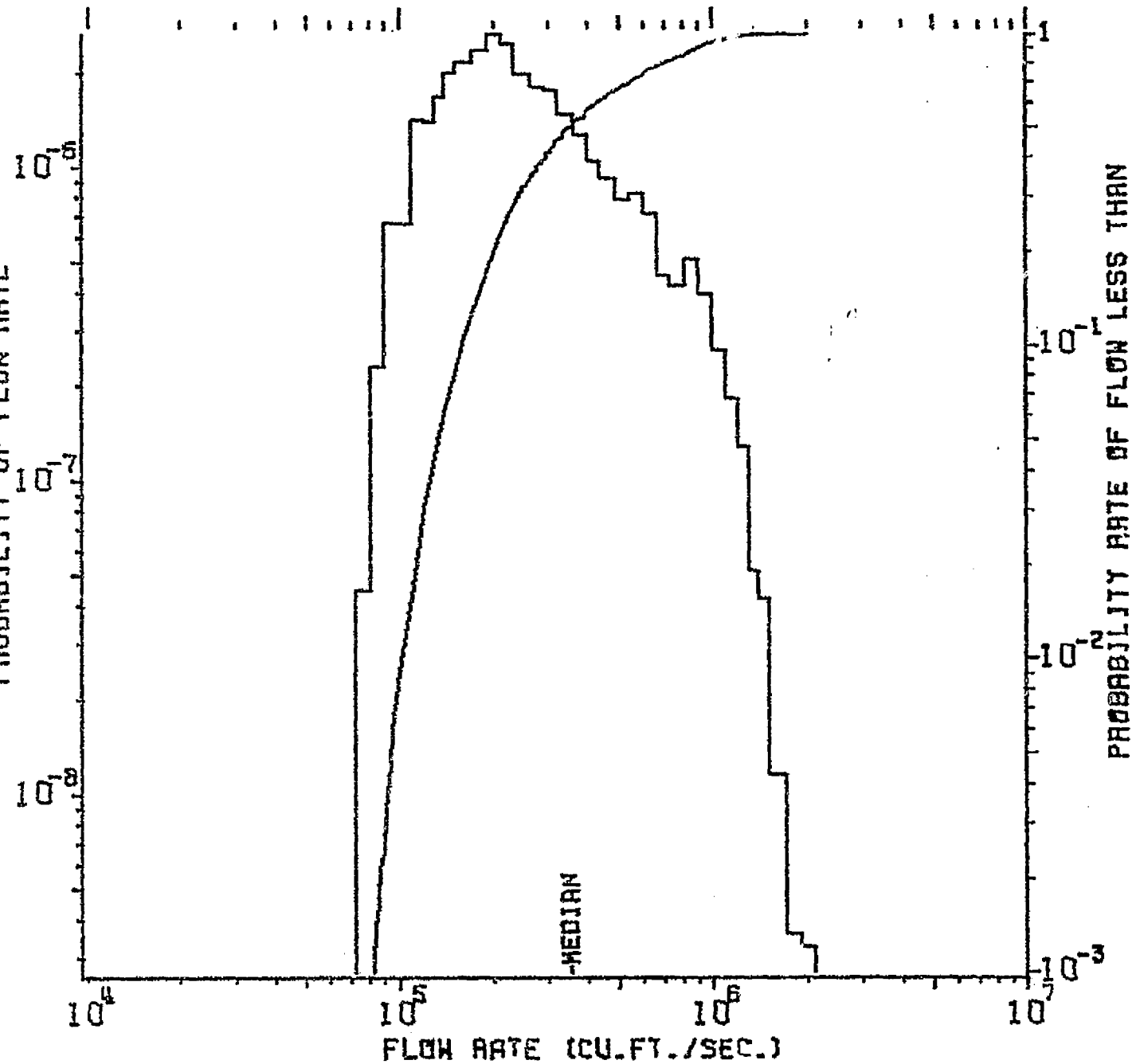

FL TAPE AYFLT4 F10 BLK. 33

MISSISSIPPI RIVER

ST. 7/2890 NEAR VICKSBURG, MISS 1931-1970

IN TAPE AAH154 F1 RCDS. 3703-4170

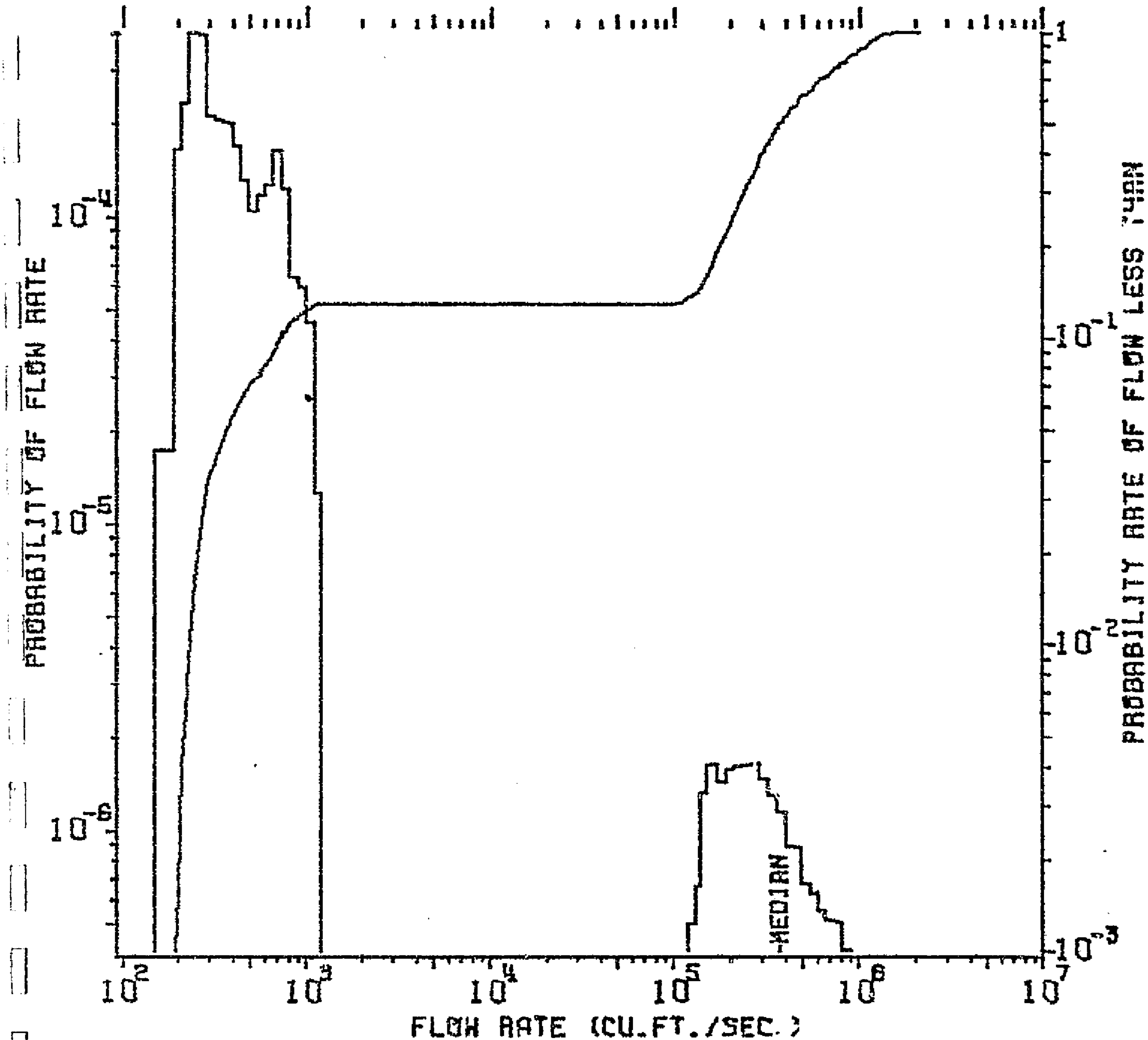

FL TAPE AVPLTH F10 BLK. 45

MISSISSIPPI RIVER

874 DATA PTS / 85 SPEC ESTS

4.1×10^6 FT REACH

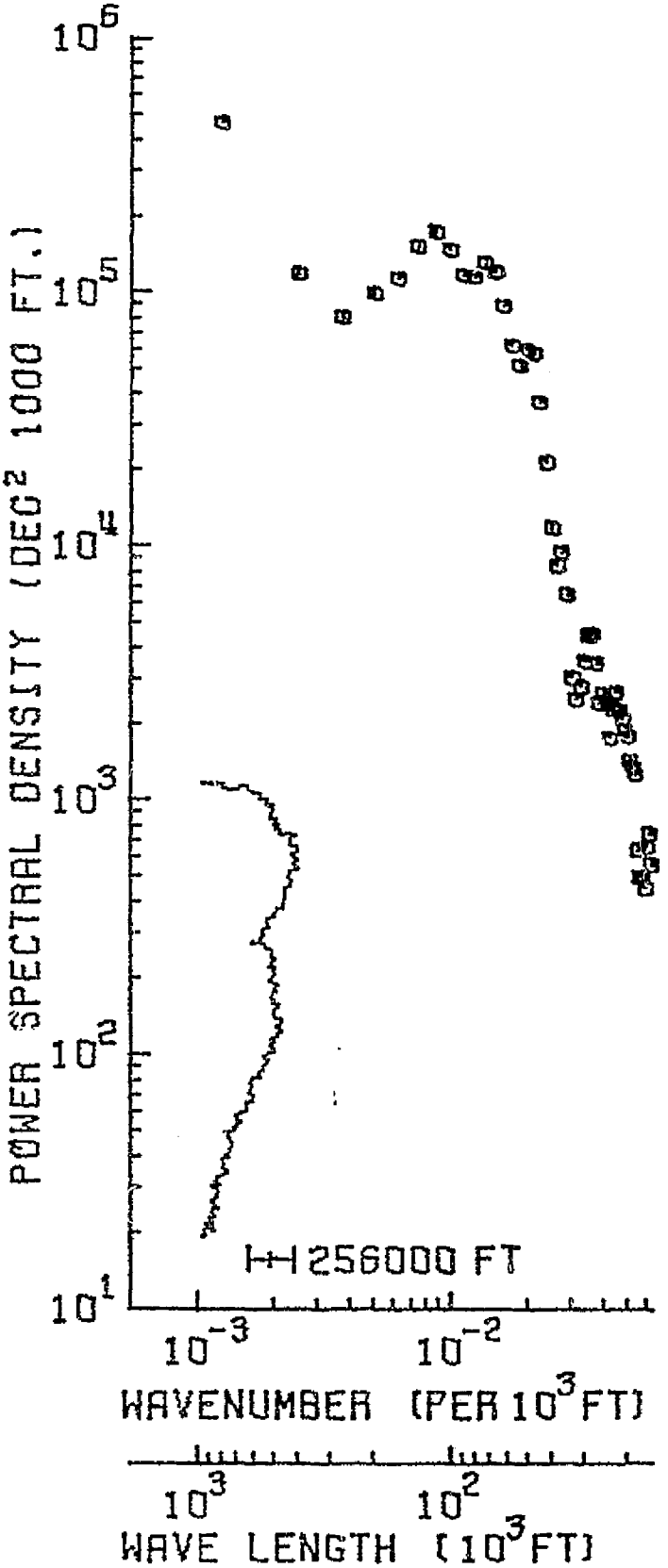

1 / 5249

PLT TAPE PSPLT1 F6 BLK 59 IN DISK KAUDSK PIS096.MAJ.LMISS1
74 295 OCT 22 03:49:10.1

SACRAMENTO RIVER

ST. 11/3780 NR RED BLUFF, CA. 1891-1968

IN TAPE AAH154 F1 RCDS. 7751 -8674

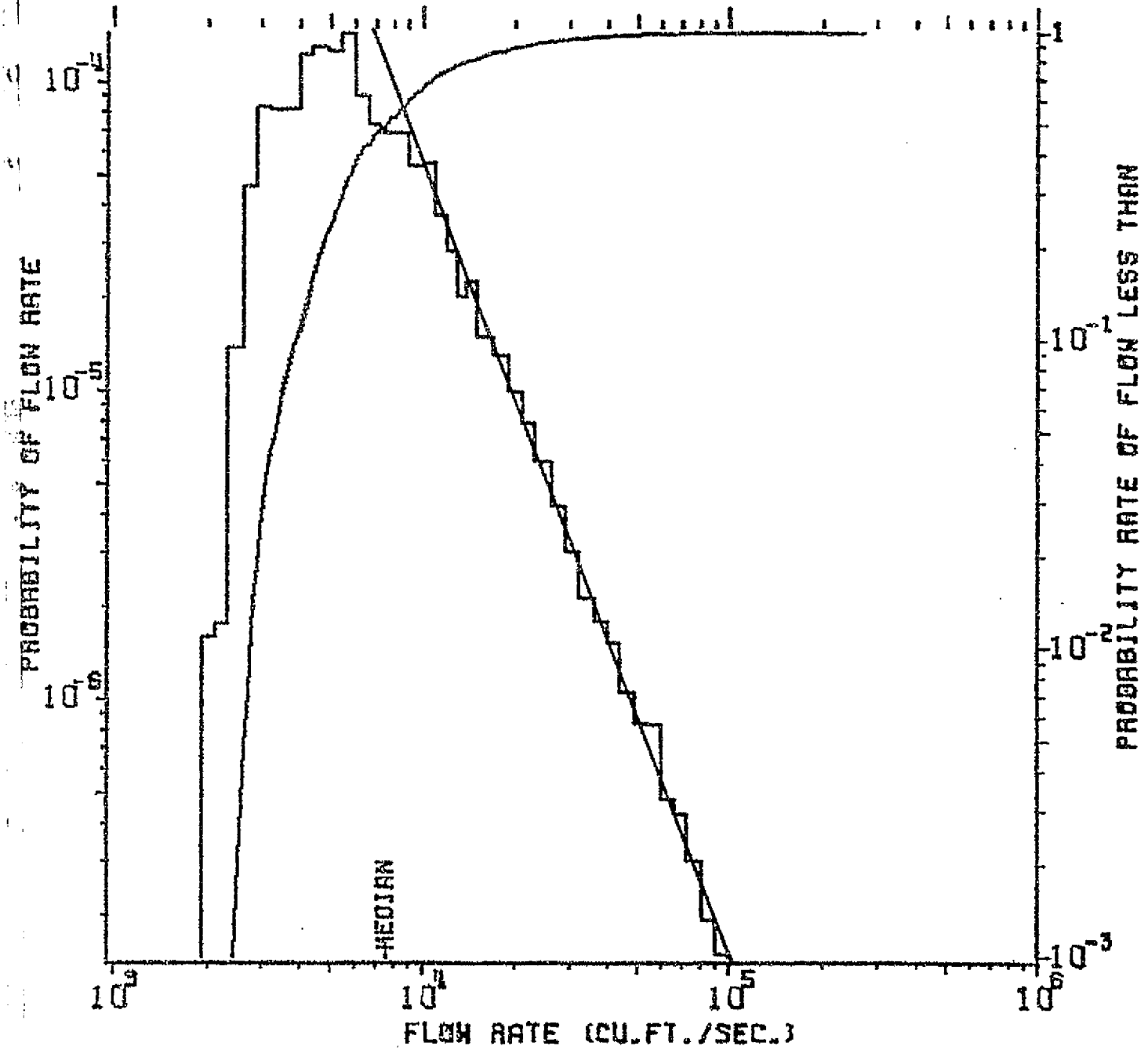

FL TAPE SYPLTN F10 BLK. 56

SACRAMENTO RIVER

ST. 11/3890 AT BUTTE CITY, CA. 1938-1970

IN TAPE AAH154 F1 RCDS. 8675 -9058

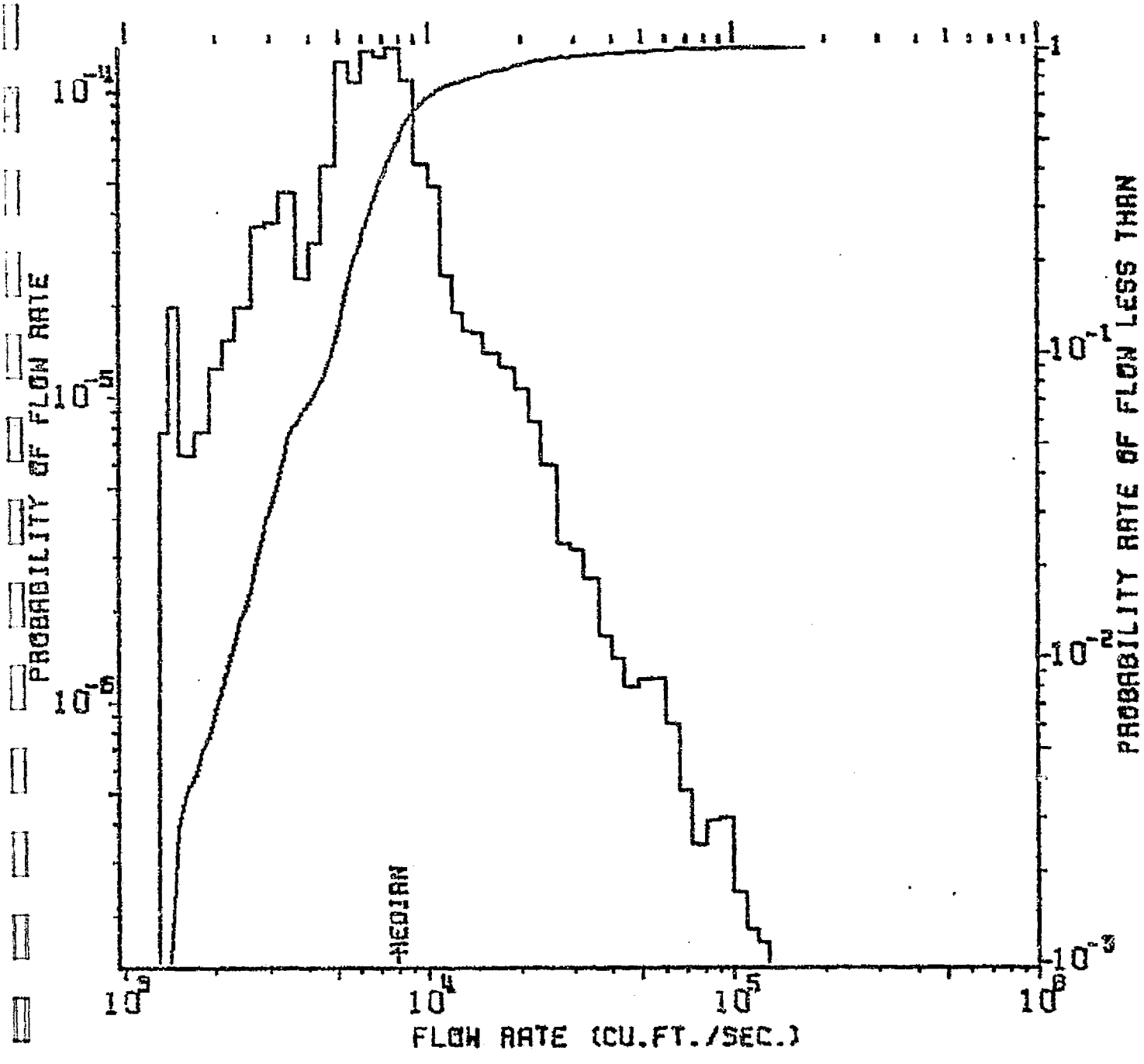

FL TAPE AVFLTN F10 BLK. 57

SACRAMENTO RIVER

ST. 11/3895 AT COLUSA, CA. 1940-1970

IN TAPE AAH154 F1 ACOS. 9059 -9418

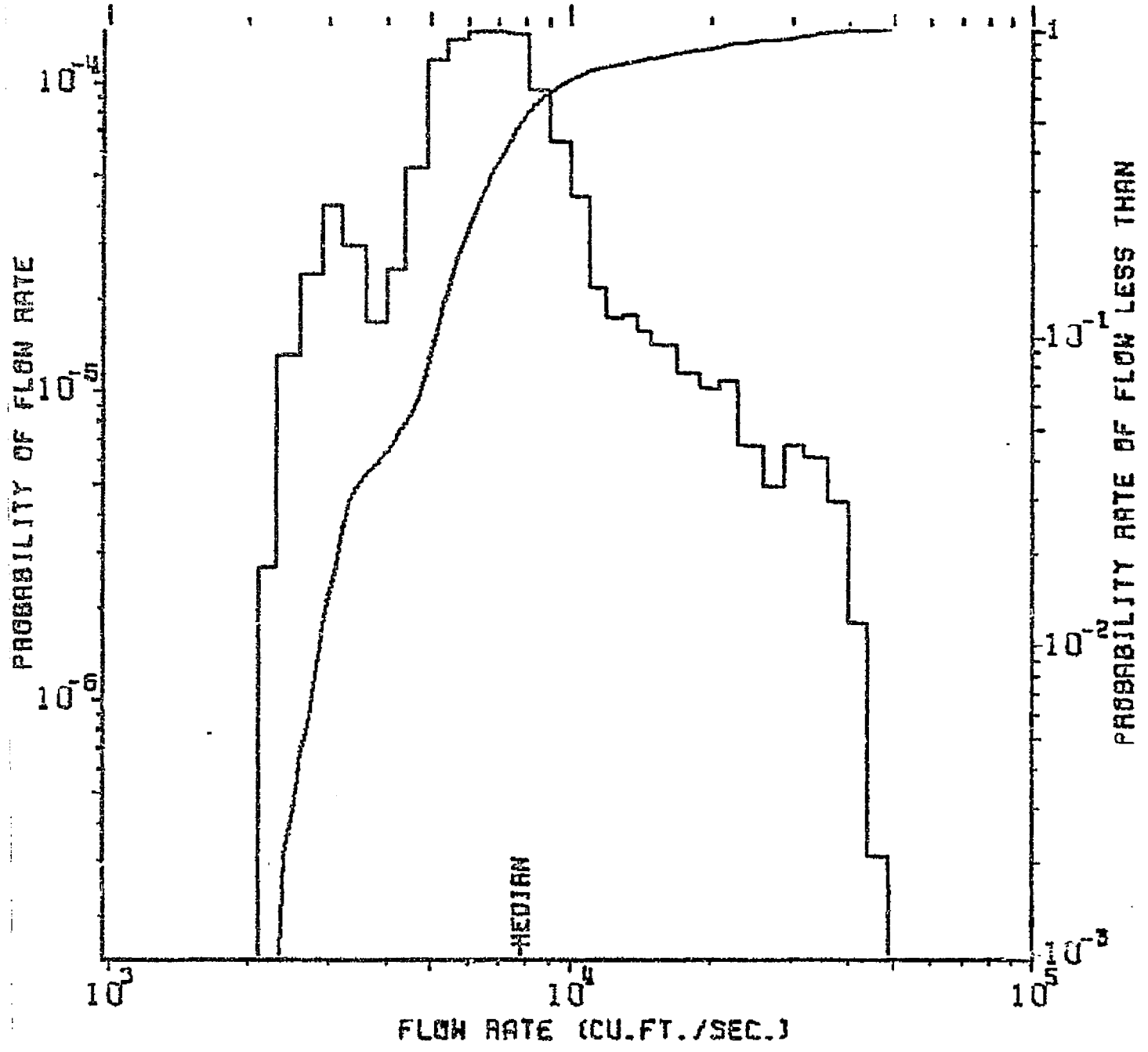

FL TAPE AVrL79 F10 BLK. 50

RIVER SACR

3617 DATA PTS / 125 SPEC ESTS

5.0×10^{5} FT REACH

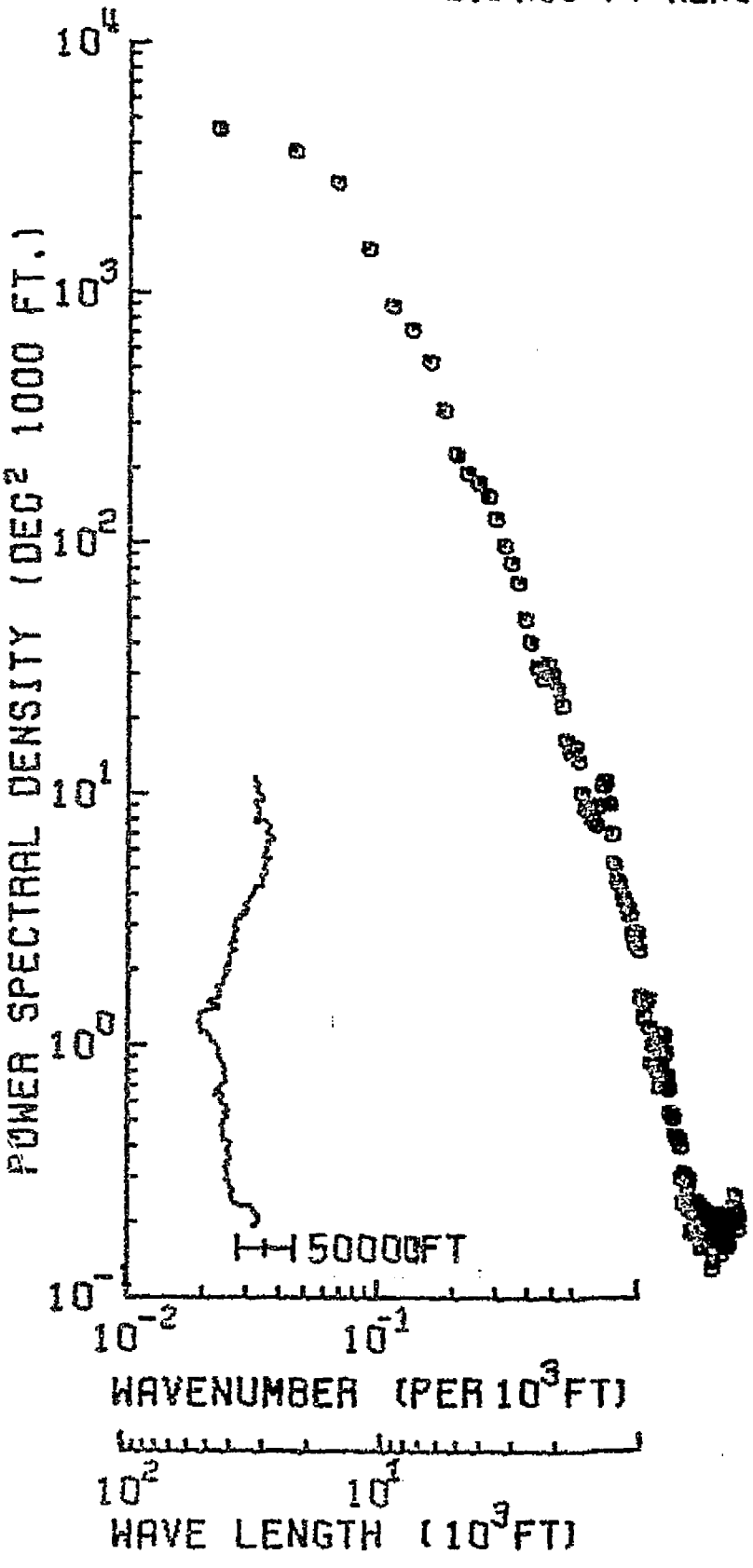

1 / 3618

PLT TAPE PSPLT1 FS BLK 38 C IN DISK KAU05K PIS096.KAJ.SACR.L2.A
70 285 OCT 12 01:18:07.0

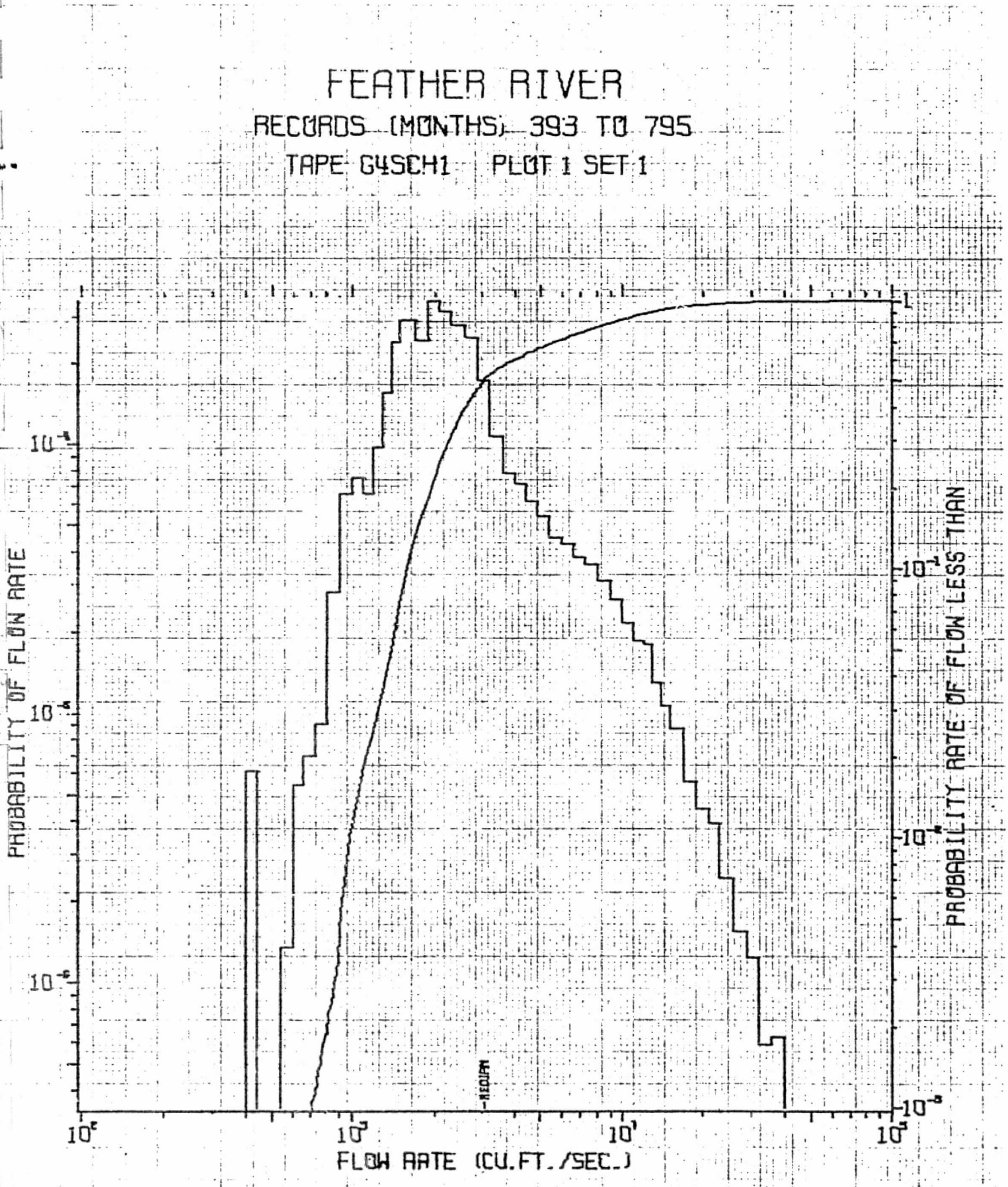
FEATHER RIVER
RECORDS (MONTHS) 393 TO 795
TAPE G4SCH1 PLOT 1 SET 1
PROBABILITY OF FLOW RATE
PROBABILITY RATE OF FLOW LESS THAN
FLOW RATE (CU.FT./SEC.)
MEDIAN

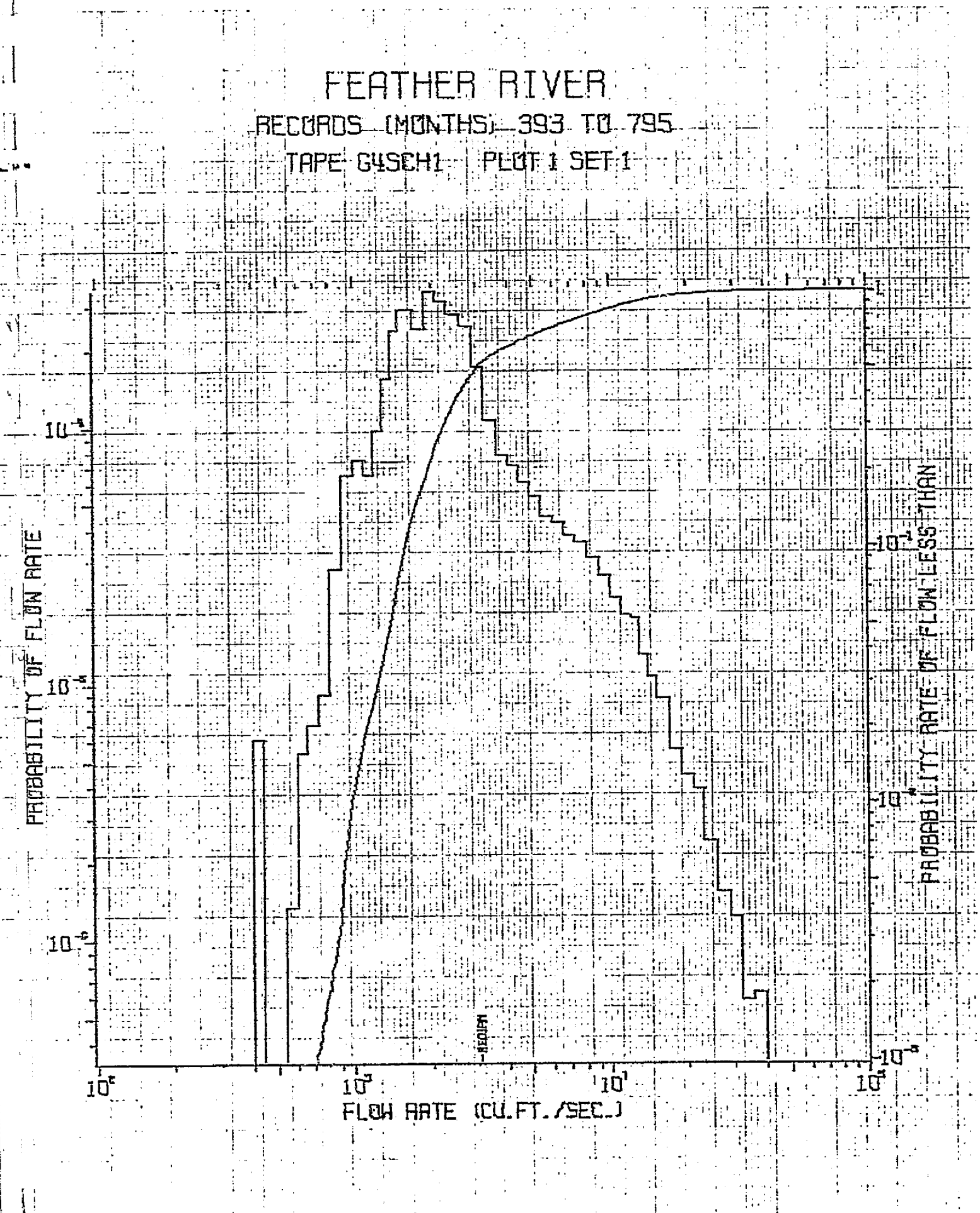
FEATHER RIVER
RECORDS (MONTHS) 393 TO 795
TAPE G4SCH1 PLOT 1 SET 1
PROBABILITY OF FLOW RATE
PROBABILITY RATE OF FLOW LESS THAN
FLOW RATE (CU.FT./SEC.)

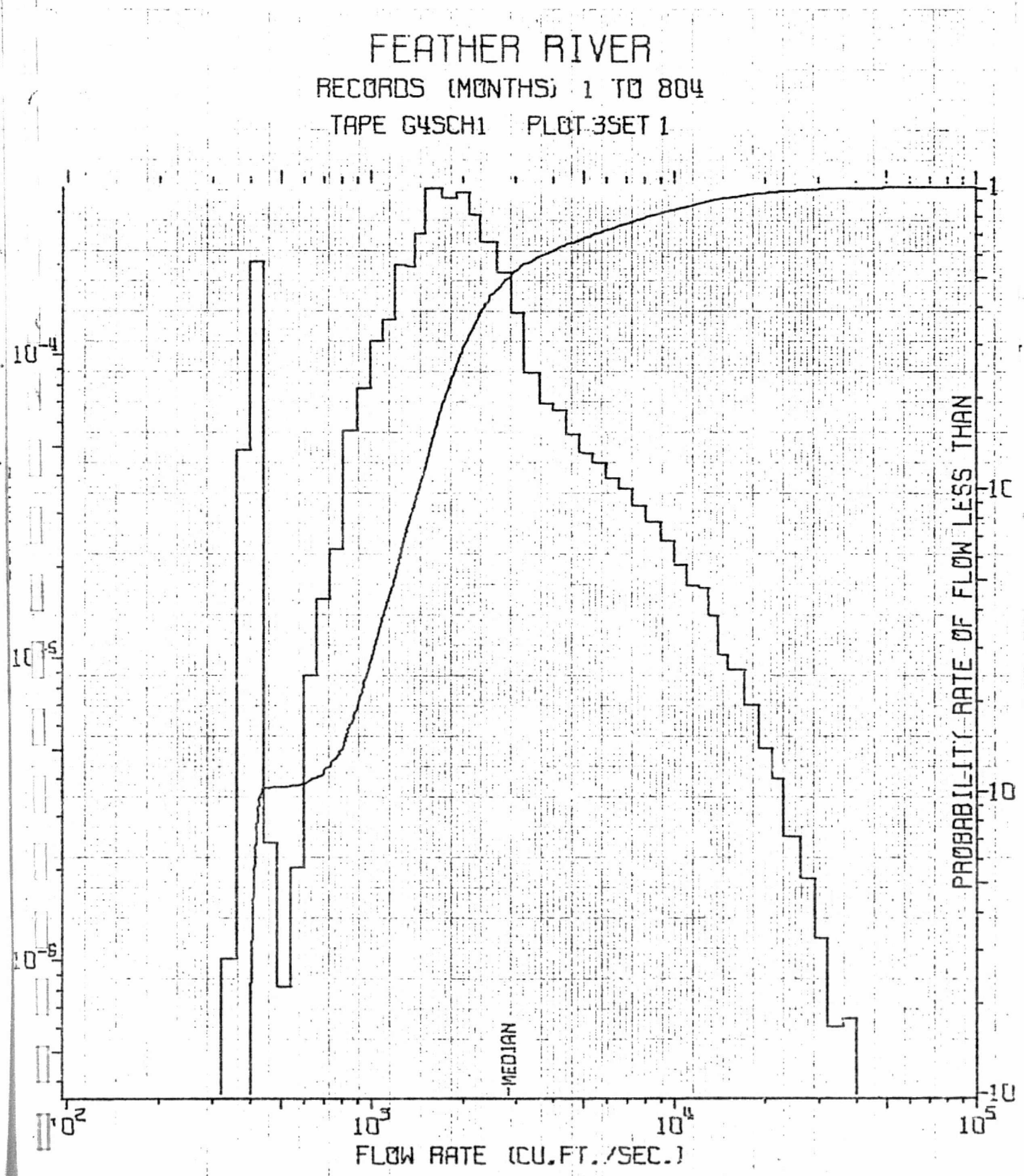
FEATHER RIVER
RECORDS (MONTHS) 1 TO 804
TAPE G4SCH1 PLOT 3SET 1
10⁻⁴
10⁻⁵
10⁻⁶
1
10
10
10
10²
10³
10⁴
10⁵
MEDIAN
PROBABILITY-RATE OF FLOW LESS THAN
FLOW RATE (CU.FT./SEC.)

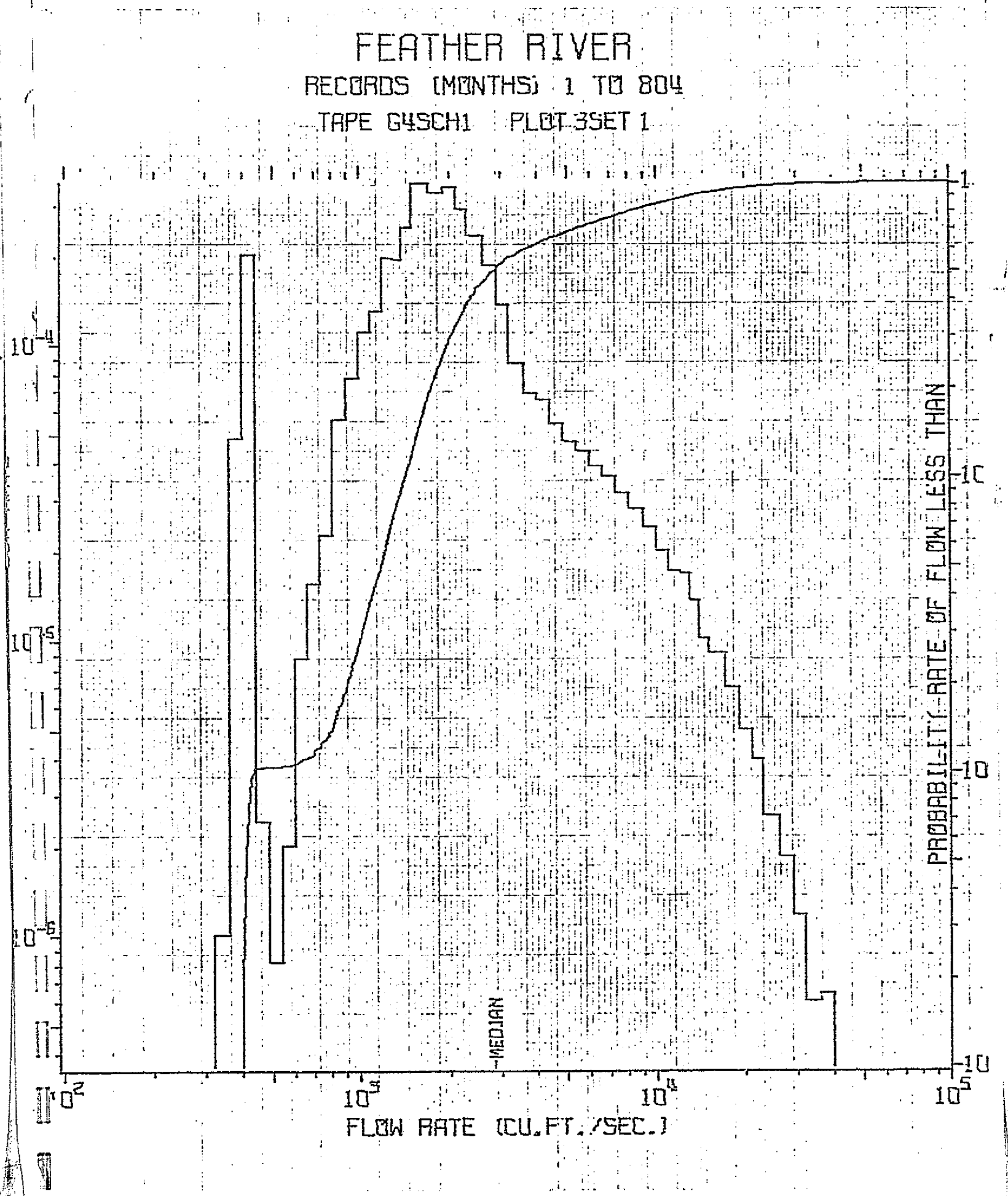
FEATHER RIVER
RECORDS (MONTHS) 1 TO 804
TAPE G4SCH1 PLOT 3SET 1
PROBABILITY-RATE OF FLOW LESS THAN
MEDIAN
FLOW RATE (CU.FT./SEC.)

HOMOCHITTO RIVER

STATION 7/2945 DOLOROSO, MISS. 1939-1951

TAPE 001621 RECORDS 4074-4193 PLOT50 SET 1

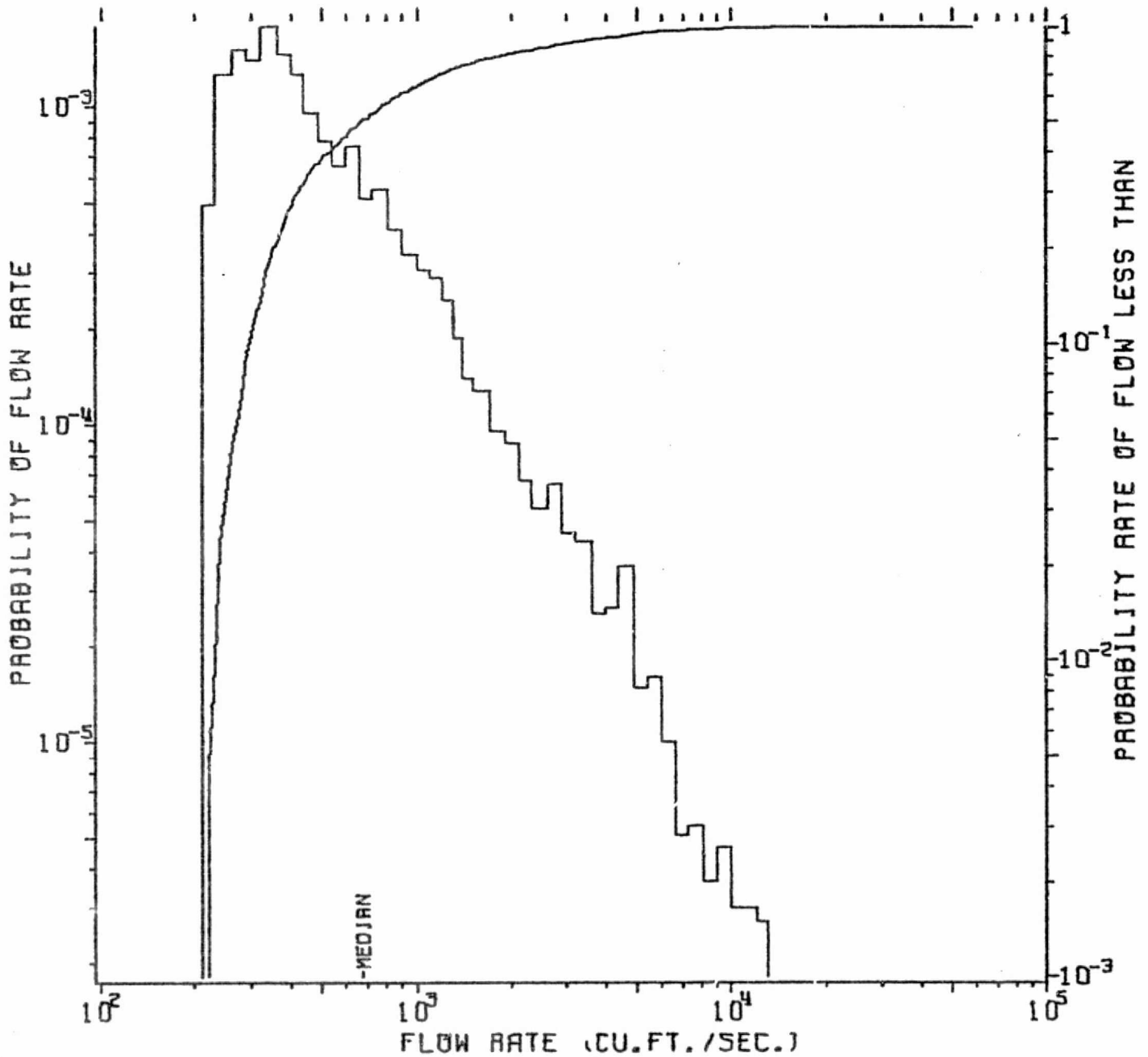

HOMOCHITTO RIVER

STATION 7/2945 DOLOROSO, MISS. 1939-1951

TAPE 001621 RECORDS 4074-4193 PLOT50 SET 1

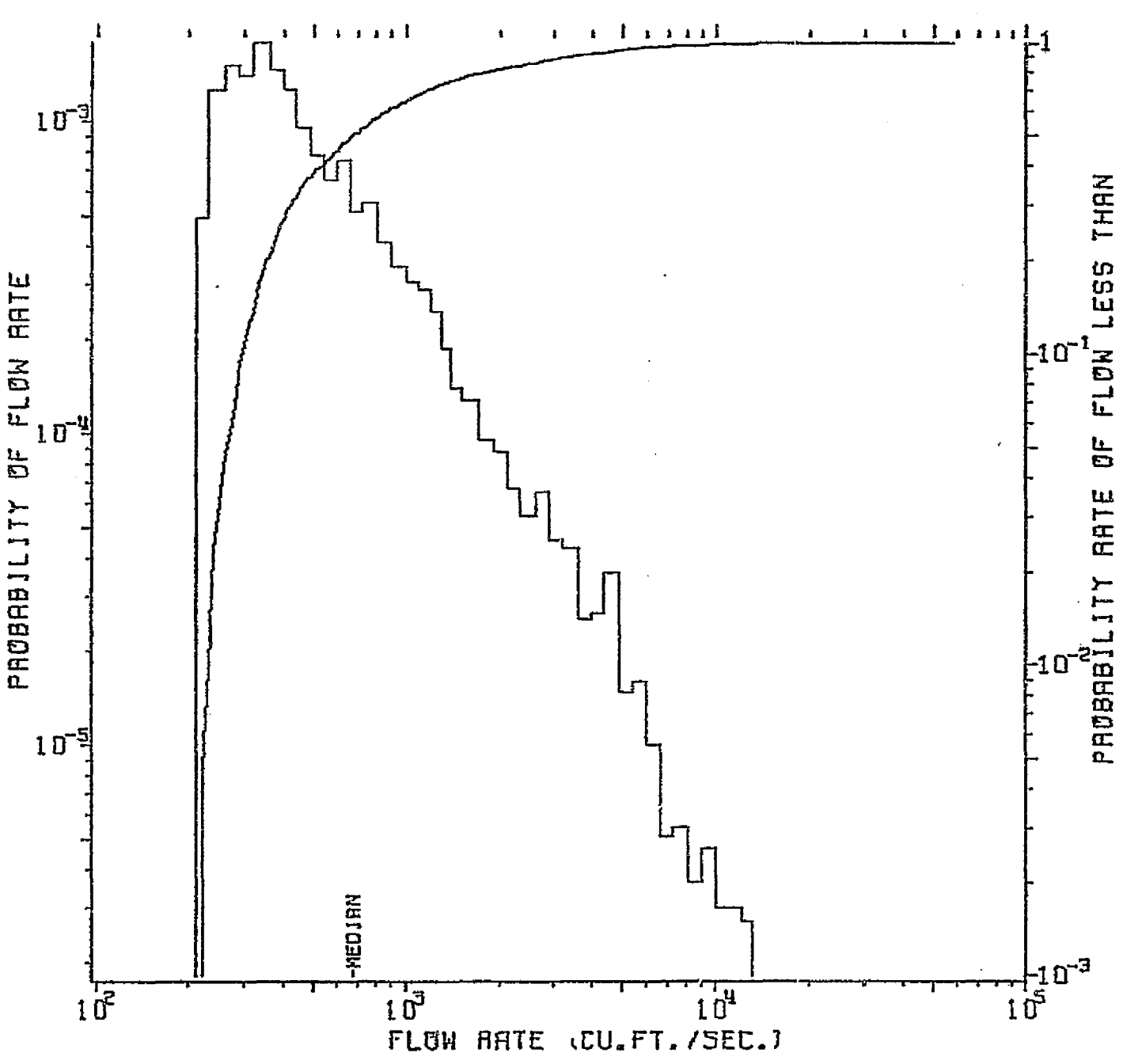

HOMOCHITTO RIVER

STATION 7/2910 EDDICETON, MISS. 1938/10-1969/9

TAPE 001621 RECORDS 3498-3869 PLOT48SET1

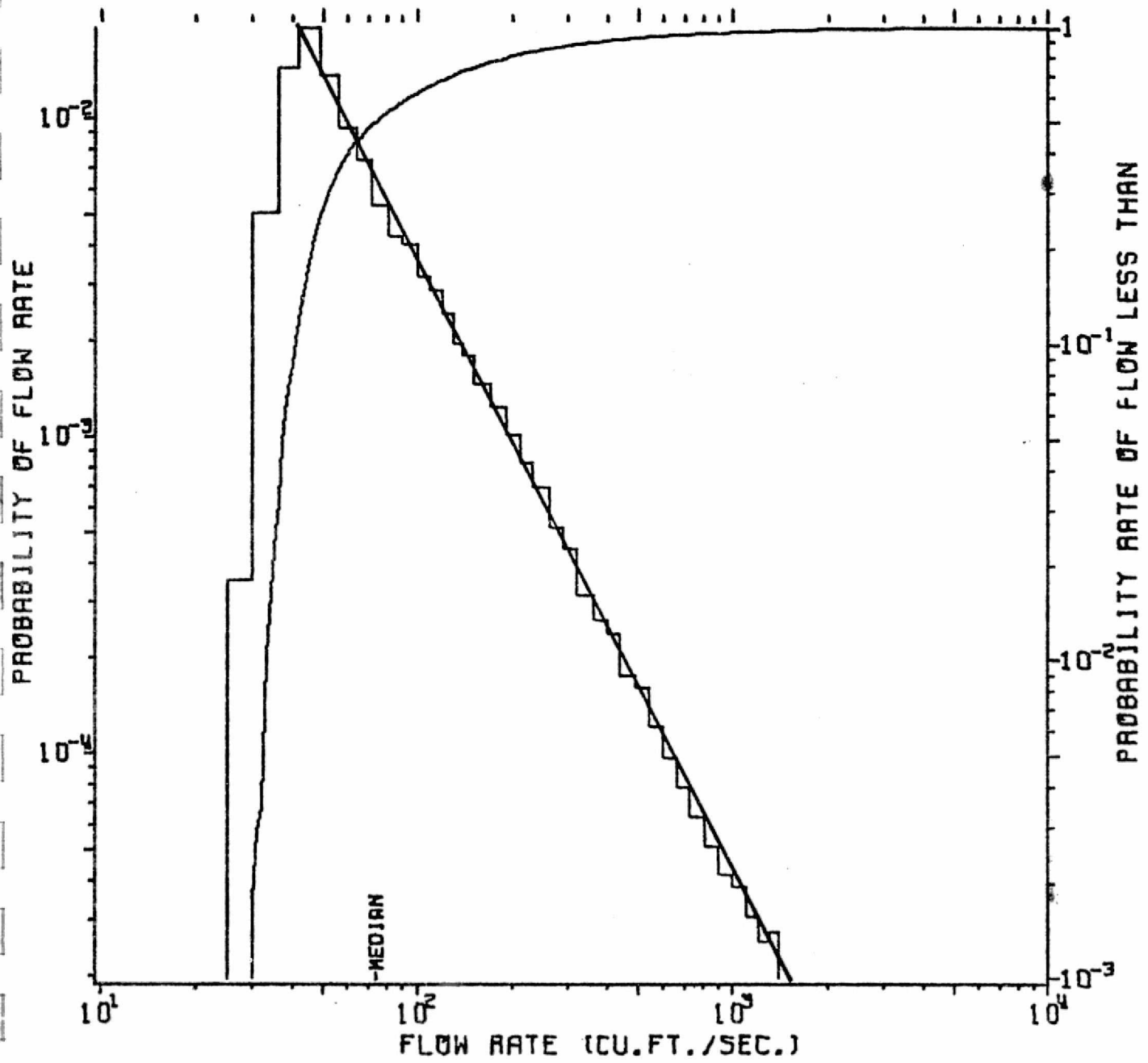

HOMOCHITTO RIVER

STATION 7/2910 EDDICETON, MISS. 1938/10-1969/9

TAPE 001621 RECORDS 3498-3869 PLOT48SET1

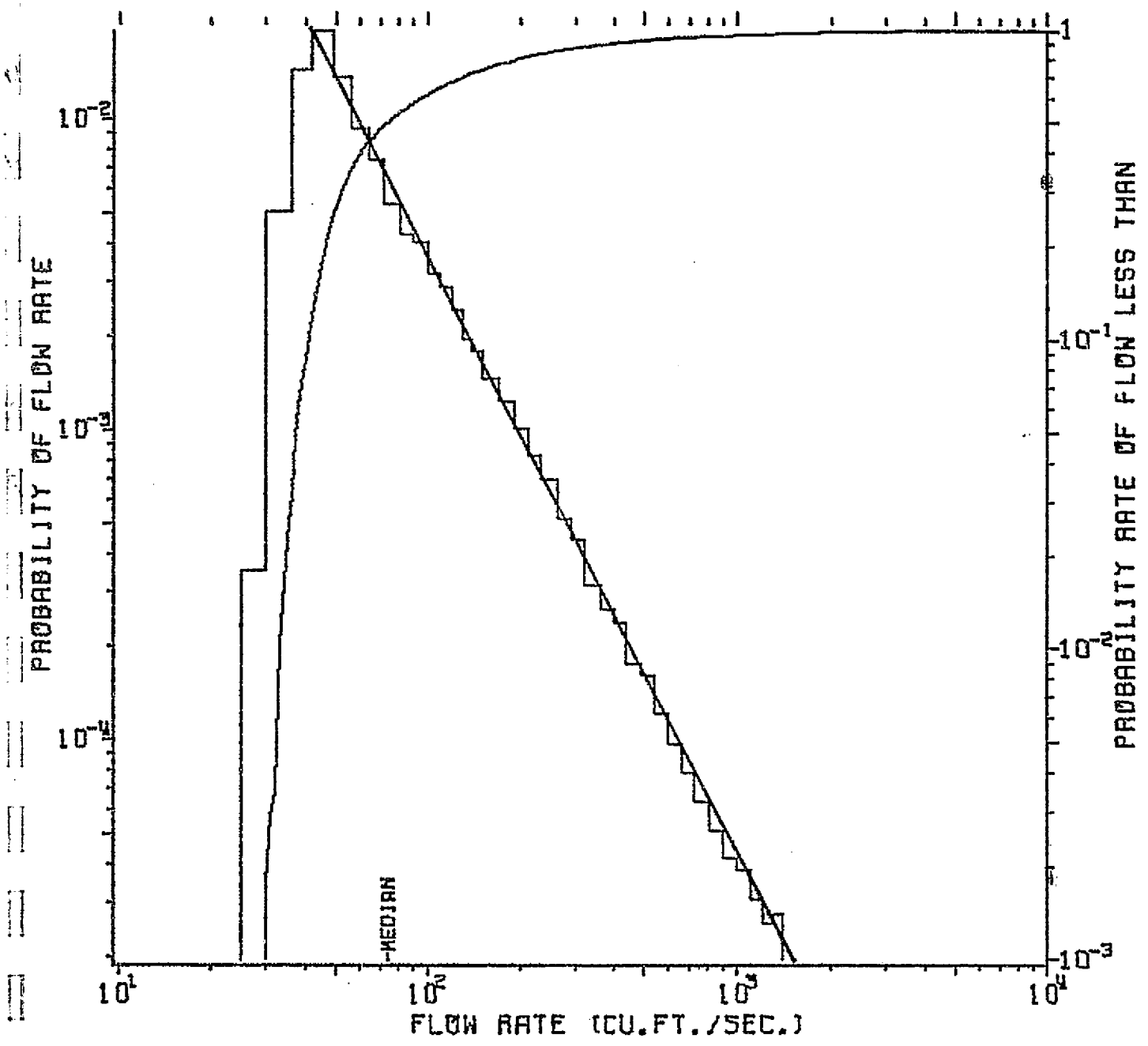

HOMOCHITTO RIVER

STATION 7/2925 ROSETTA, MISS. 1951-1969

TAPE 001621 RECORDS 3870-4073 PLOT 49 SET 1

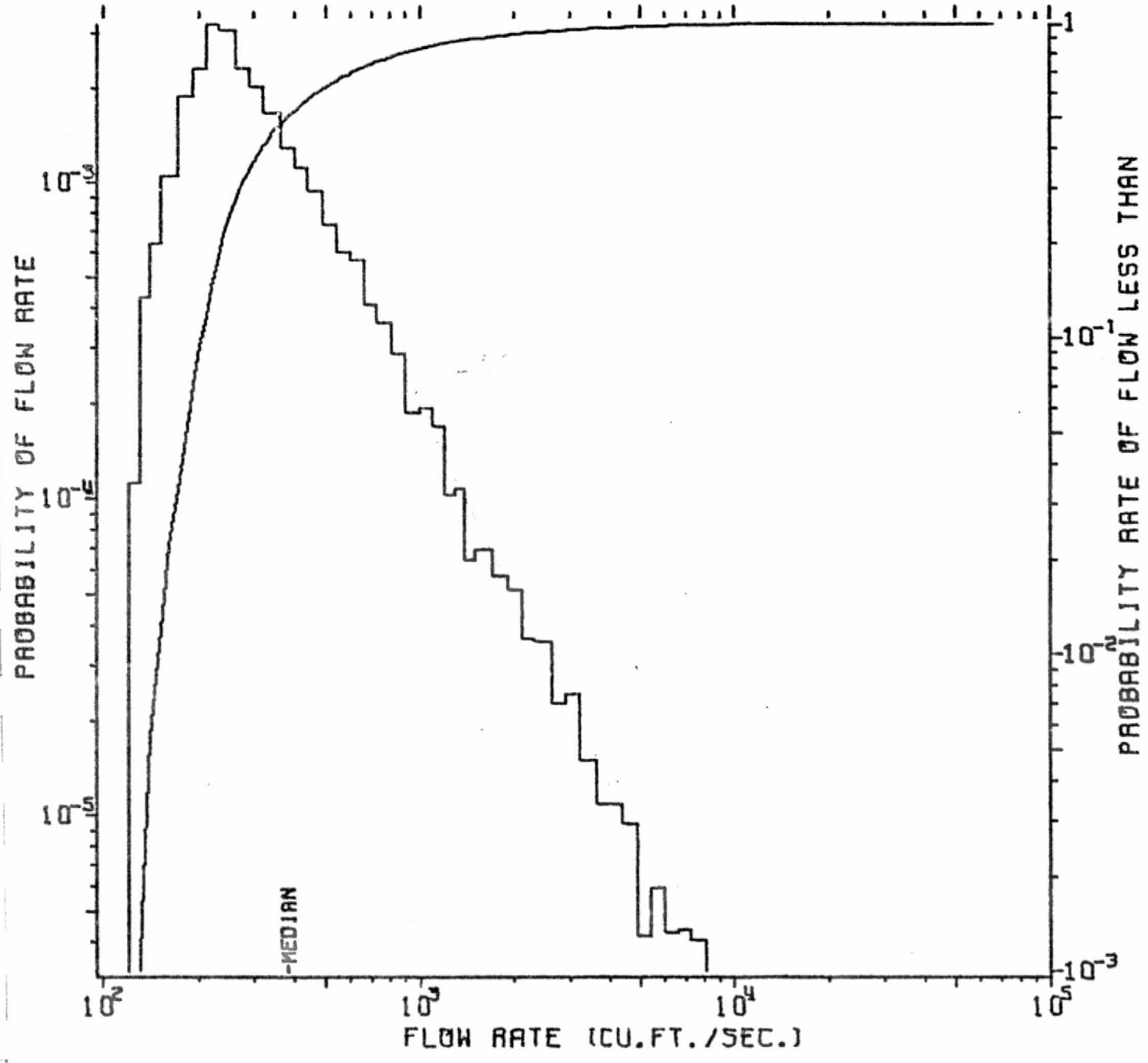

HOMOCHITTO RIVER

STATION 7/2925 ROSETTA, MISS. 1951-1969

TAPE 001621 RECORDS 3870-4073 PLOT 49 SET 1

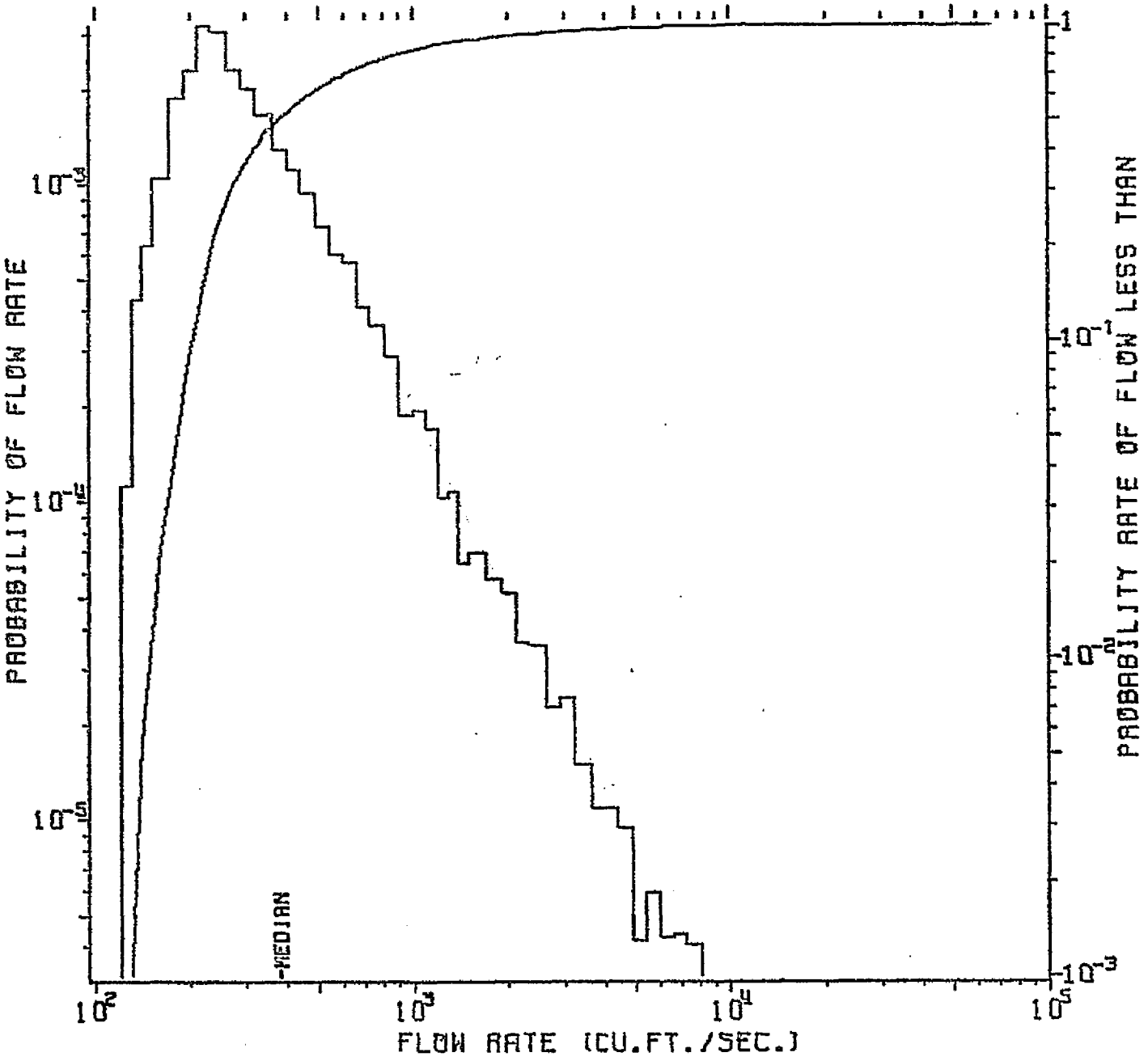

RIVER MNQD

7280ATA PTS / 75 SPEC ESTS

7.8×10^4 FT REACH

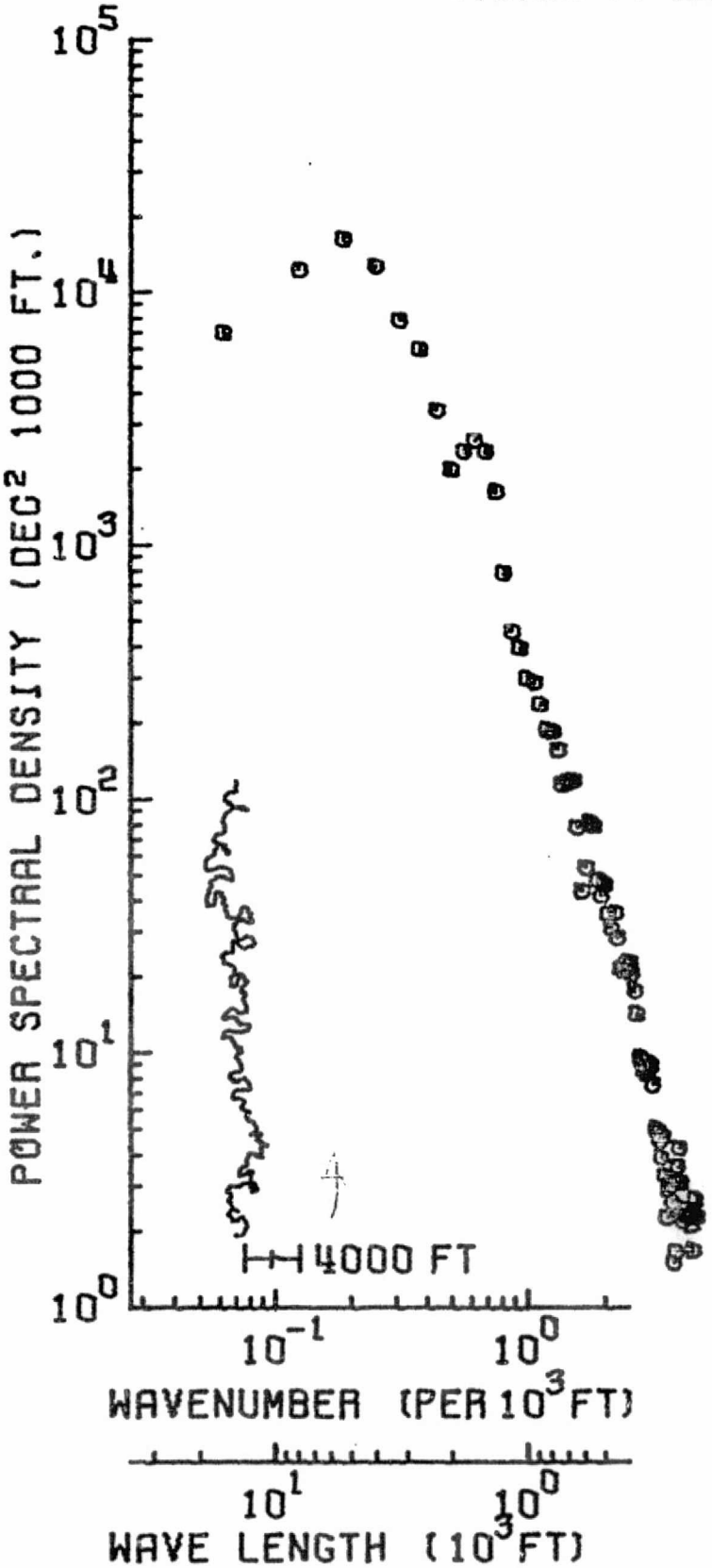

3200 / 6109

PLT TAPE PSPLT1 FY BLK. 31 IN DISK KAU03X PI5096.MAJ.MNQD.L
74 283 OCT 10 00:27:10.9

RIVER MNQD

728DATA PTS / 75 SPEC ESTS

$7.8X10^{4}$ FT REACH

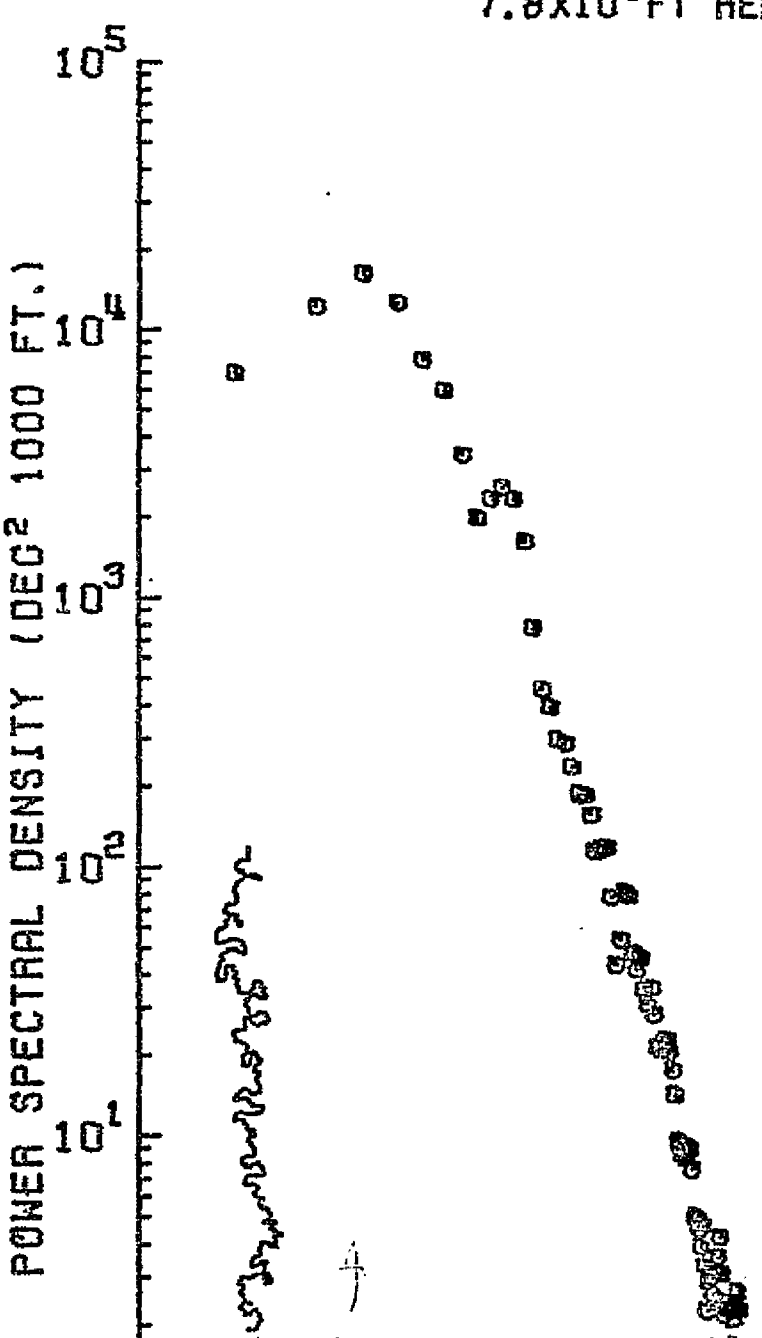

5200 / 6109

PLT TAPE PSPLT1 FW BLK. 31 IN DISK KAUDSK P15096.MAJ.MNQD.L
74 283 OCT 10 00:27:10.9

RIVER MNQD

1527 DATA PTS / 125 SPEC ESTS

1.6 X 10^5 FT REACH

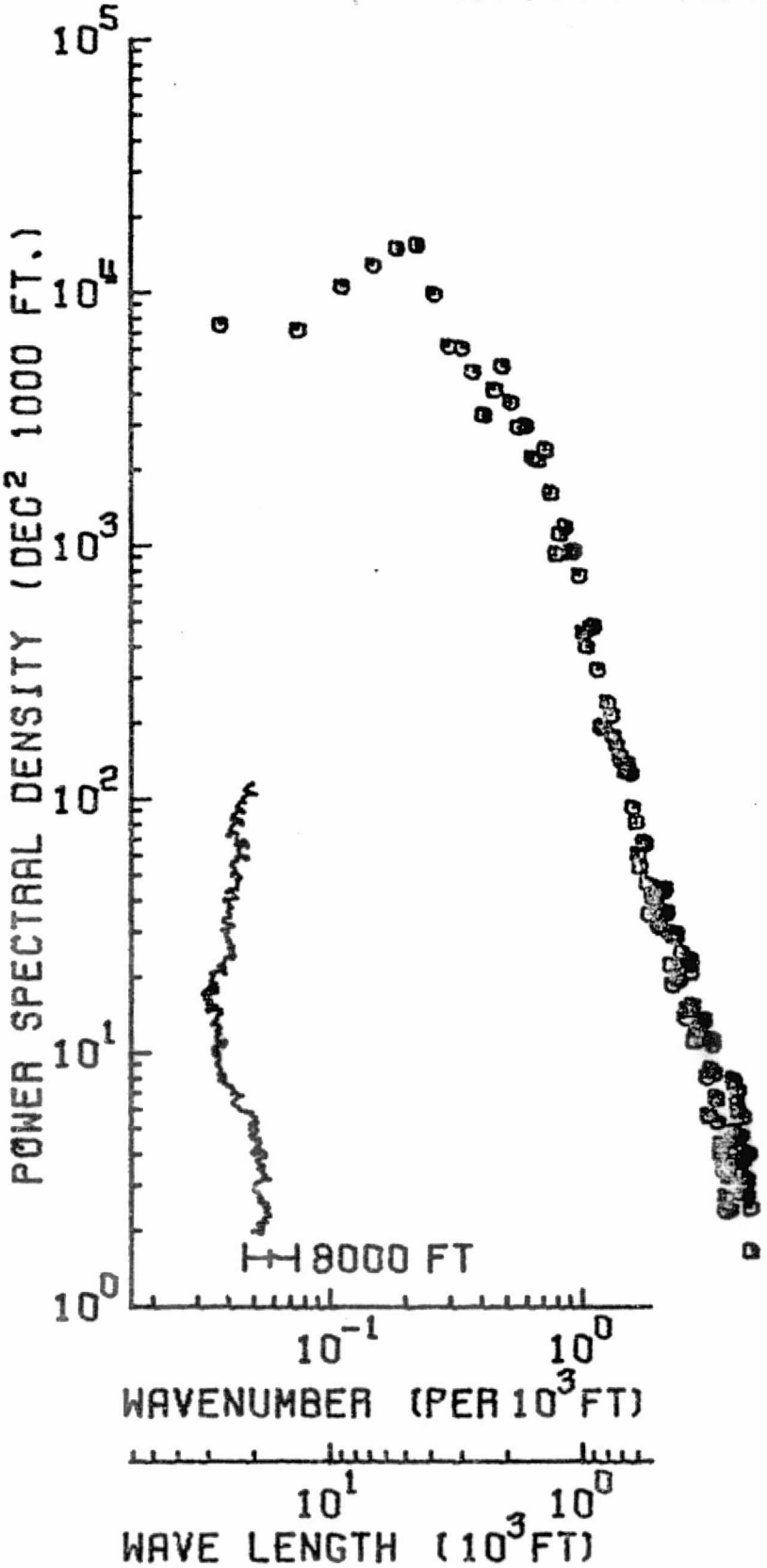

1 / 6109

PLT TAPE PSPLT: F4 BLK. 32 IN DISK KAUDSK PIS096.NAJ.MNQD.L
74 293 OCT 10 00:27:18.9

RIVER MNQD

1527 DATA PTS / 125 SPEC ESTS

1.6×10^5 FT REACH

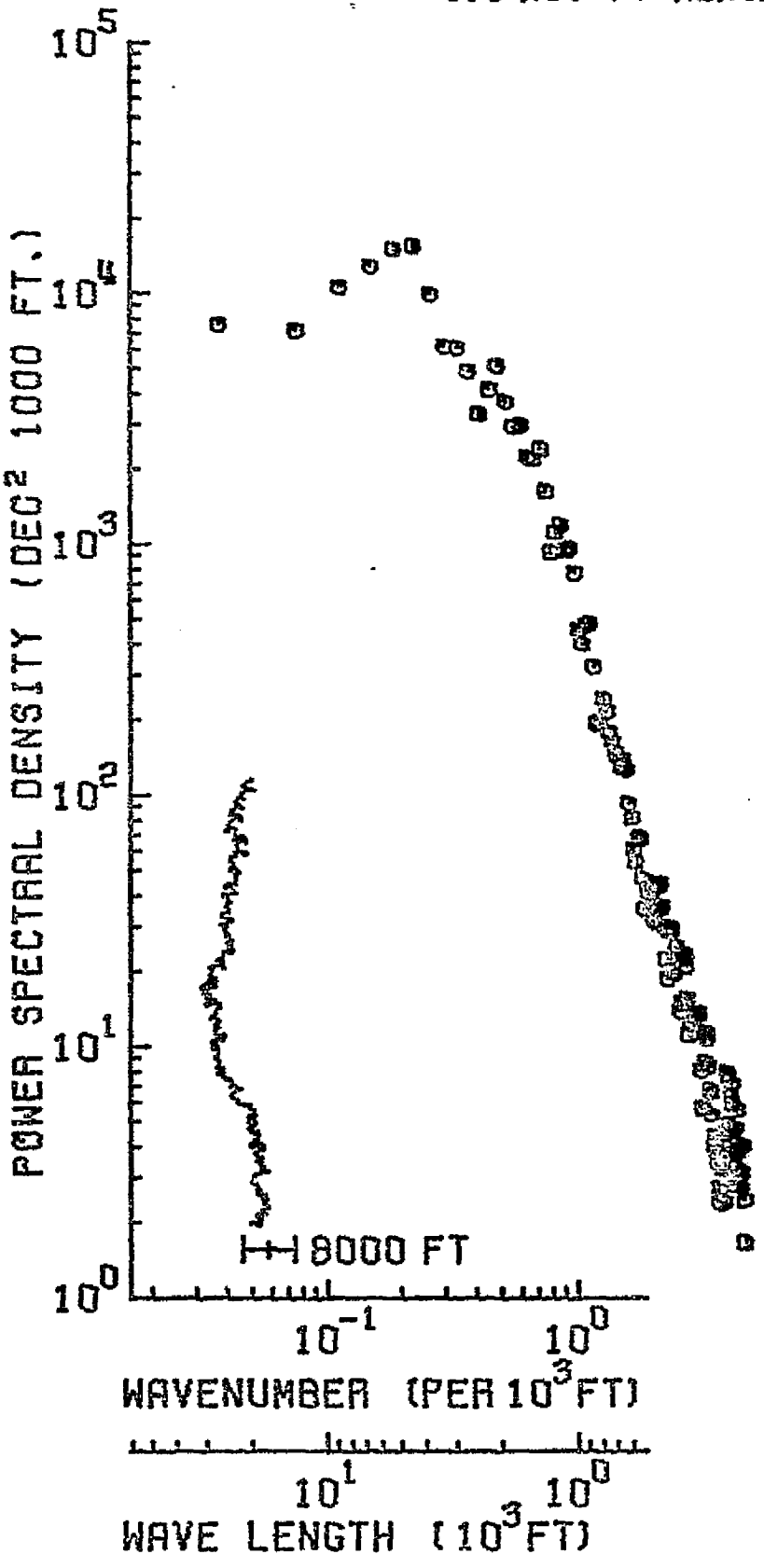

1 / 6109

PLT TAPE PSPLT1 FU BLK 32 IN DISK KAUDSK PIS096.MAJ.MNQD.L
74 295 OCT 10 00:27:10.9

MANISTIQUE RIVER

STATION 4/0565 MANISTIQUE, MICH. 1938-1969

TP 4552, FIL 2, RECDS 3294-3662 PLOT 17 SET 1

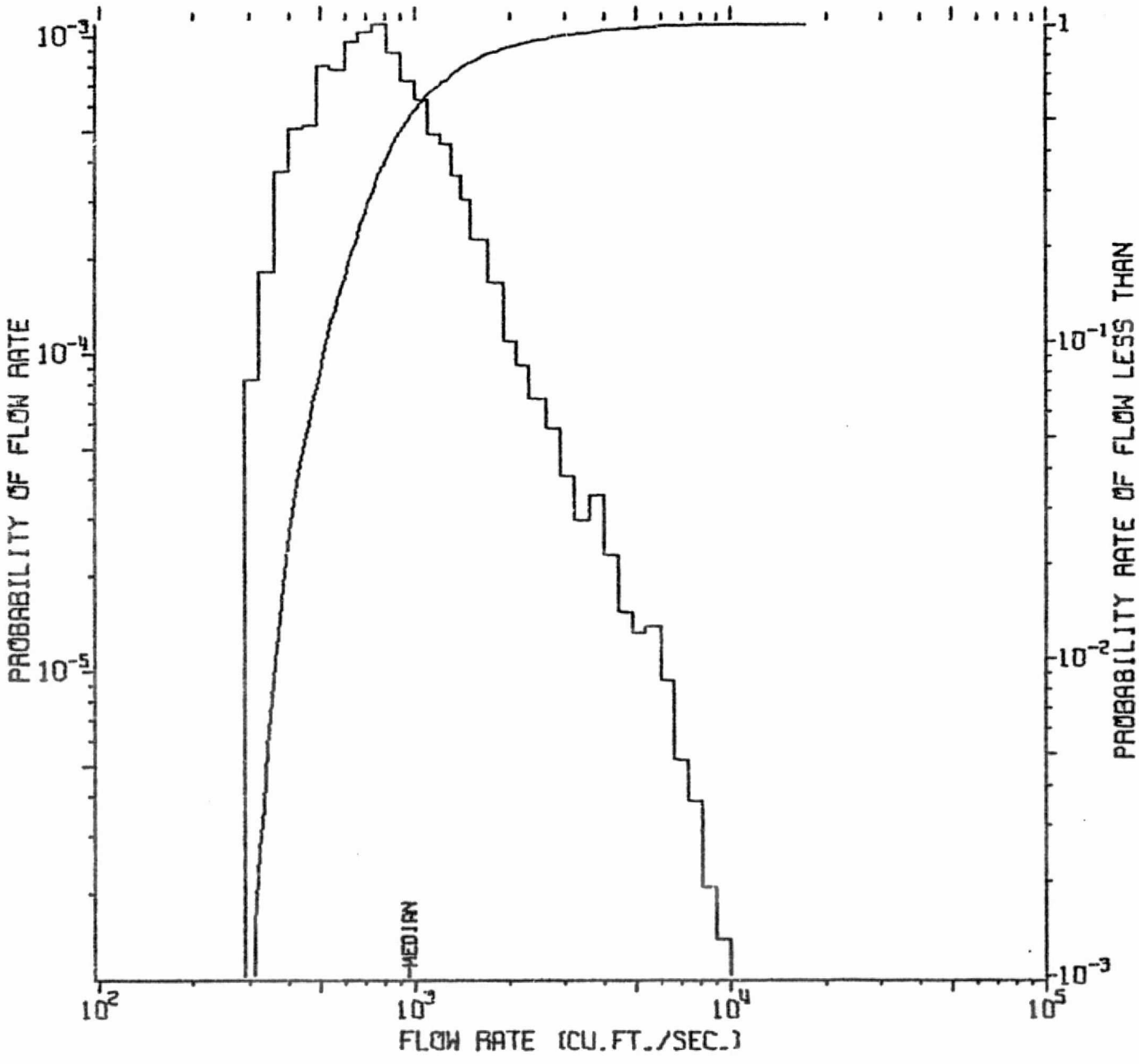

MANISTIQUE RIVER

STATION 4/0550 BLANEY, MICH. 1938-1969

TP 4552, FIL 2, RECDS 2706-3071 PLOT 15 SET 1

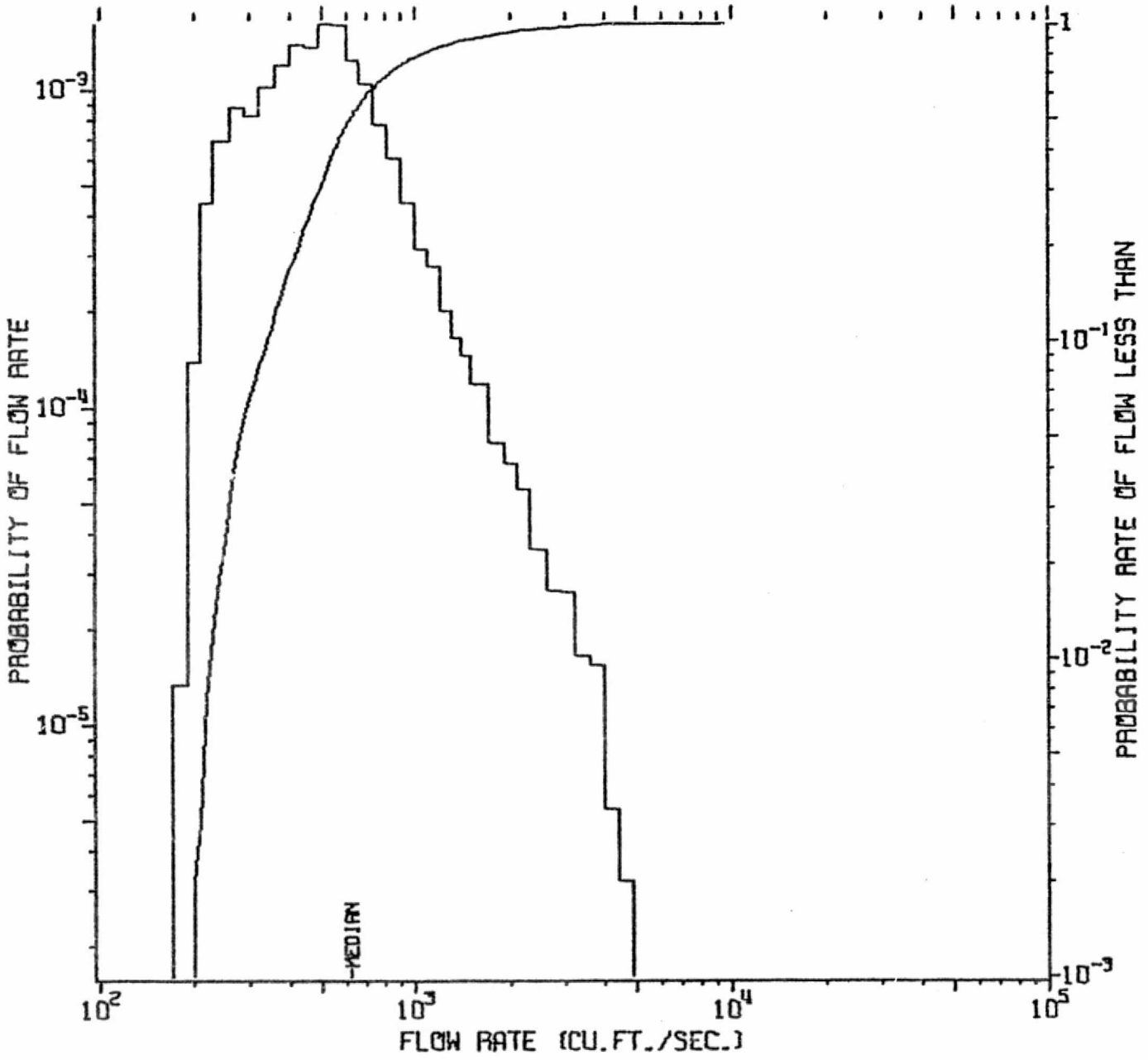

MANISTIQUE RIVER

STATION 4/0495 GERMFASK, MICH. 1938-1969

TP 4552, FIL 2, RECDS 2340-2705 PLOT 14 SET 1

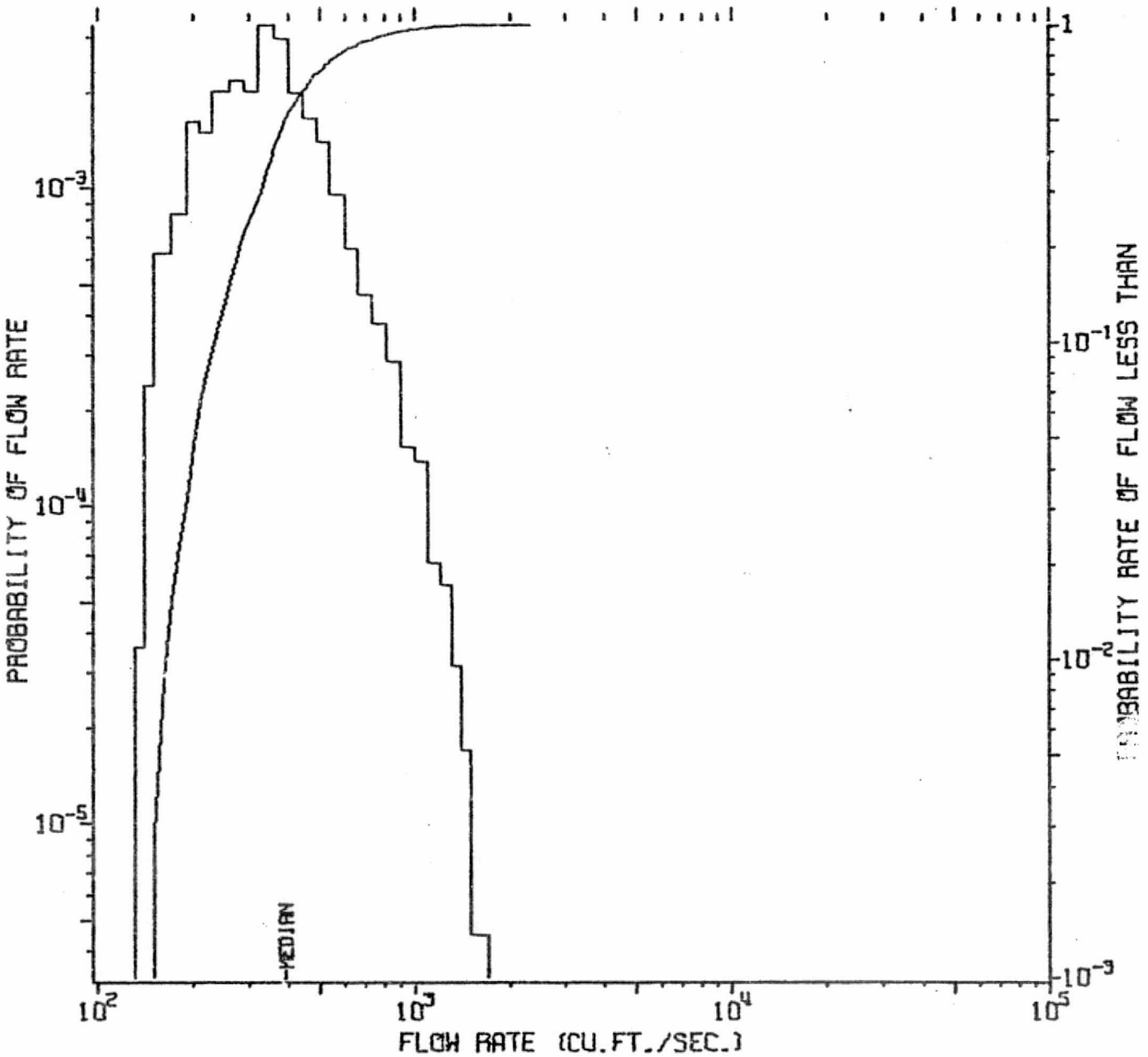

RIVER MUSK

934 DATA PTS / 90 SPEC ESTS

1.2×10^5 FT REACH

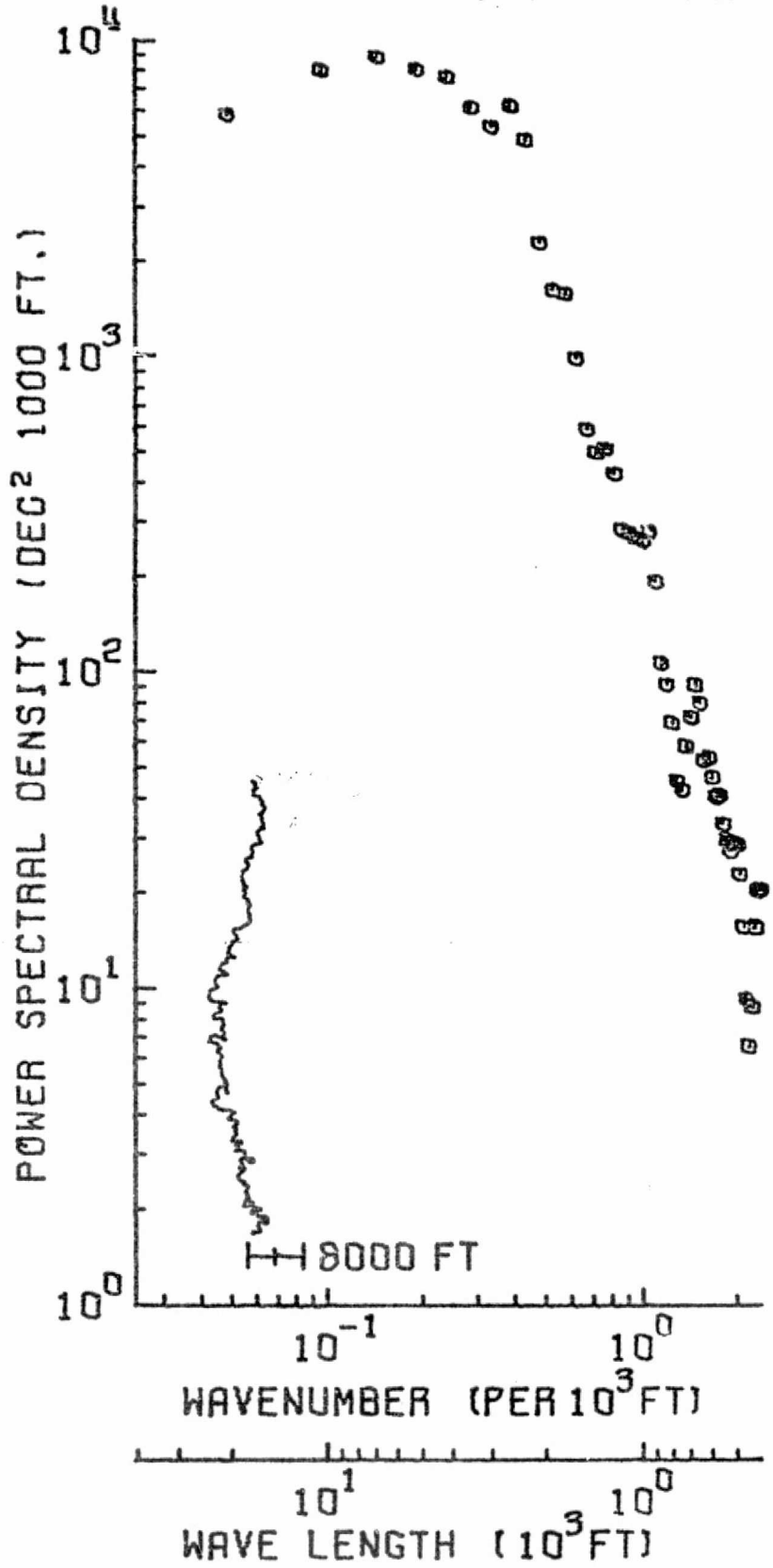

1 / 3579

PLT TAPE PSPLT1 F6 BLK. 57 IN DISK KAUD3K PI3D36.MAJ.MUSK8
74 295 OCT 22 03:49:10.1 IN DISK KAUD3K PI3D36.MAJ.MUSK8.ANG2

MUSKEGON RIVER

STATION 4/1215 EVART, MICH. 1933/10-1970/9

TP 4552, FIL 2, RECDS 3663-4106 PLOT 18 SET 1

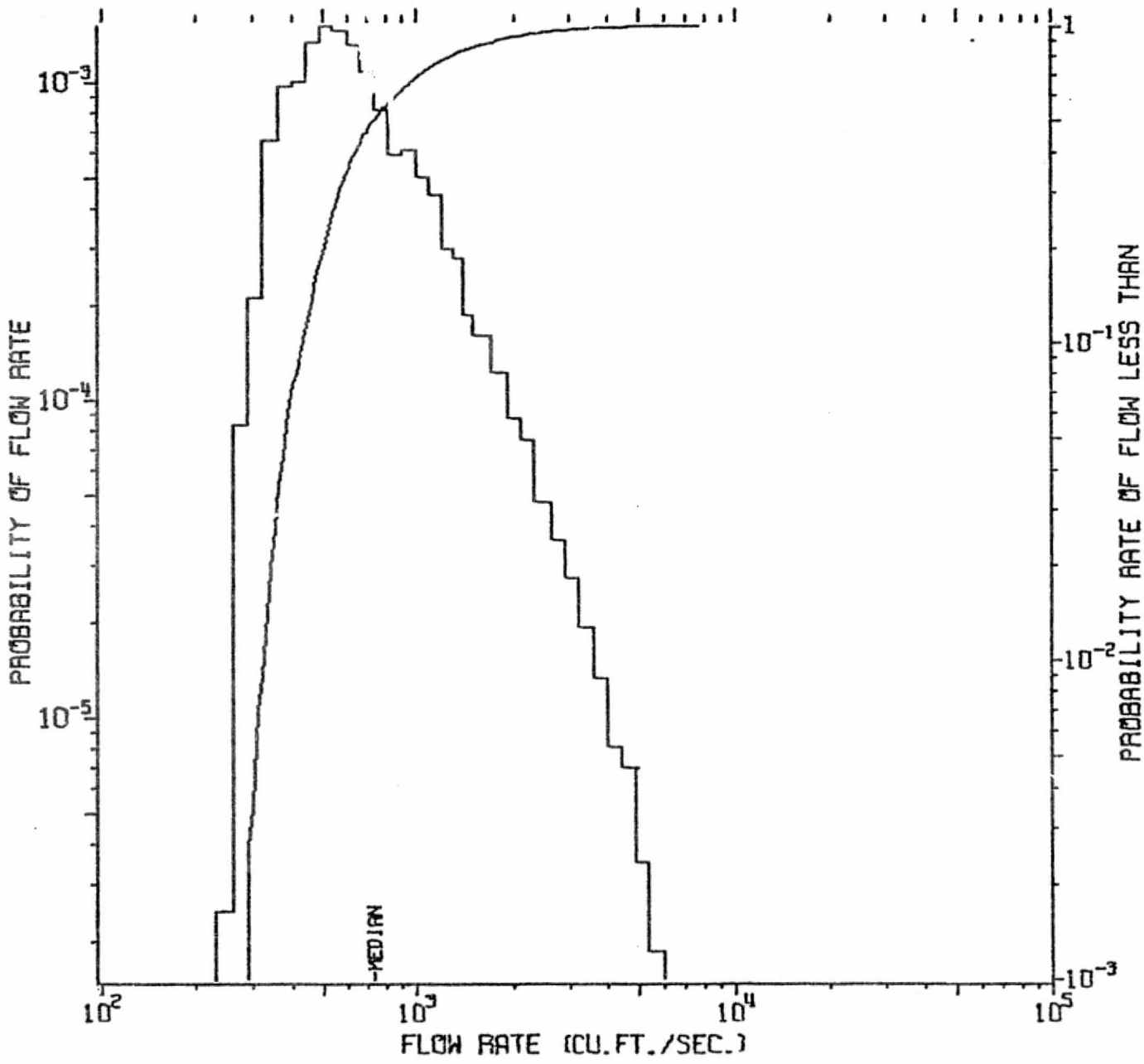

FLAM RIVER

1136 DATA PTS / 90 SPEC ESTS

1.3×10^5 FT REACH

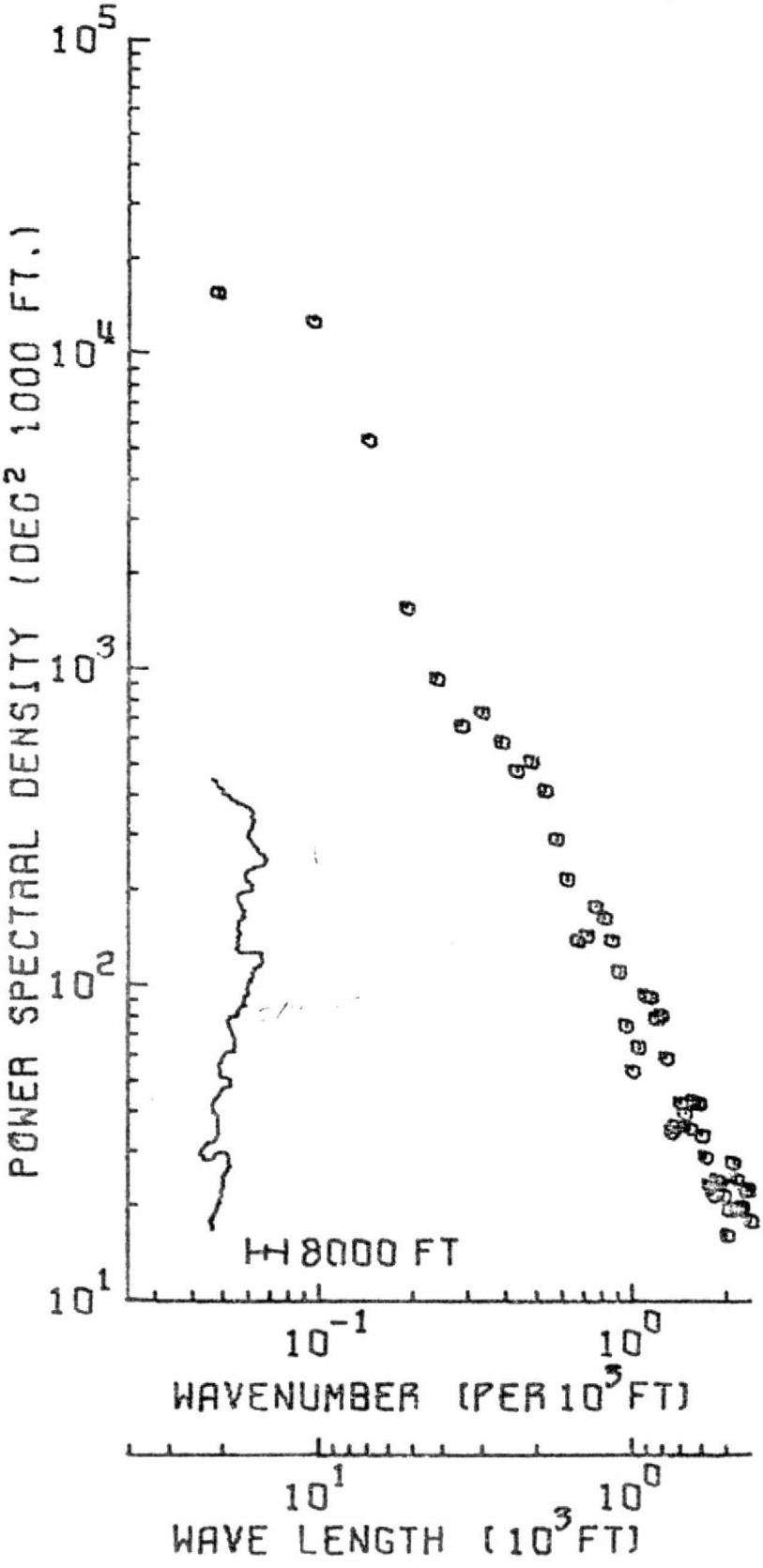

1 / 4547

PLT TAPE P3PLT1 F6 BLK. 53 IN DISK KAU03K PIS096.MAJ.FLAM
74 295 OCT 22 03:49:10.1 IN DISK KAU03K PIS096.MAJ.FLAM.ANG2

FLAMBEAU RIVER AT BABBS ISLAND

STATION 5/3585 WINTER, WIS. 1960/10-1969/9

TP 4552, FIL 2, RECDS 7269-7376 PLOT 31 SET 1

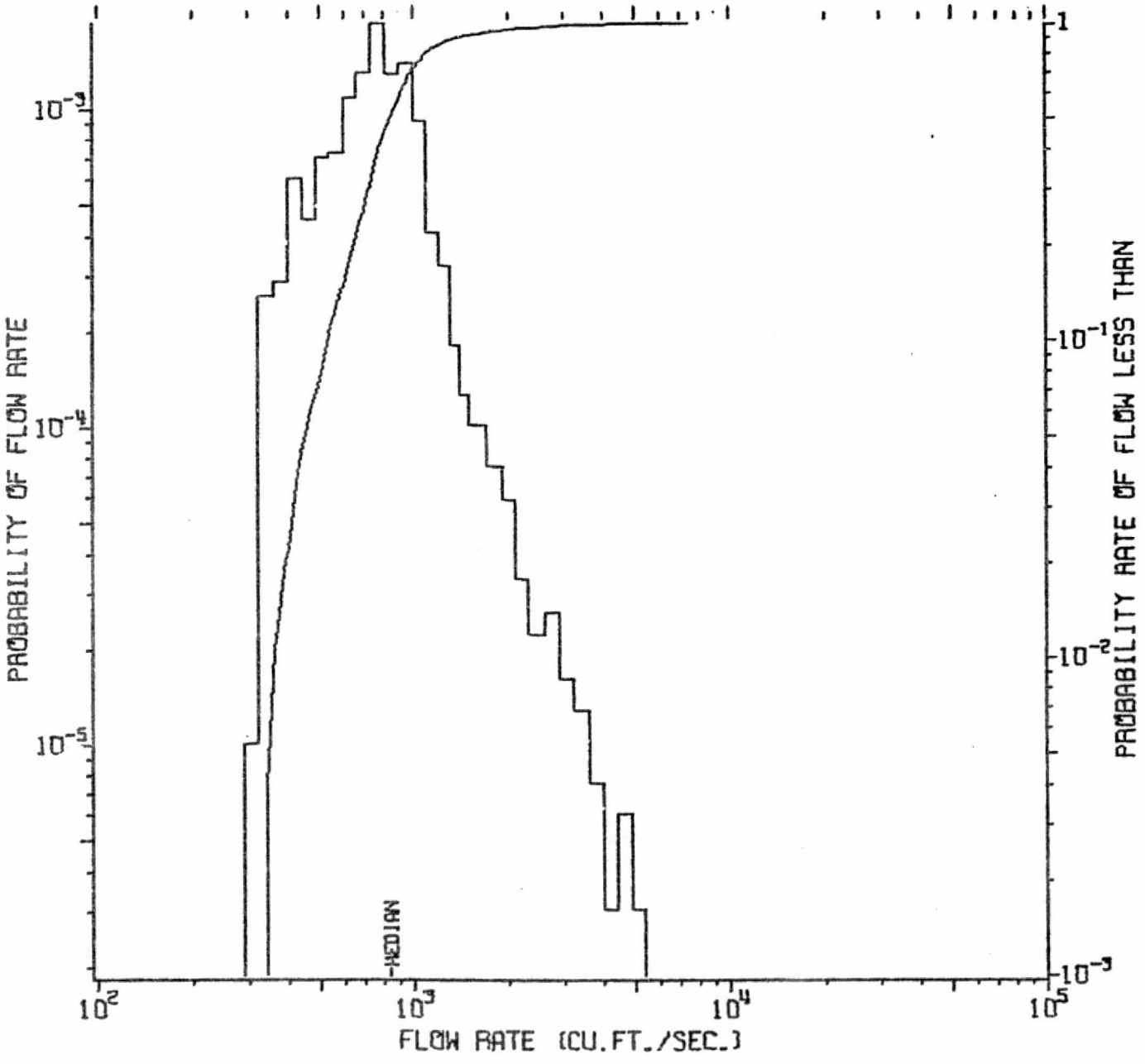

ONTONAGON RIVER, MICH

1299 DATA PTS / 190 SPEC ESTS

7.5×10^4 FT REACH

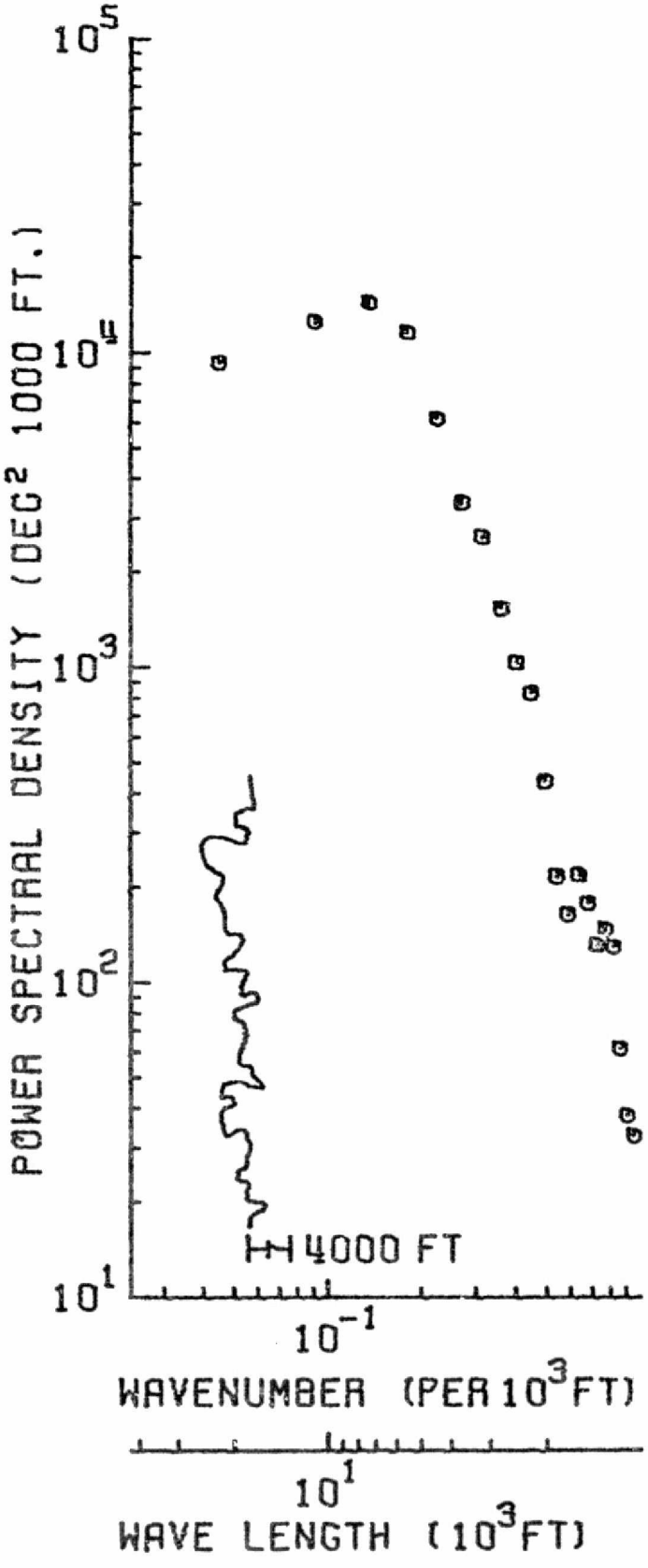

1 / 2600

PLT TAPE ISTPLT F1 BLK 5 IN DISK KRUDSK PIS095.RAJ.ONTR
74 270 SEP 27 11:22:58.4 IN DISK KRUDSK PIS095.RAJ.ONTR.ANG2

ONTONAGON RIVER

STATION 4/0400 ROCKLAND, MICH. 1942/10-1969/9

TAPE 001621 RECORDS 2149-2472 PLOT44 SET1

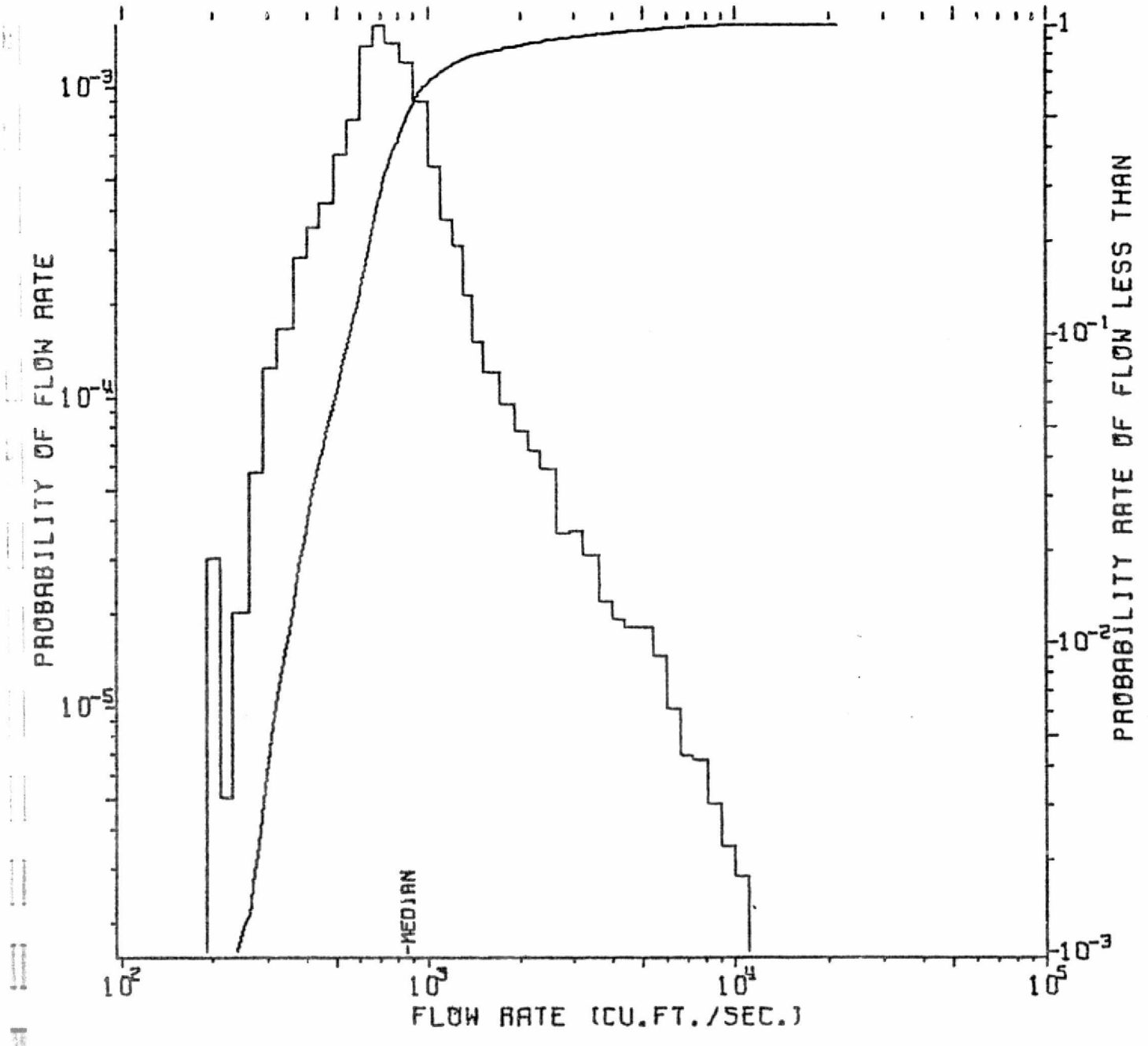

CHIP RIVER (1)

749 DATA PTS / 75 SPEC ESTS

8.7×10^4 FT REACH

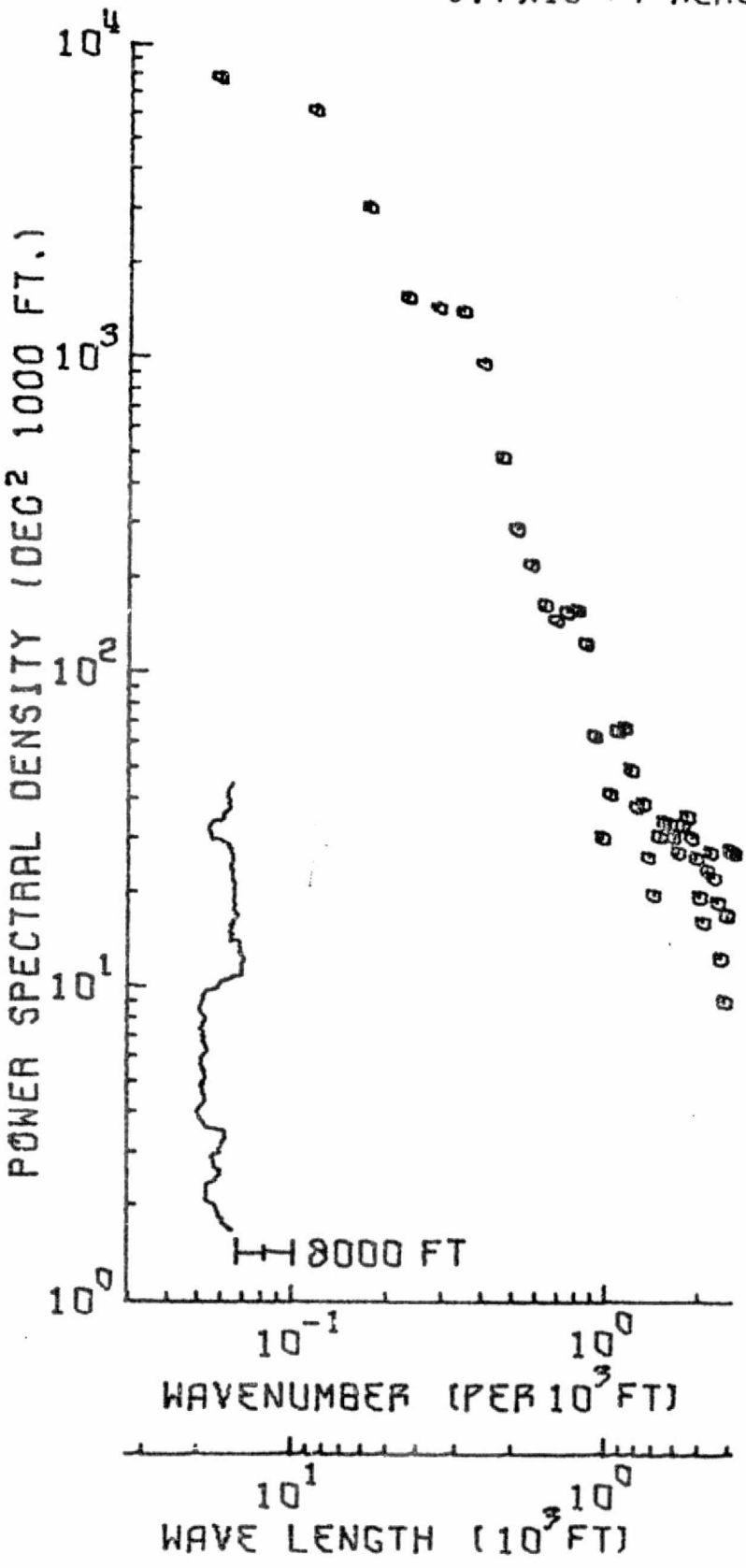

1 / 3000

PLT TAPE P3PLT1 F6 BLK. 49 IN DISK KAUO3K PI5096.MAJ.CHPM
74 295 OCT 22 09:49:10.1 IN DISK KAUO3K PI5096.MAJ.CHPM.ANGZ

CHIP RIVER (2)

749 DATA PTS / 75 SPEC ESTS

8.7×10^4 FT REACH

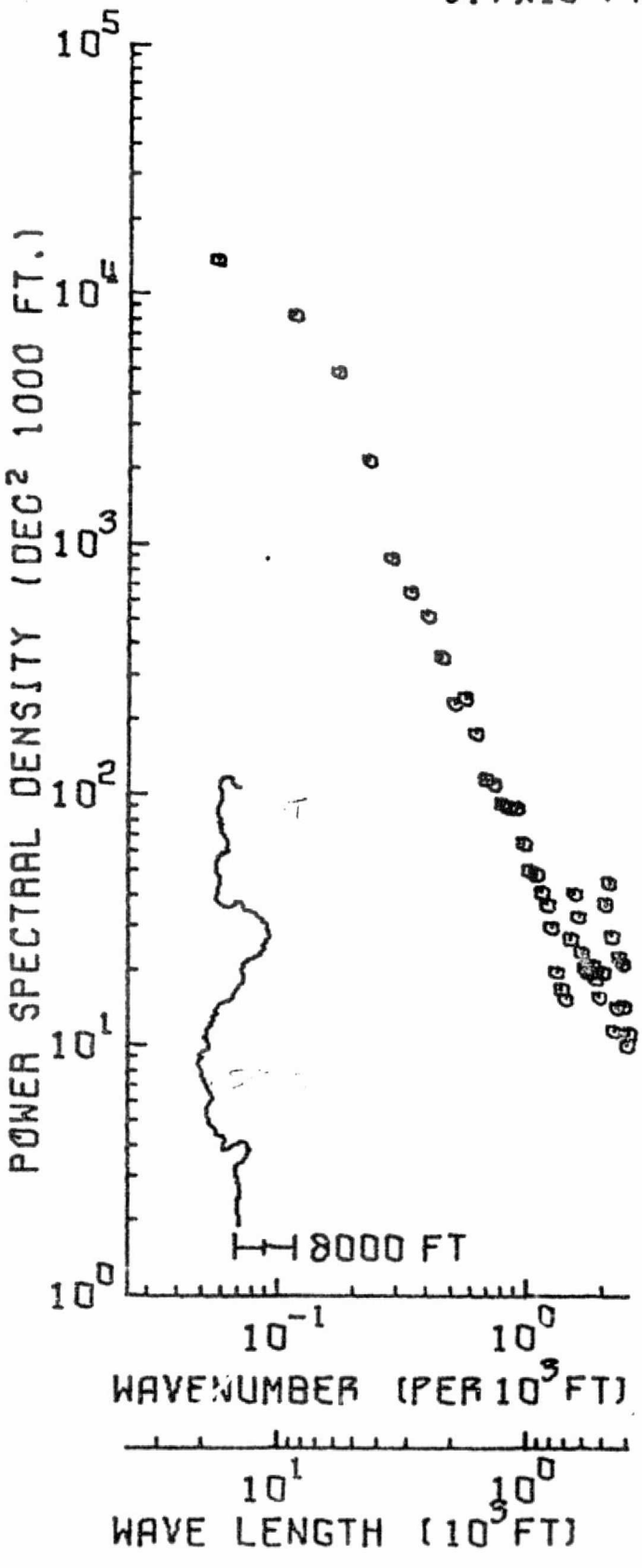

3000 / 6000

PLT TAPE P3PLT1 F6 BLK. 50 IN DISK KAUO3K PI3096.MAJ.CHPR
74 295 OCT 22 03:49:10.1 IN DISK KAUO3K PI3096.MAJ.CHPR.ANG2

CHIP RIVER

791 DATA PTS / 85 SPEC ESTS

1.8×10^5 FT REACH

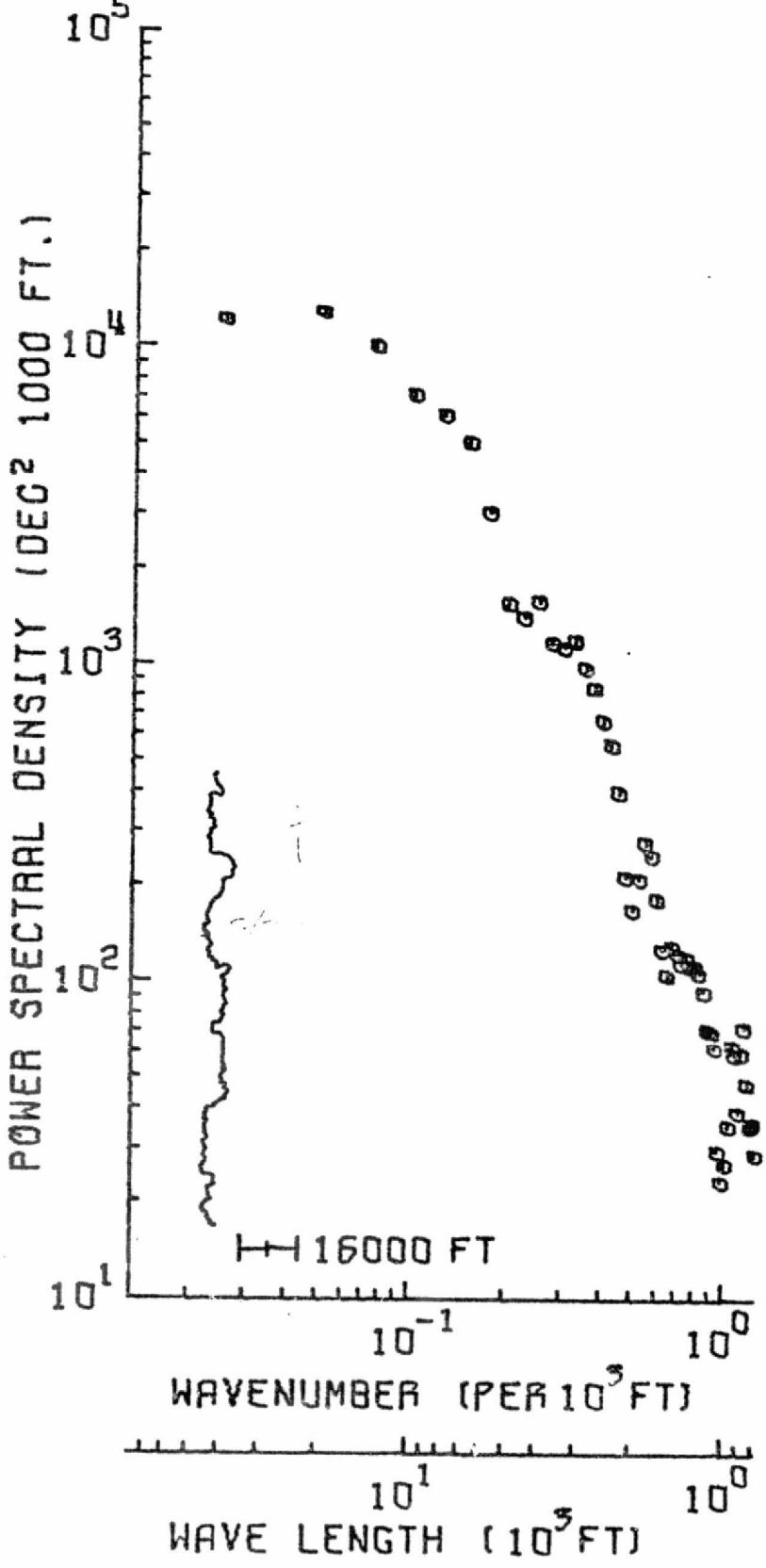

1 / 6331

RLT TAPE P3PLT1 PS BLK. 51 IN DISK KAU03K PI3096.MAJ.CHPA
74 295 OCT 22 03:49:10.1 IN DISK KAU03K PI3096.MAJ.CHPA.ANGZ

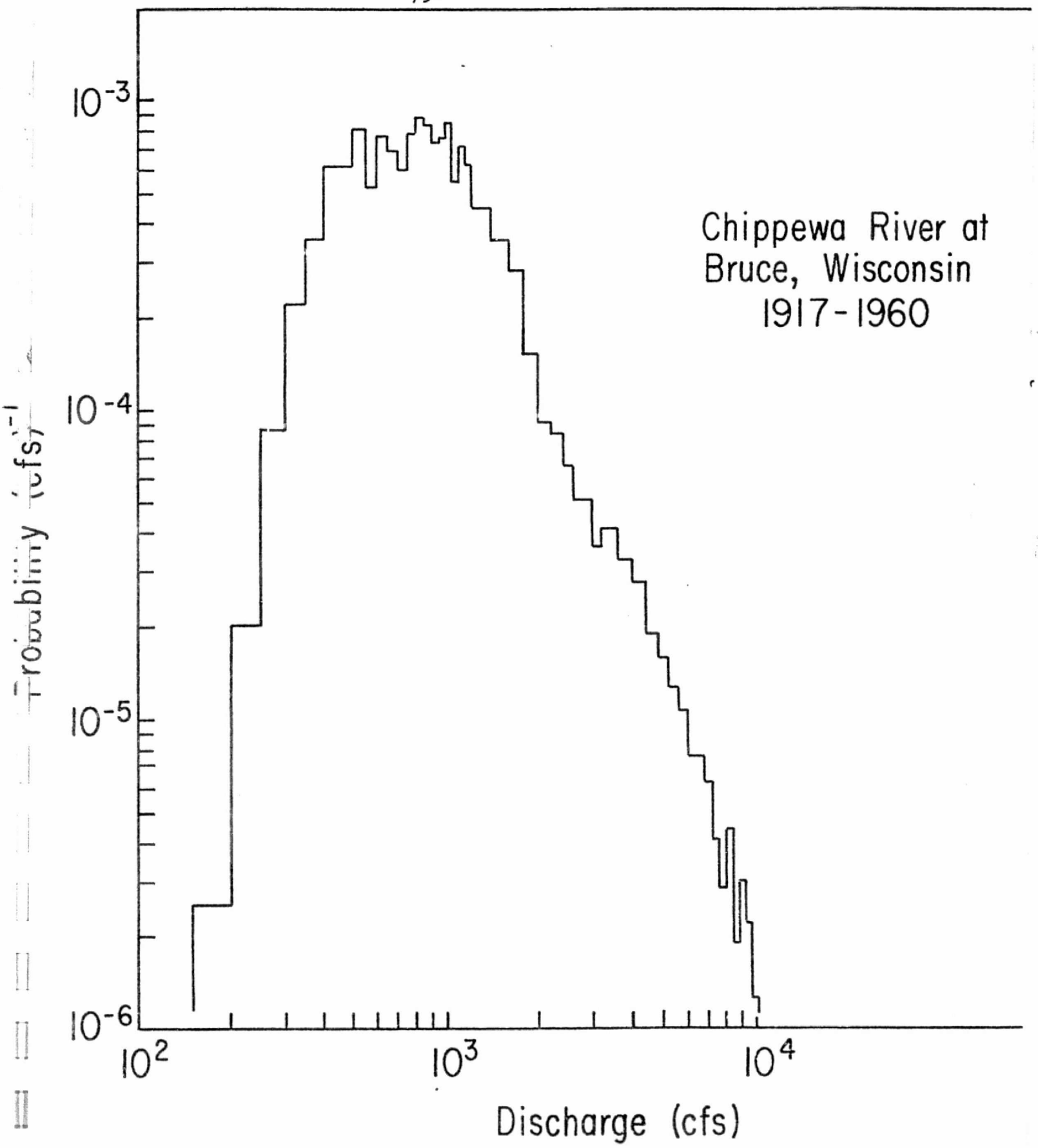
Chippewa River at
Bruce, Wisconsin
1917-1960
10^{-3}
10^{-4}
10^{-5}
10^{-6}
Probability (cfs)$^{-1}$
10^2
10^3
10^4
Discharge (cfs)

RIVER MNSM

1103DATA PTS / 80 SPEC ESTS

5.9×10^4 FT REACH

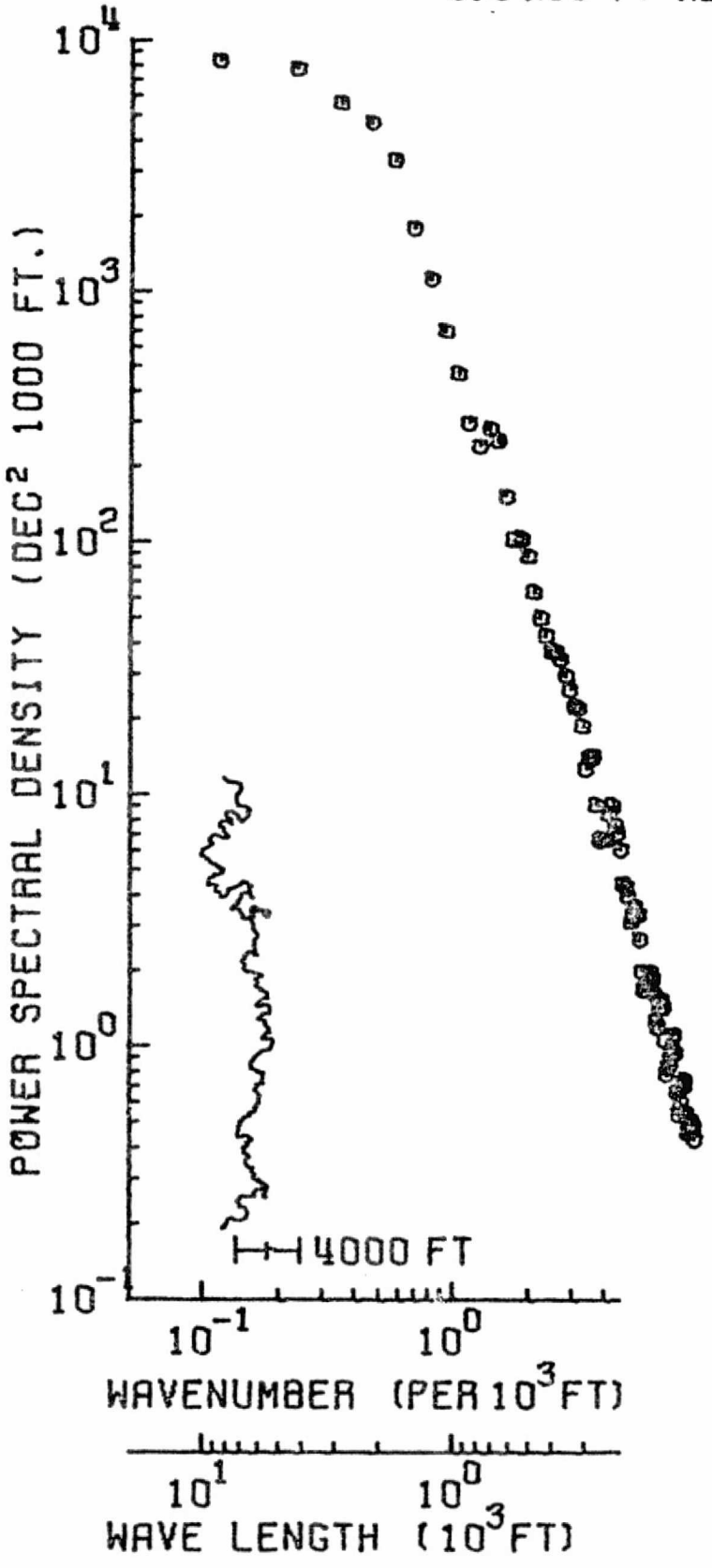

1 / 2209

PLT IBGE_PSPLT1 FZ BLK=9 IN DISK KAUDSK PIS096.MAJ.MNSM.L

RIVER MNSM

754 DATA PTS / 125 SPEC ESTS

4.0×10^4 FT REACH

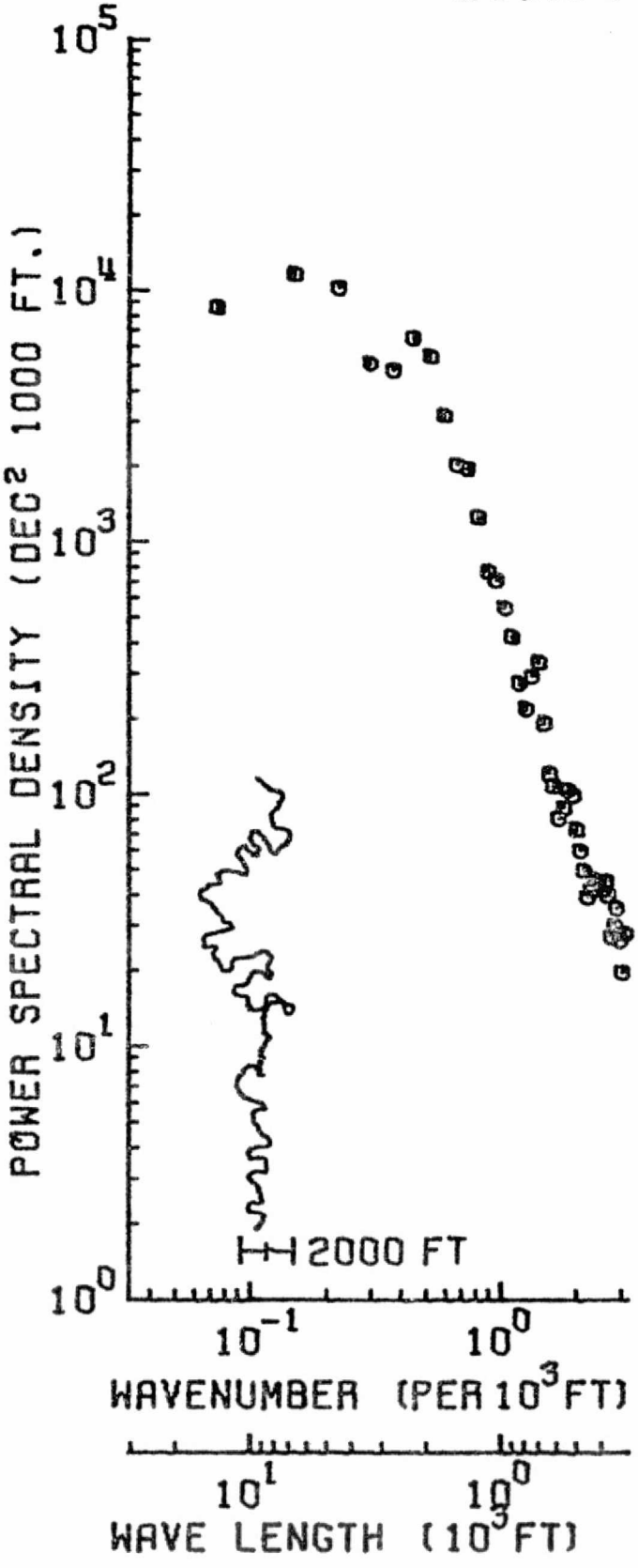

700 / 2209

PLT TAPE ISTPLT F2 BLK 15 IN DISK KAUDSK PIS096.MAJ.MNSM.L
74 274 OCT 1 02:24:07.4

RIVER MNSW

1125 DATA PTS / 100 SPEC ESTS

1.2 X10^5 FT REACH

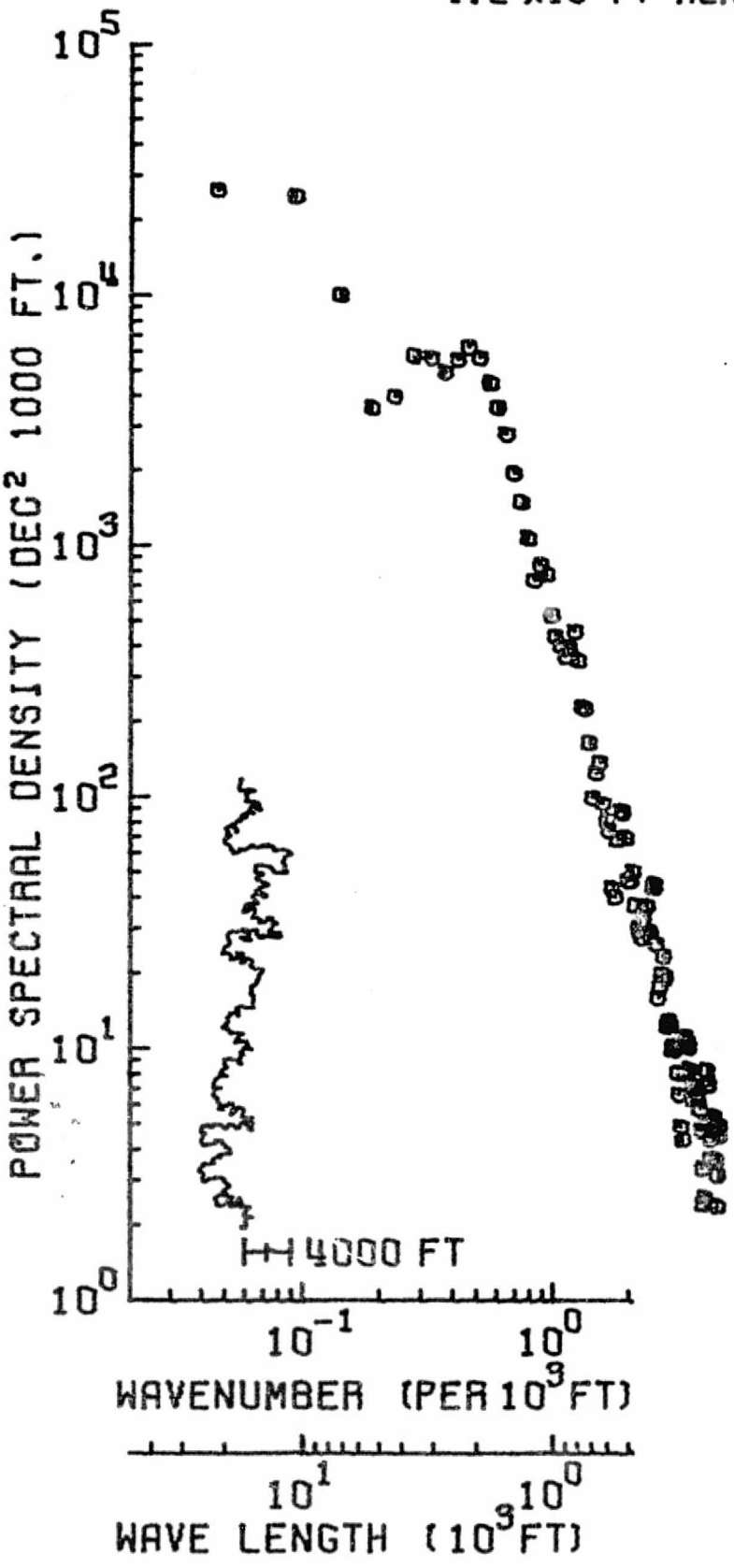

5500 / 10000

PLT TAPE PSPLT1 F4 BLK 23 IN DISK KAUDSK PIS096.MAJ.MNSW.L
74 283 OCT 10 00:27:18.9

RIVER MNSW

525 DATA PTS / 60 SPEC ESTS

5.6 X 10^4 FT REACH

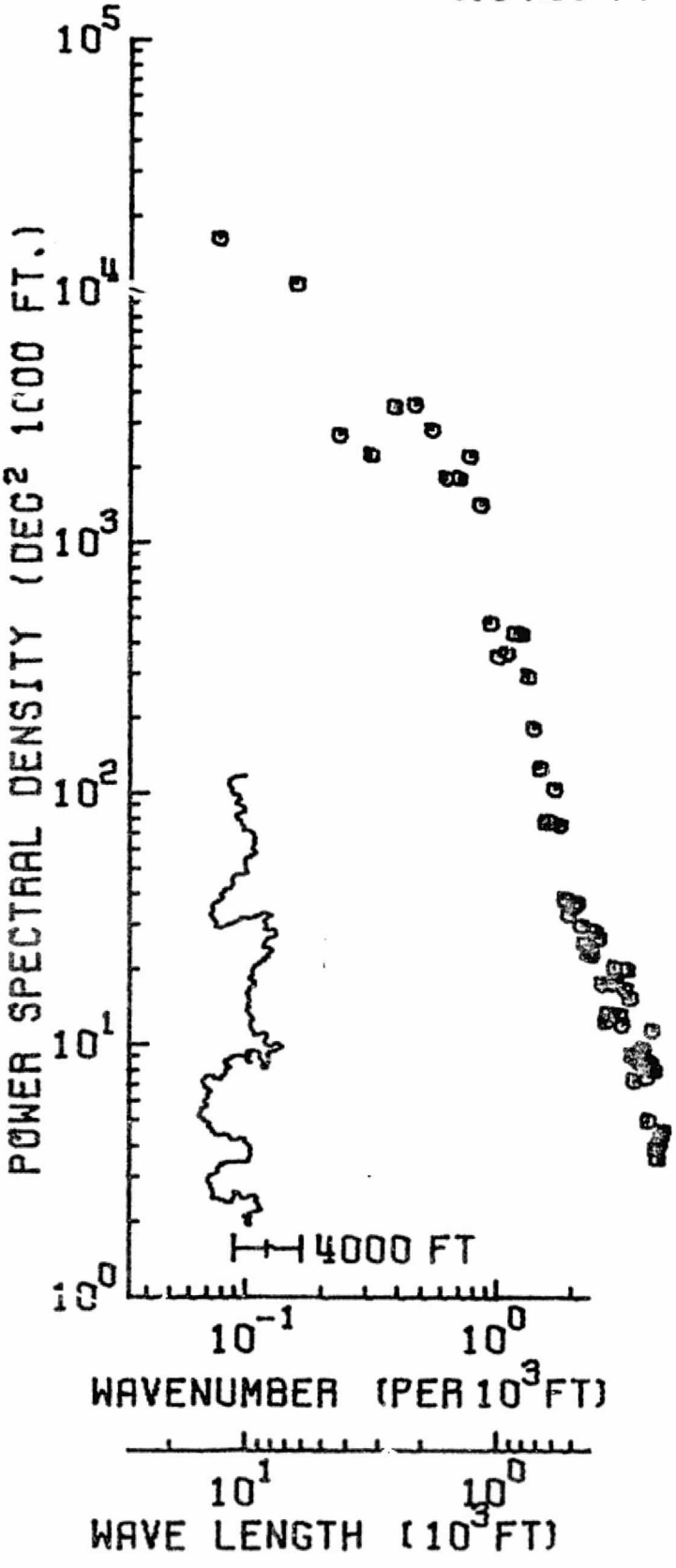

3400 / 5500

PLT TAPE PSPLT1 F4 BLK 22 IN DISK KAUDSK PIS096.MAJ.MNSW.L
74 283 OCT 10 00:27:19.9

RIVER MNSW

849 DATA PTS / 85 SPEC ESTS

9.1×10^4 FT REACH

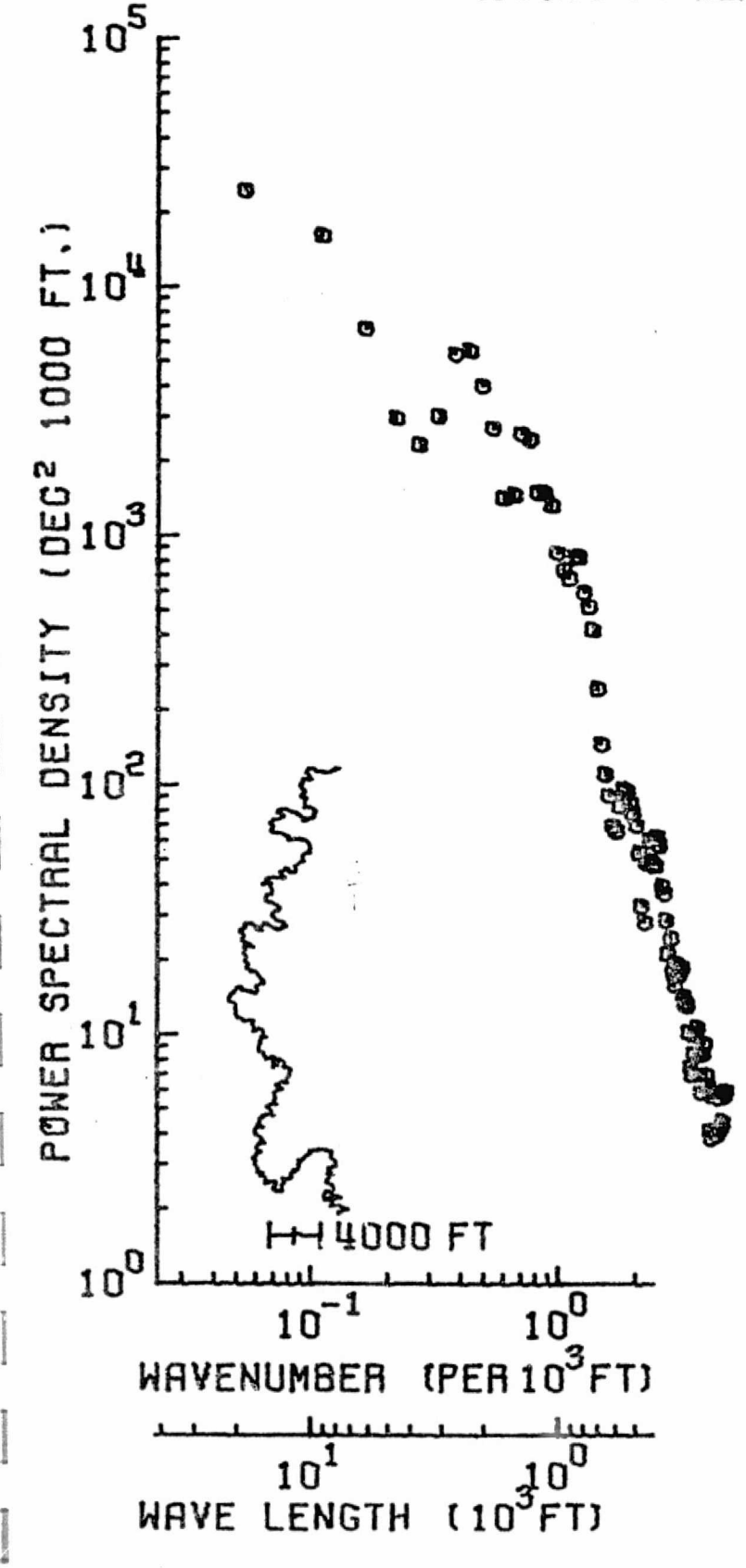

1 / 3400

PLT TAPE PSPLT1 F4 BLK 21 IN DISK KAUB3K P15096.NAJ.MN5W.L
74 293 OCT 10 00:27:38.9

RIVER MNSW

1380 DATA PTS / 100 SPEC ESTS

3.0 X10^5 FT REACH

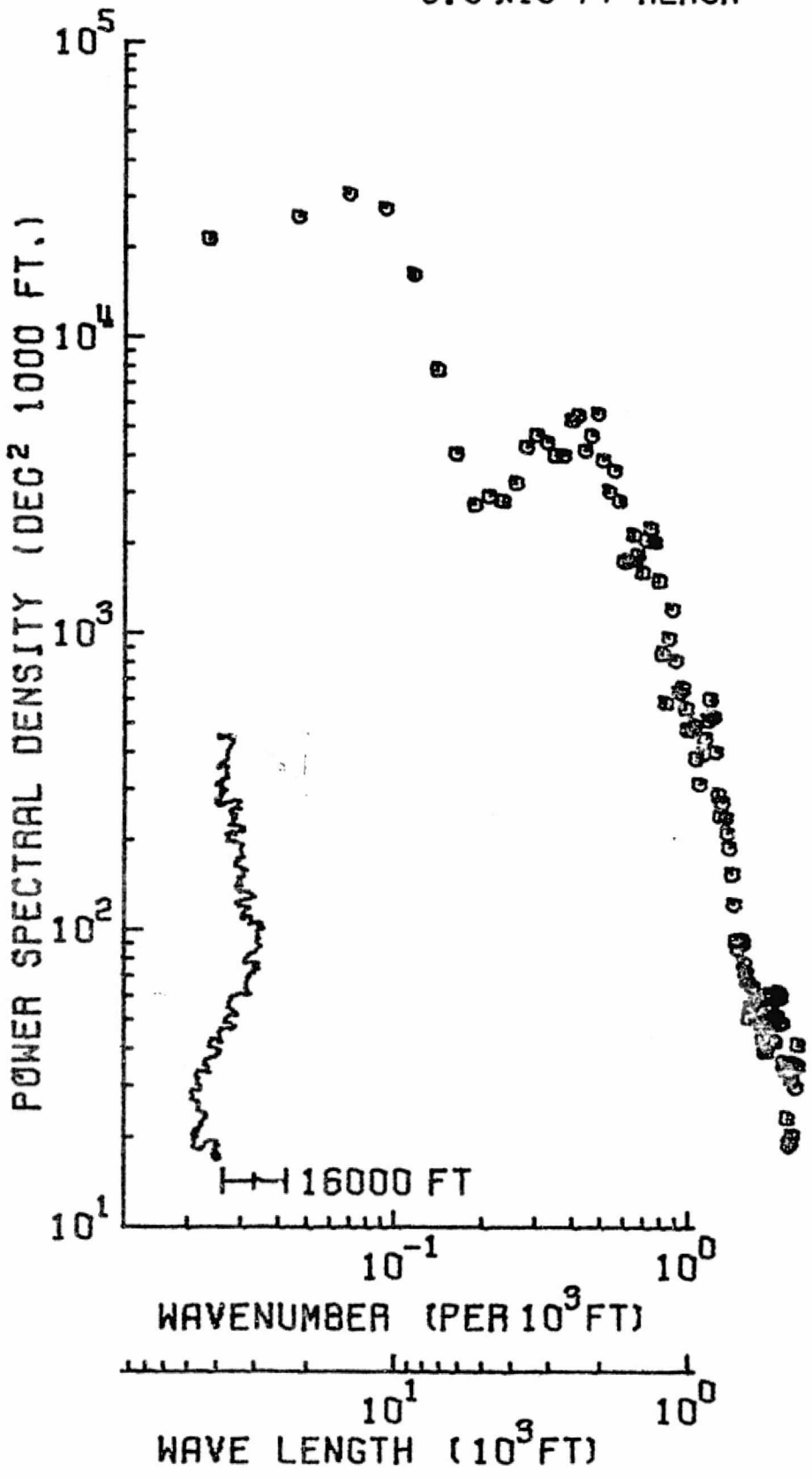

1 / 11049

PLT TAPE PSPLT1 F4 BLK 24 IN DISK KAUD3X PI5096.MAJ.MNSW.L
74 283 OCT 10 00:27:10.9

MANISTEE RIVER, MICH

2543DATA PTS / 200 SPEC ESTS

4.4×10^5 FT REACH

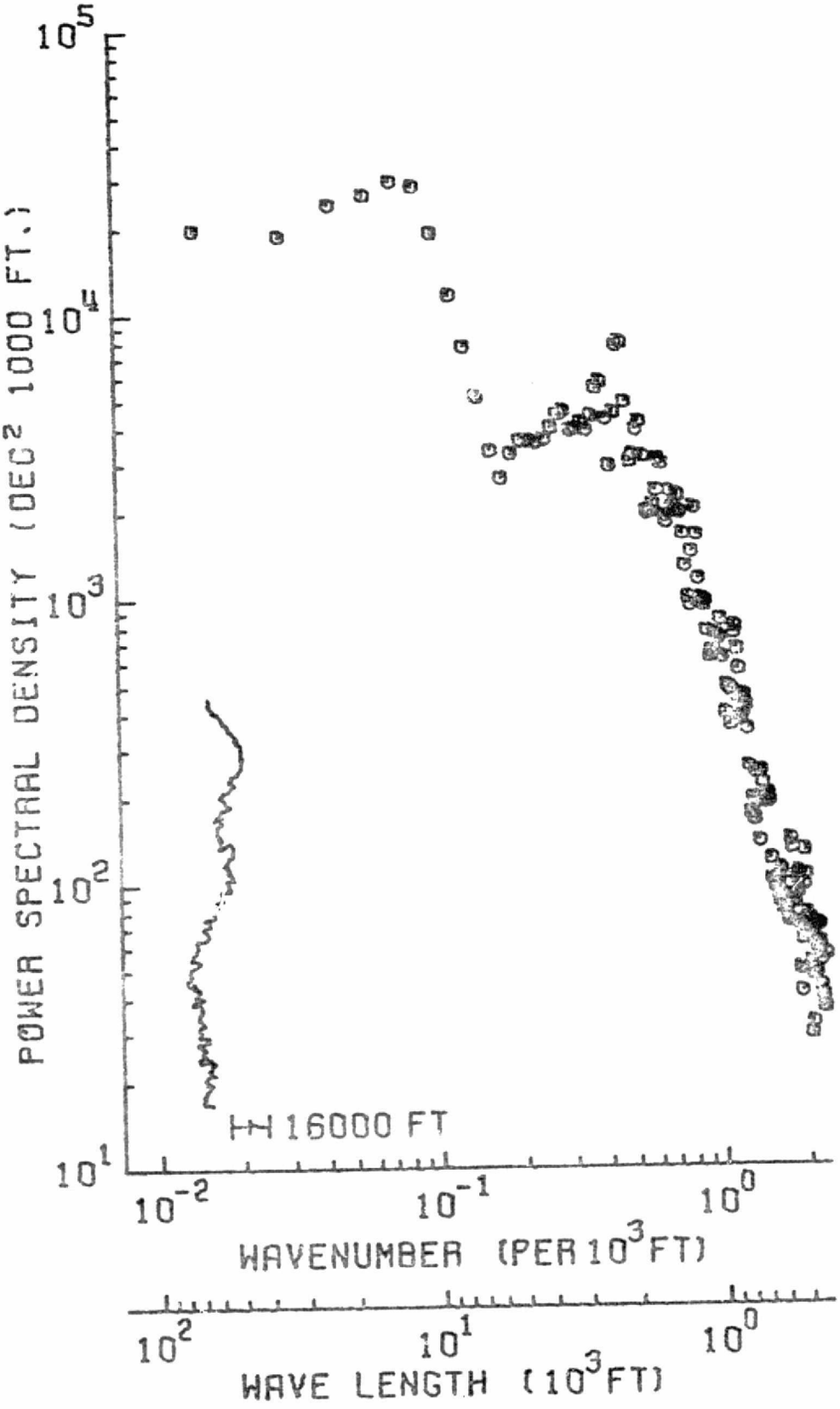

1 / 15259

PLT TAPE ISTPLT F1 BLK 3 IN DISK KAUDSK P15096.MAJ_MN5
74 270 SEP 27 11:22:50.4 IN DISK KAUDSK P15096.MAJ_MN5.ANG2

MANISTEE RIVER

STATION 4/1260 MANISTEE, MICH. 1951/10-1969/9

TP 4552, FIL 2, RECDS 5378-5593 PLOT 23 SET 1

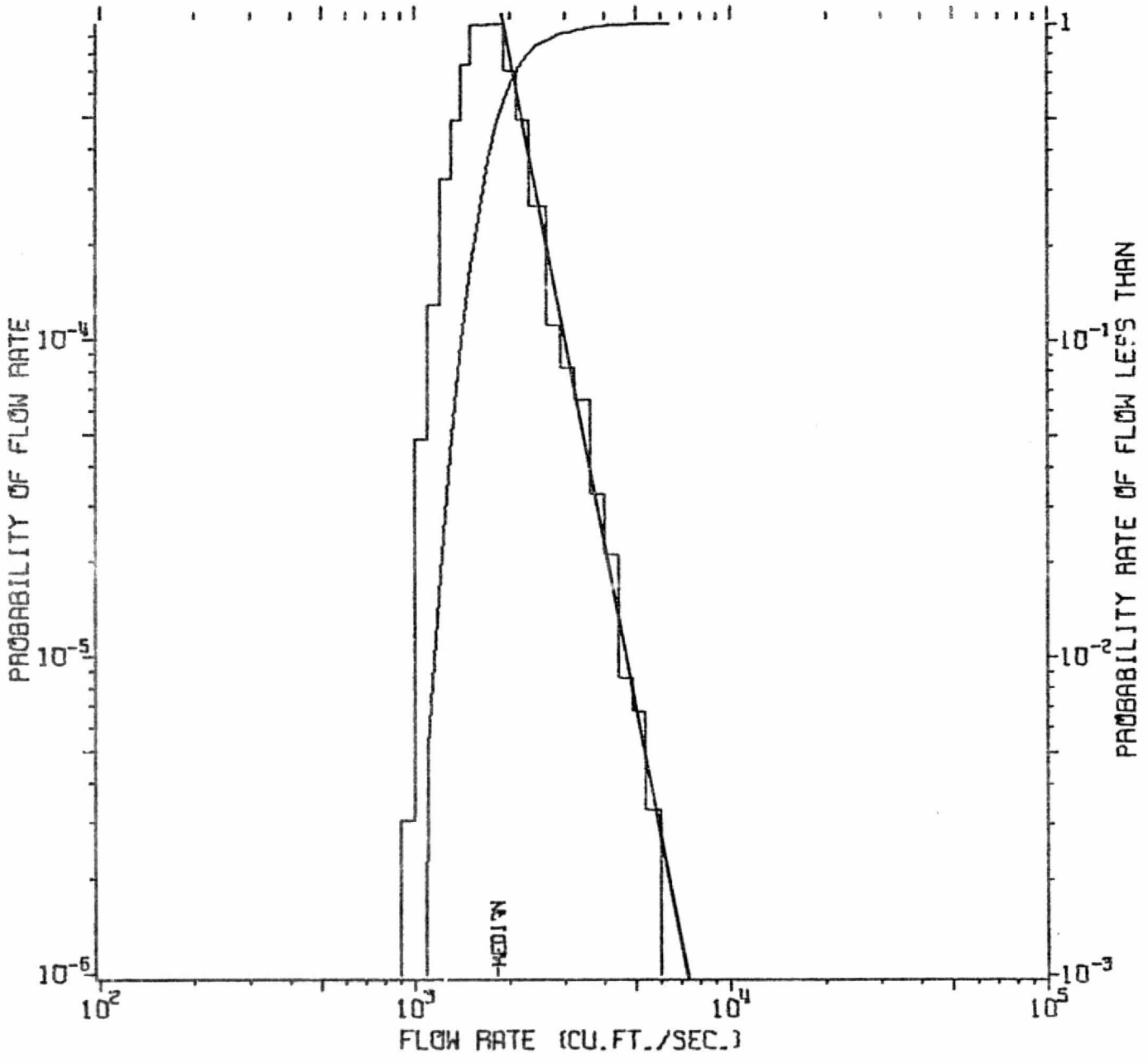

MANISTEE RIVER

STATION 4/1240 SHERMAN, MICH. 1933/10-1970/9

TP 4552, FIL 2, RECDS 4610-5053 PLOT 20 SET 1

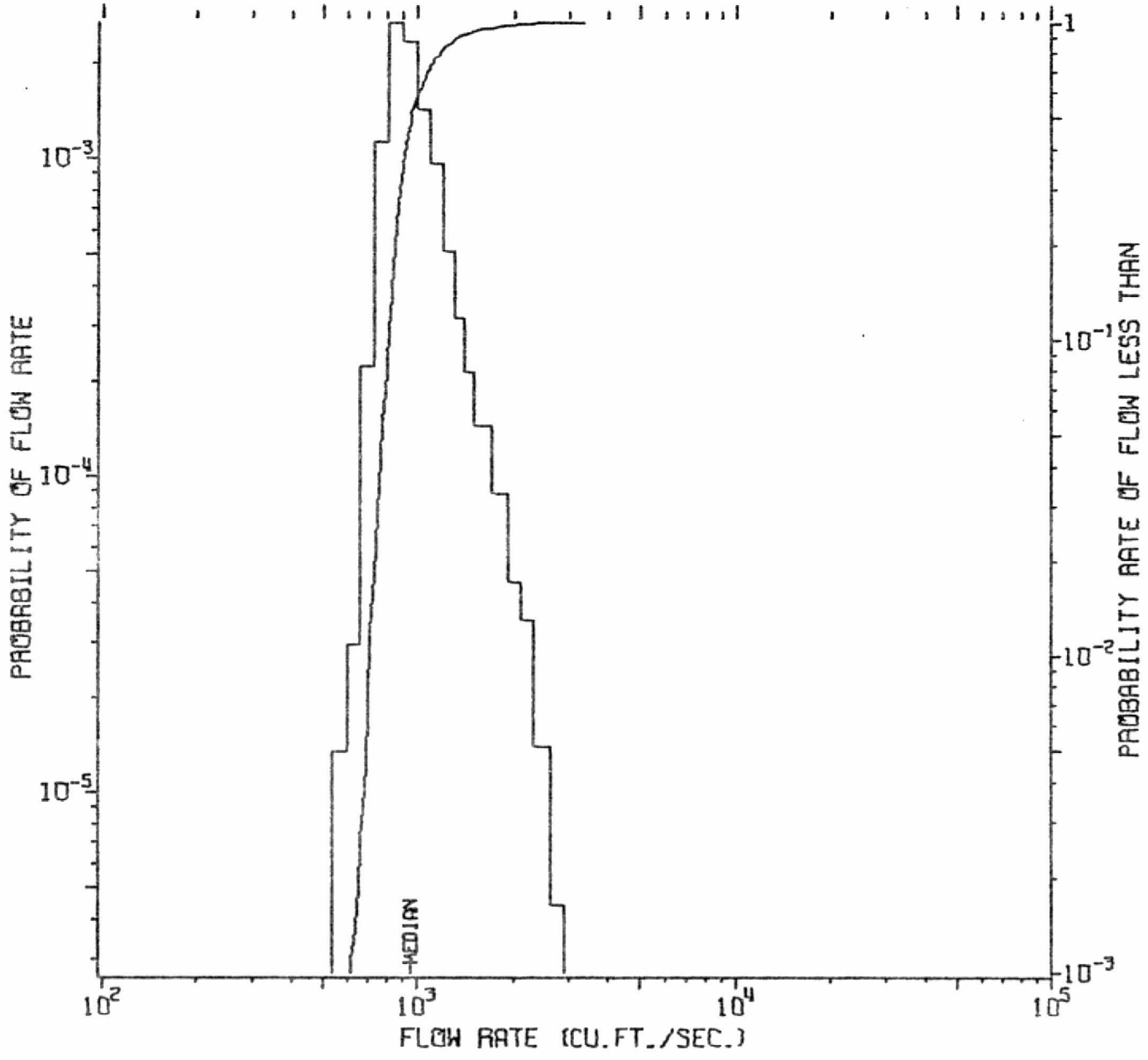

MANISTEE RIVER

STATION 4/1235 GRAYLING, MICH. 1942/10-1970/9

TP 4552, FIL 2, RECDS 4107-4442 PLOT 19 SET 1

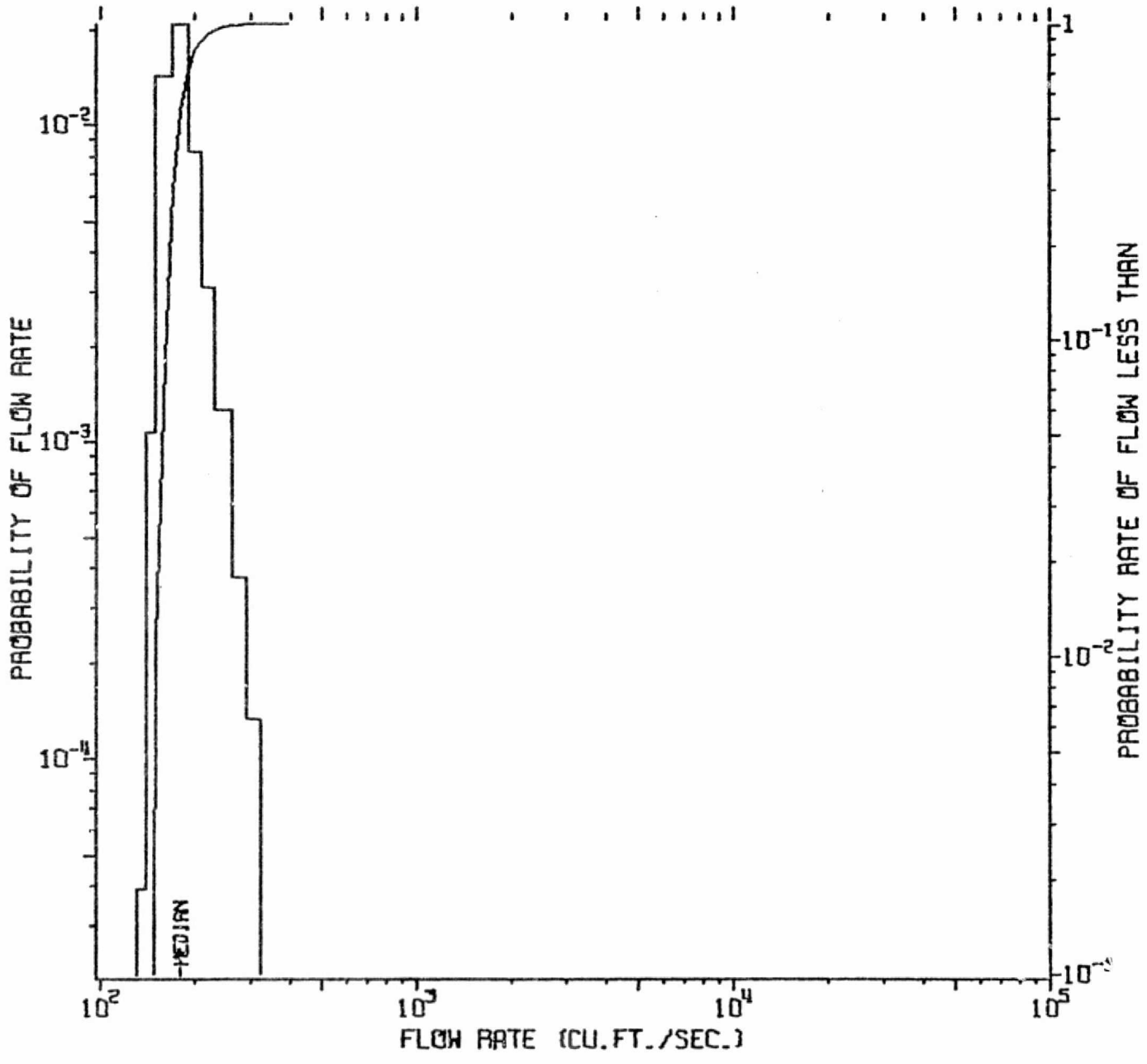

FEATHER RIVER

667 DATA PTS / 100 SPEC ESTS

1.2×10^5 FT REACH

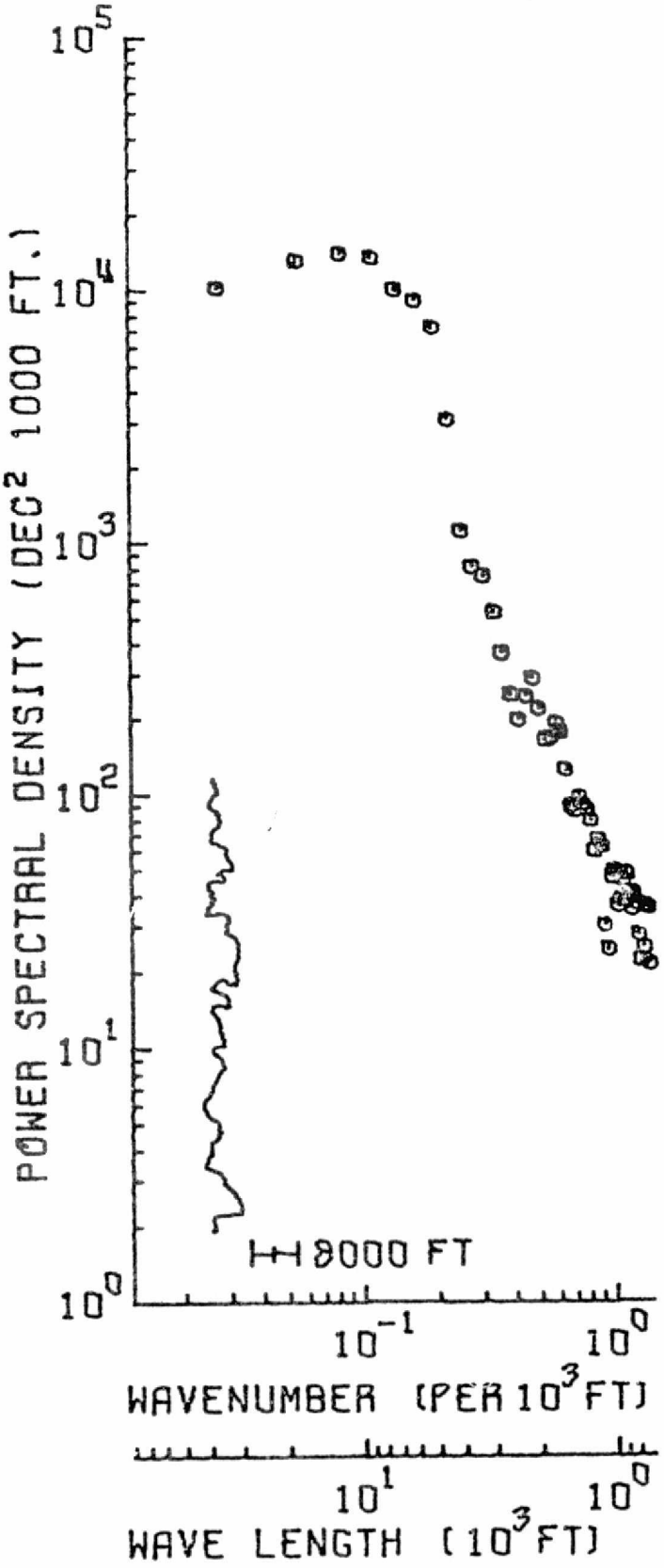

1 / 1337

PLT TAPE P3PLT1 F6 BLK. 41 C IN DISK KAUDSK PIS096.MAJ.FEAT1.82
74 295 OCT 22 03:49:10.1 IN DISK KAUDSK PIS096.MAJ.FEATA.82.ANG1

HOMOCHITTO RIVER, MISS

2196 DATA PTS / 200 SPEC ESTS

2.6 X10^5 FT REACH

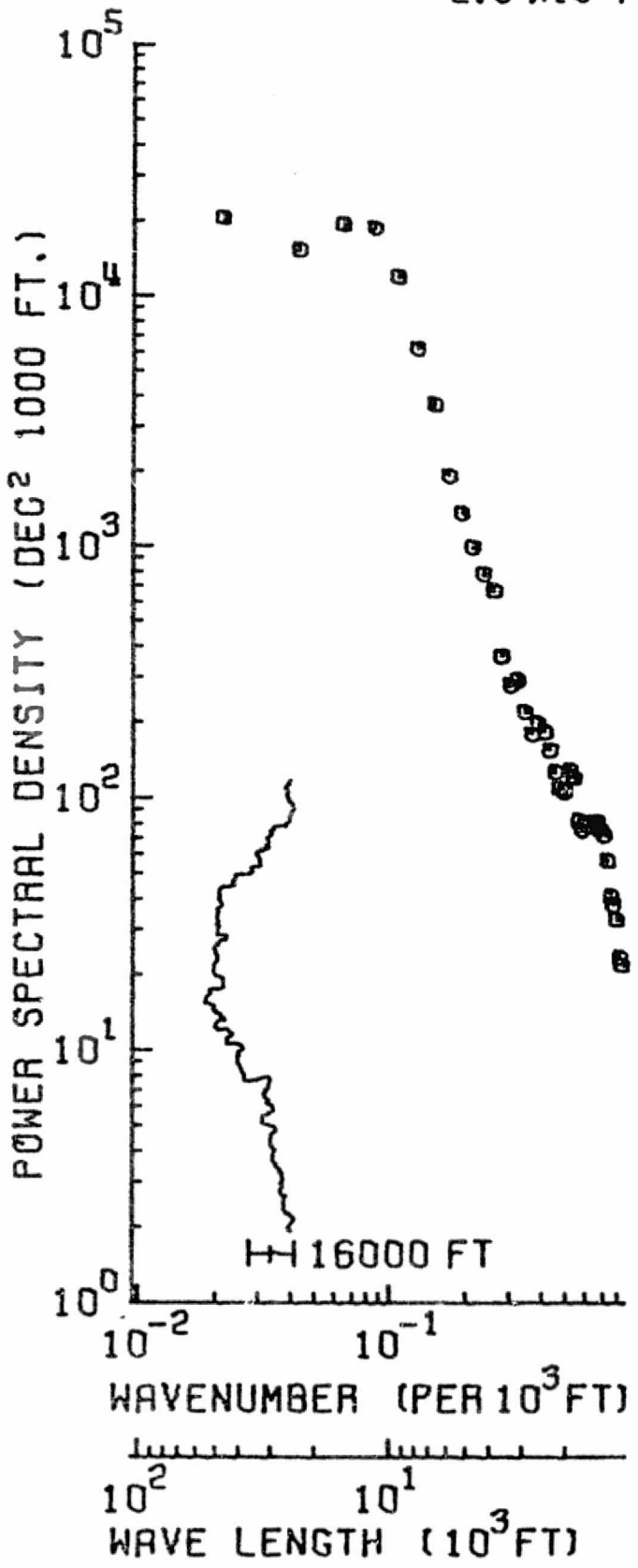

1 / 8785

PLT TAPE TSTPLT F2 BLK 12 IN DISK KAUDSK PIS096.MAJ.HOMA
74 274 OCT 1 02:24:07.4 IN DISK KAUDSK PIS096.MAJ.HOMA.ANG2

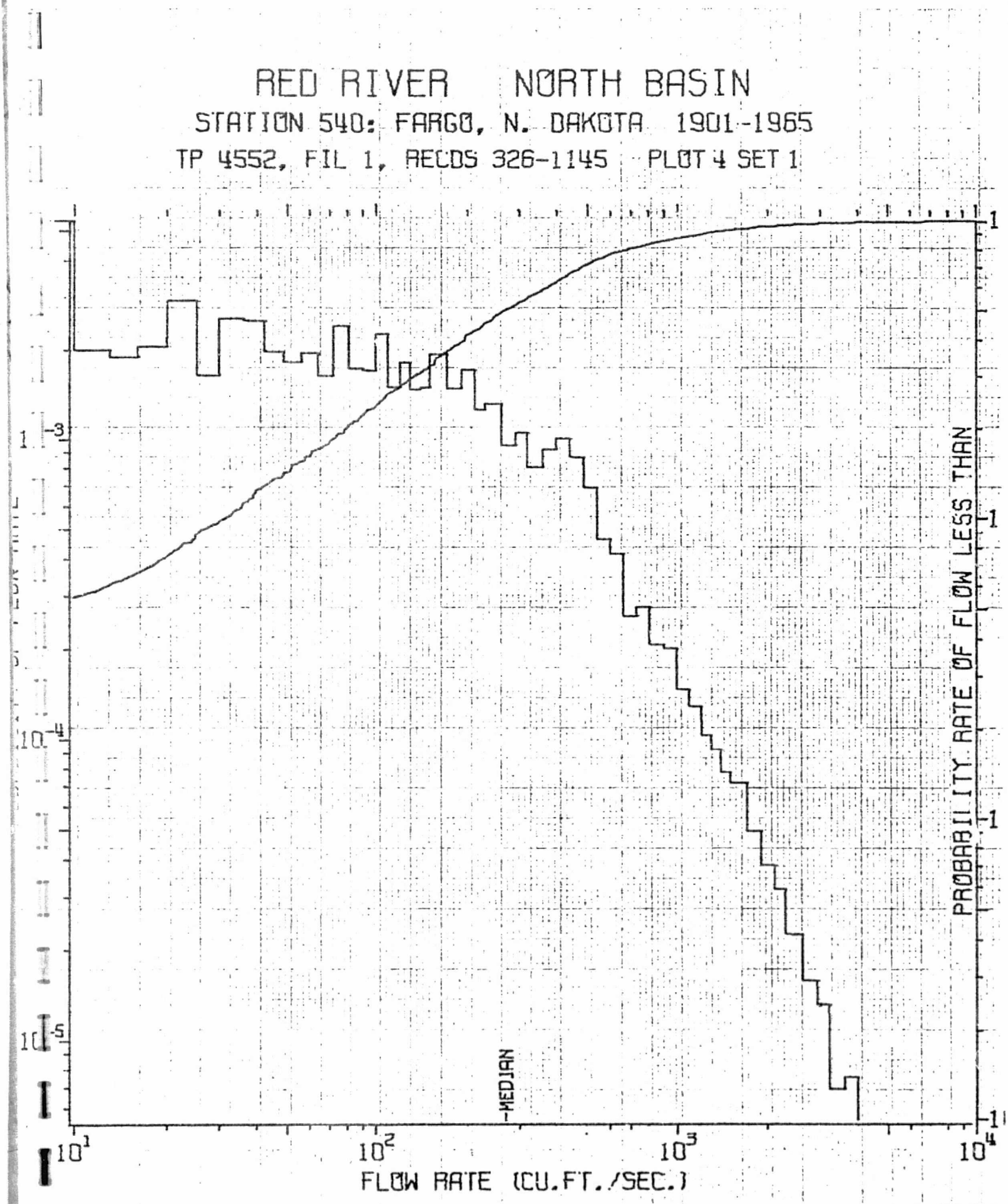
RED RIVER NORTH BASIN
STATION 540: FARGO, N. DAKOTA 1901-1965
TP 4552, FIL 1, RECDS 326-1145 PLOT 4 SET 1
PROBABILITY RATE OF FLOW LESS THAN
MEDIAN
FLOW RATE (CU.FT./SEC.)
10^{1}
10^{2}
10^{3}
10^{4}
10^{-3}
10^{-4}
10^{-5}
1
1
1
1

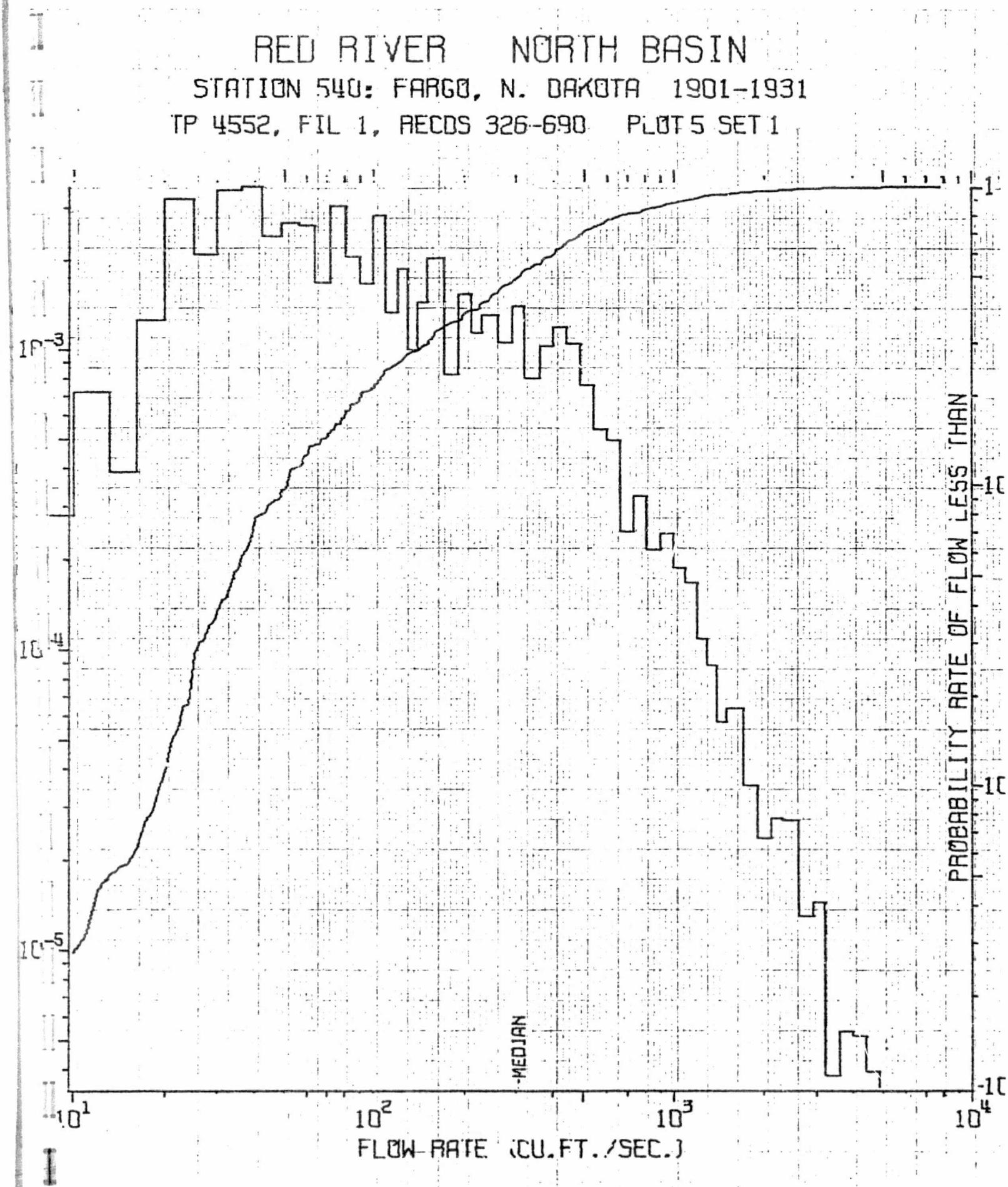
RED RIVER NORTH BASIN
STATION 540: FARGO, N. DAKOTA 1901-1931
TP 4552, FIL 1, RECDS 326-690 PLOT 5 SET 1
PROBABILITY RATE OF FLOW LESS THAN
MEDIAN
FLOW-RATE (CU.FT./SEC.)
10^{1}
10^{2}
10^{3}
10^{4}
10^{-3}
10^{-4}
10^{-5}

RED RIVER NORTH BASIN

STATION 540: FARGO, N. DAKOTA 1931-1942

TP 4552, FIL 1, RECDS 691-816 PLOT 6 SET 1

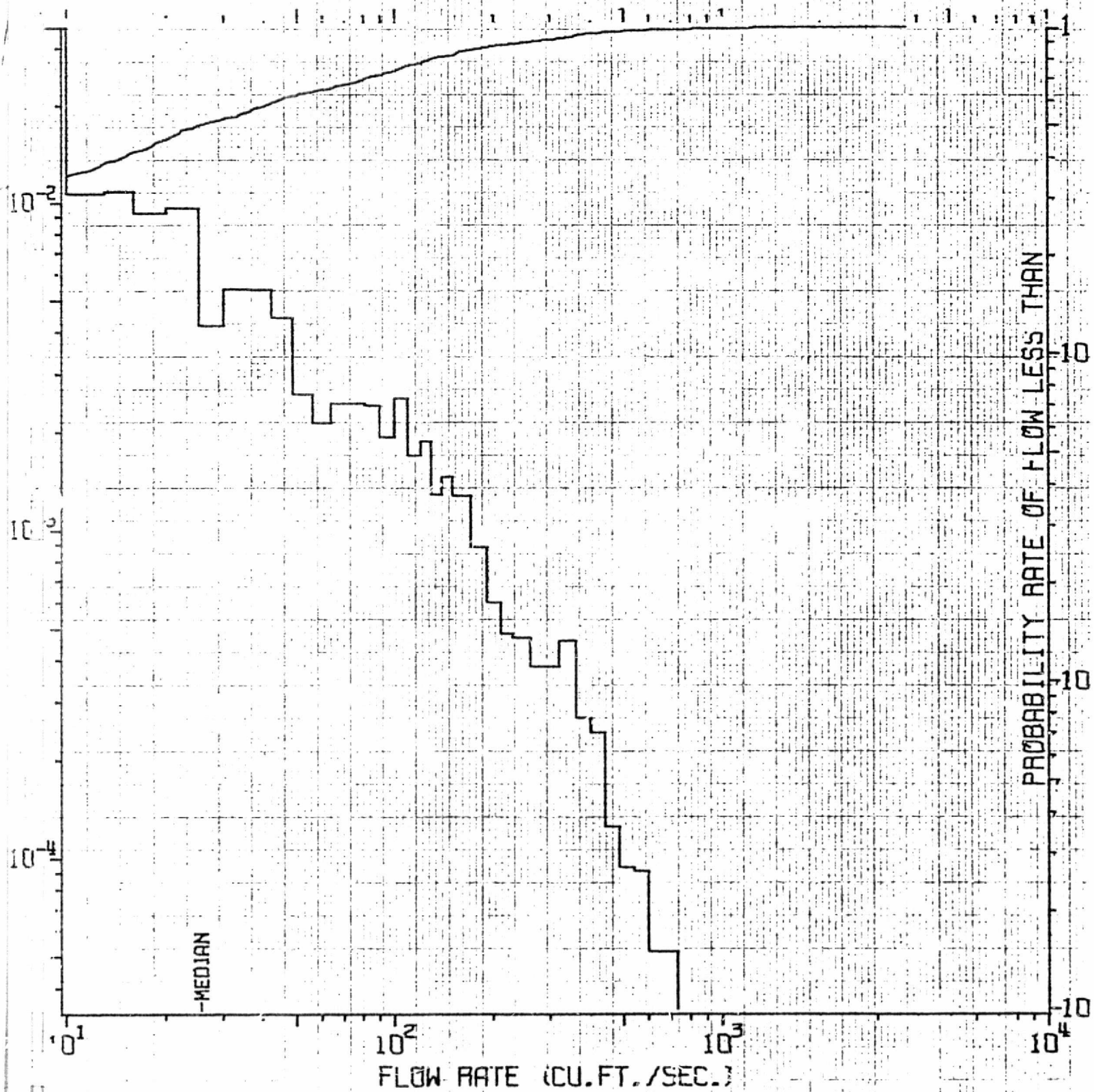

RED RIVER

1287 DATA PTS / 100 SPEC ESTS

3.9×10^5 FT REACH

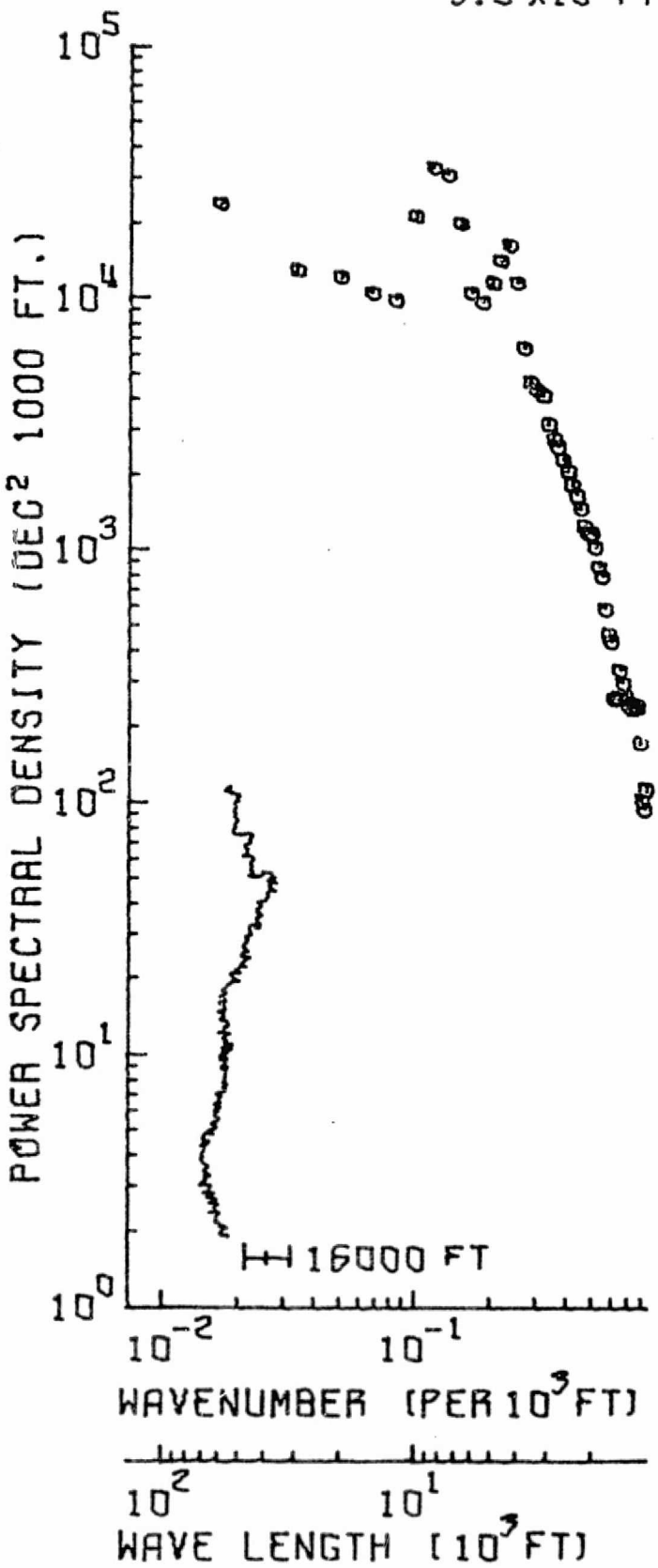

1 / 5159

PLT TAPE P3PLT1 F6 BLK. 45 C IN DISK KAUDSK PI3096.NAJ.RED.81
74 295 OCT 22 03:43:10.1 IN DISK KAUDSK PI3096.NAJ.RED.81.ANG1

RED RIVER

642 DATA PTS / 60 SPEC ESTS

1.9 X 10^5 FT REACH

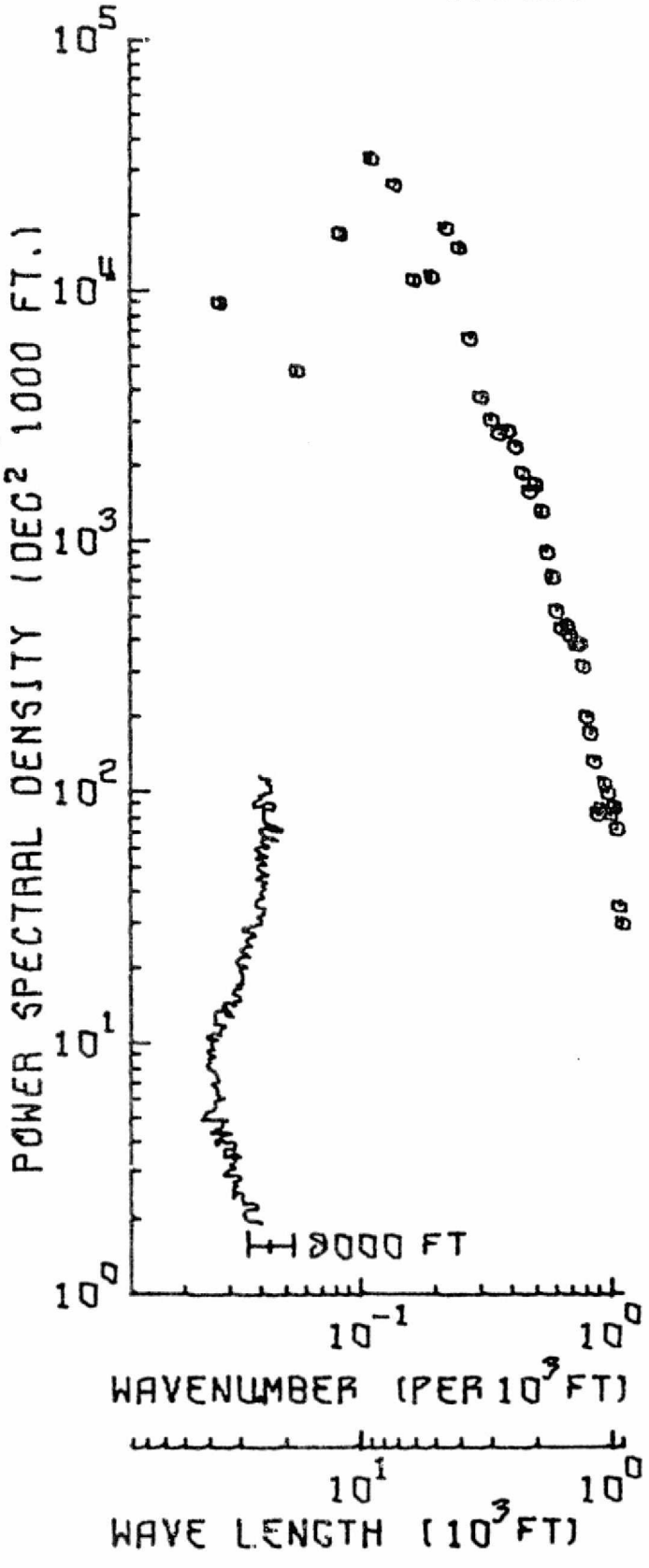

1 / 2570

RLT TAPE F3FLT1 F6 BLK. 43 C IN DISK KAUDSK FI3096.MAJ.AEO.81
74 295 OCT 22 03:49:10.1 IN DISK KAUDSK FI3096.MAJ.AEO.81.ANGL

RED RIVER

644 DATA PTS / 60 SPEC ESTS

1.9×10^5 FT REACH

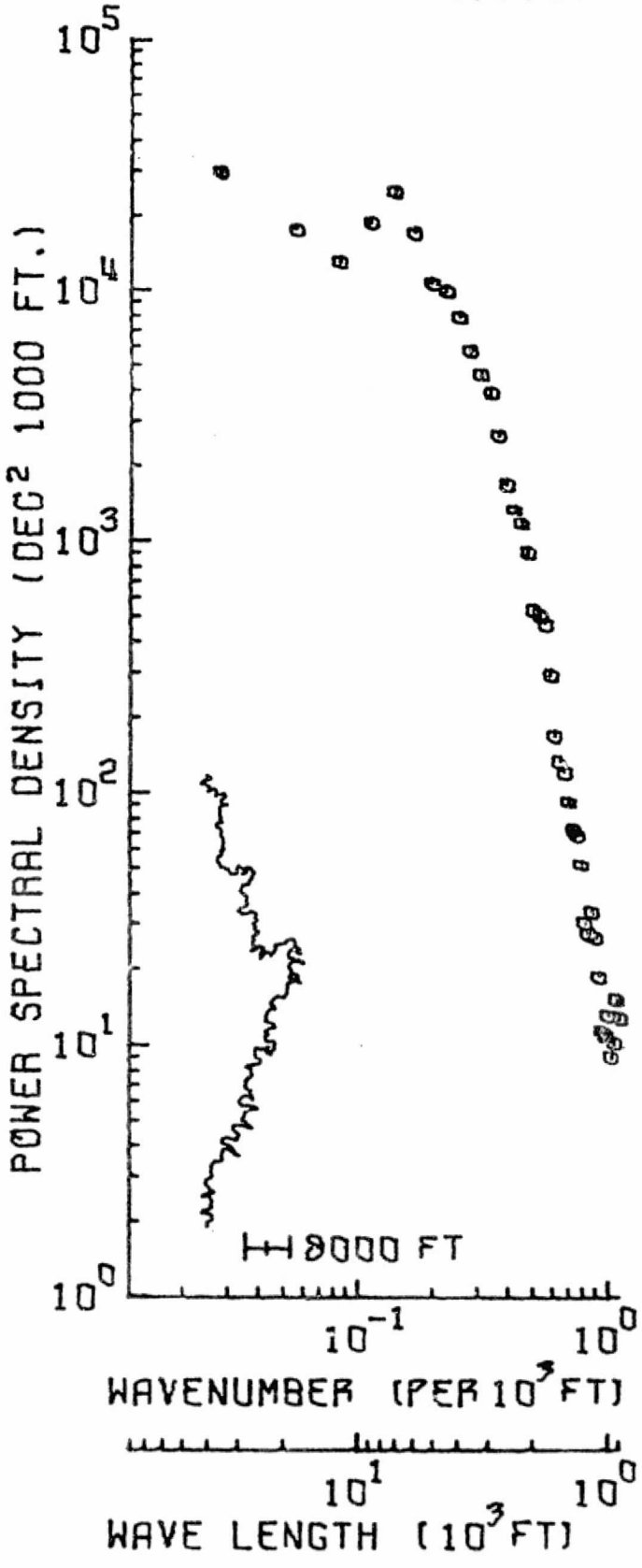

2570 / 5150

PLT TAPE P3PLT1 F6 BLK. 44 C IN DISK KAUO3K PI3036.MAJ.MED.81
74 295 OCT 22 03:43:10.1 IN DISK KAUO3K PI3036.MAJ.MED.81.ANG1

BAD RIVER

STATION 4/0270 ODANAH, WIS. 1948-1970

TP 4552, FIL 2, RECDS 426-681 PLOT 8 SET 1

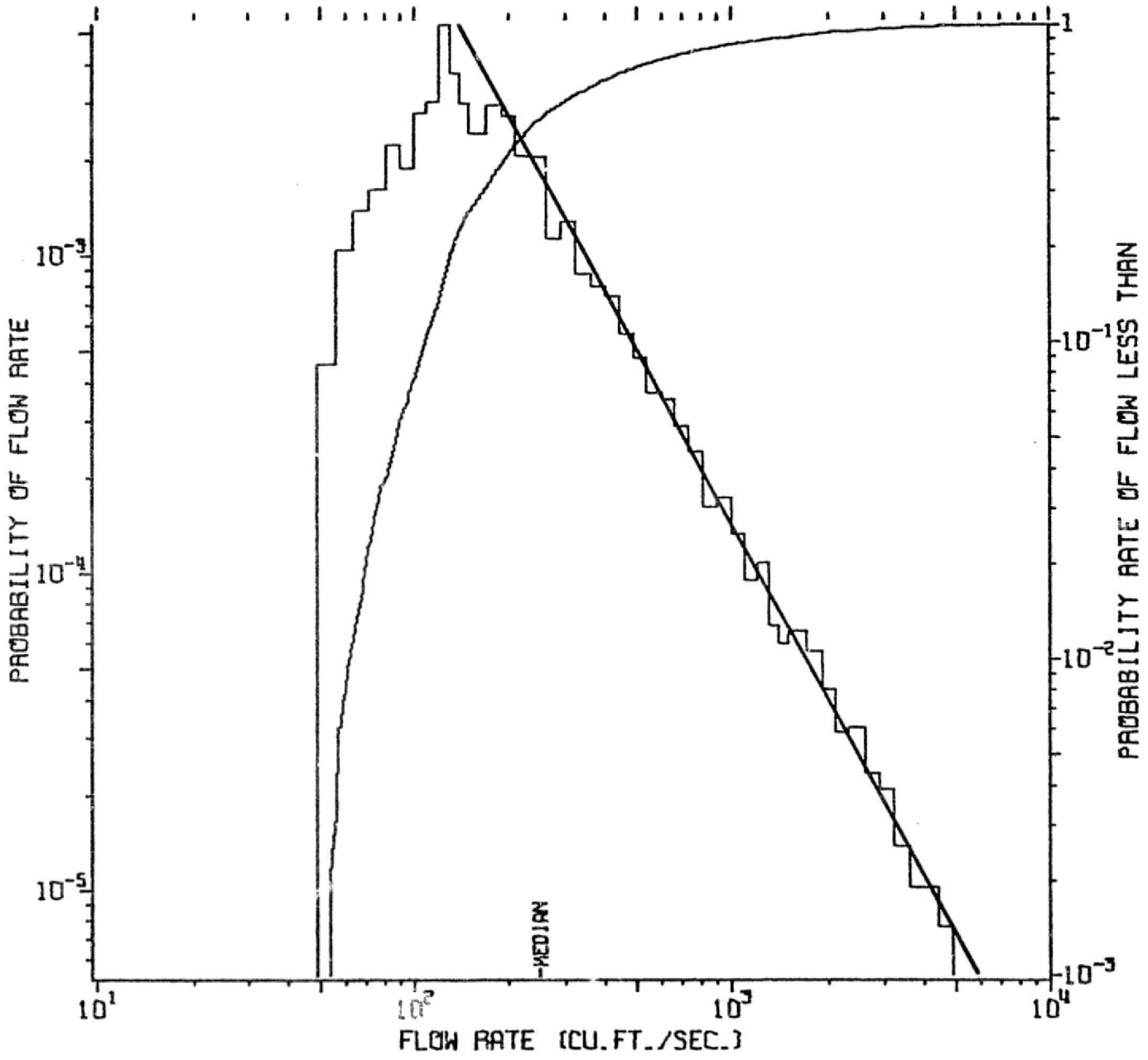

BAD RIVER

2410 DATA PTS / 150 SPEC ESTS

1.3×10^5 FT REACH

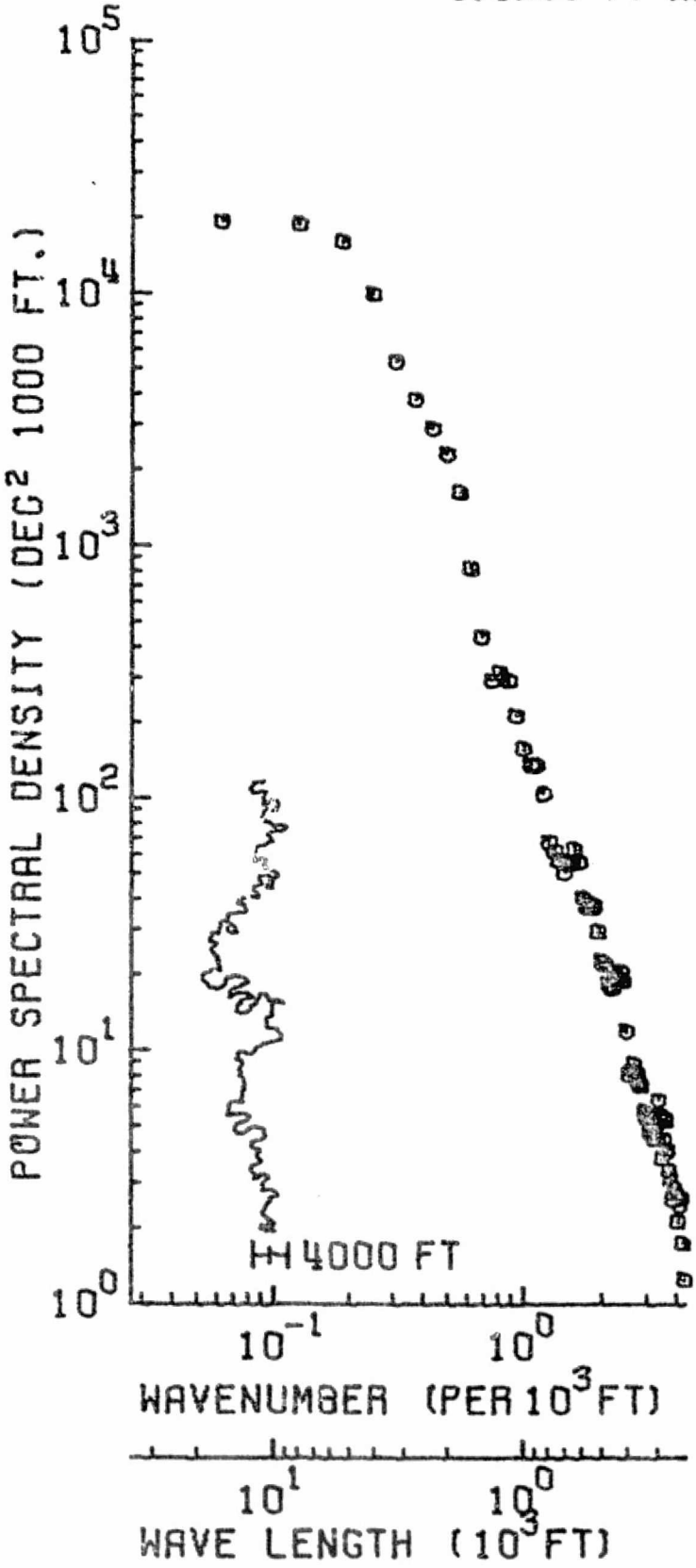

1 / 4921

PLT TAPE PSPLT1 F1 BLK 1 IN DISK KAUDSK P13G96.MAJ.BADR.L
74 273 SEP 30 12:59:45.5

C-2

BAD RIVER

1061 DATA PTS / 100 SPEC ESTS

5.7×10^4 FT REACH

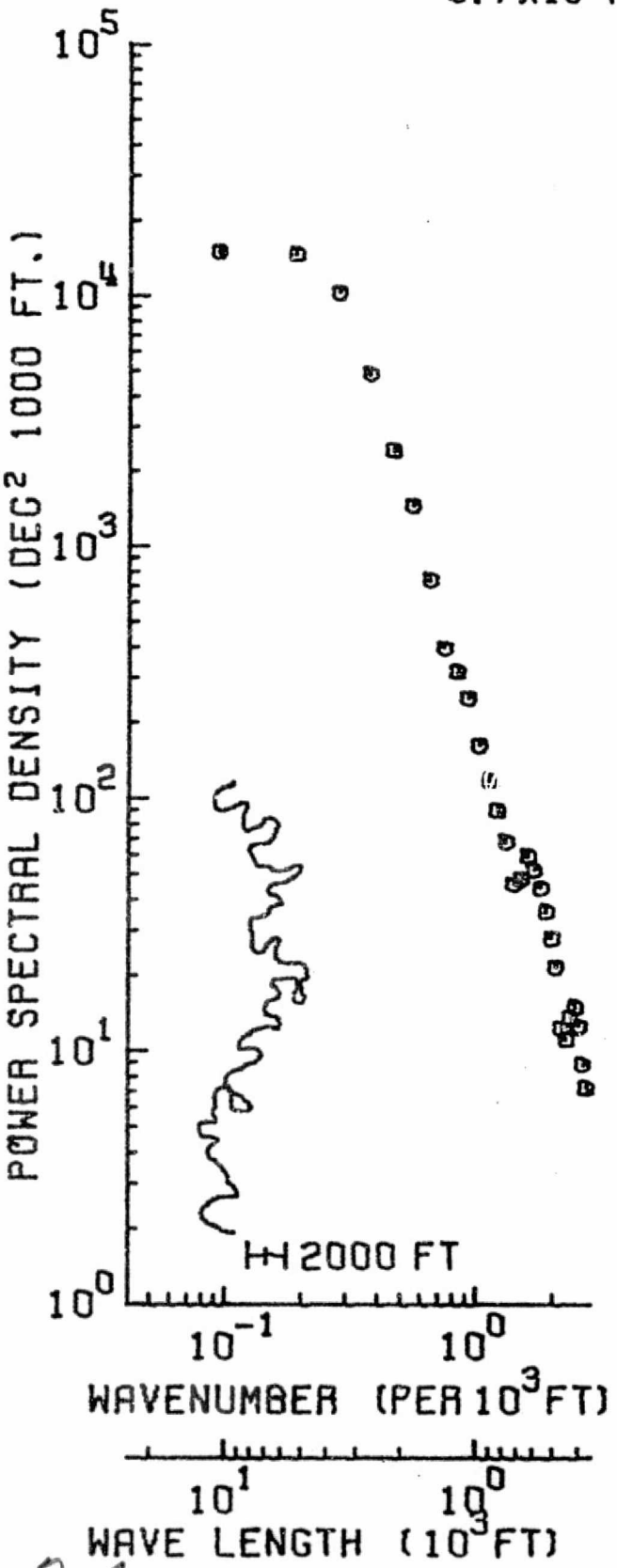

C-2

2700 / 4821

PLT TAPE PUPLT1 F1 BLK 3 IN DISK KAUDSK PISD96.MBL.BARDA.L

BAD RIVER, WISC

1310 DATA PTS / 150 SPEC ESTS

7.5×10^4 FT REACH

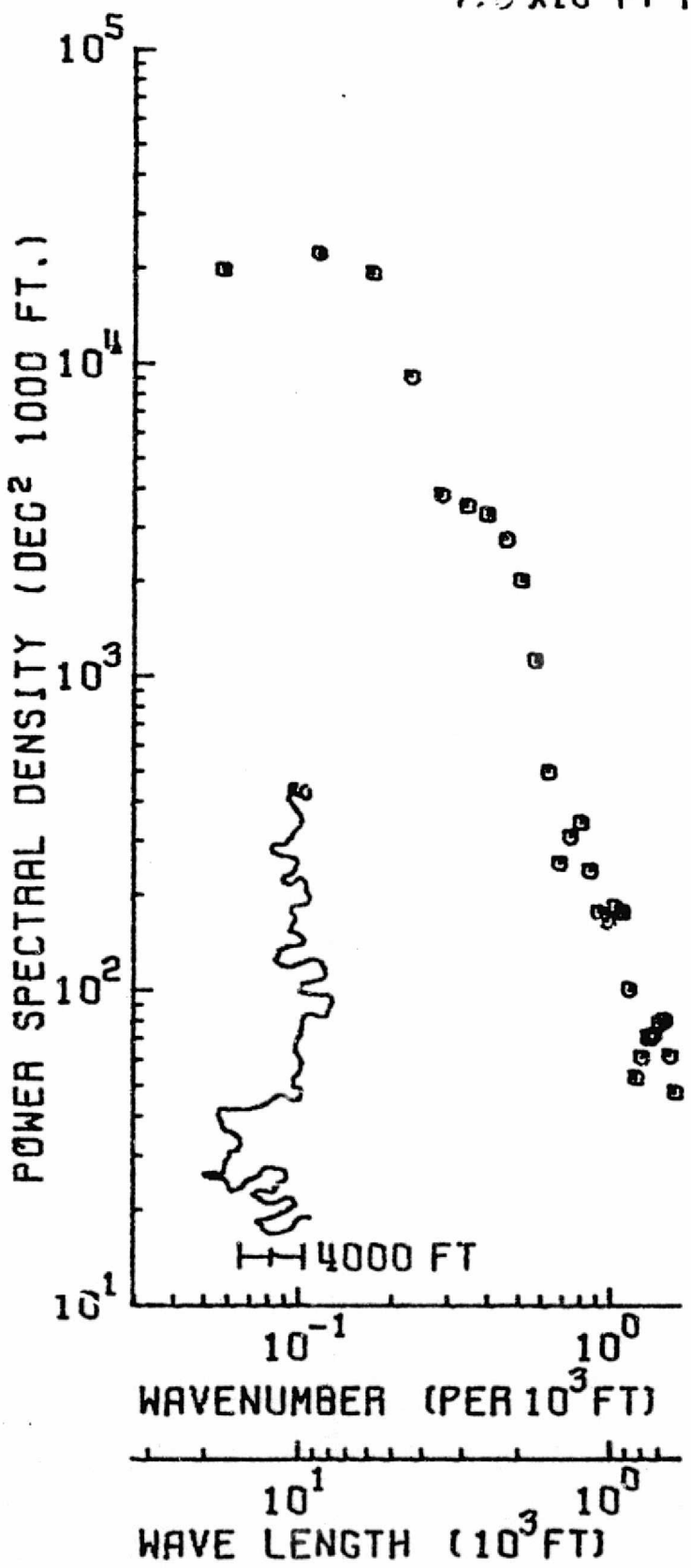

1 / 2621

PLT IAPE ISTPLT F1 BLK 7 IN DISK KAUO3K PI5096.NAJ.BAOA13
74 270 SEP 27 11:22:58.4 IN DISK KAUO3K PI5096.NAJ.BAOA13.ANG2

BAD RIVER

1300 DATA PTS / 100 SPEC ESTS

7.0 X 10^4 FT REACH

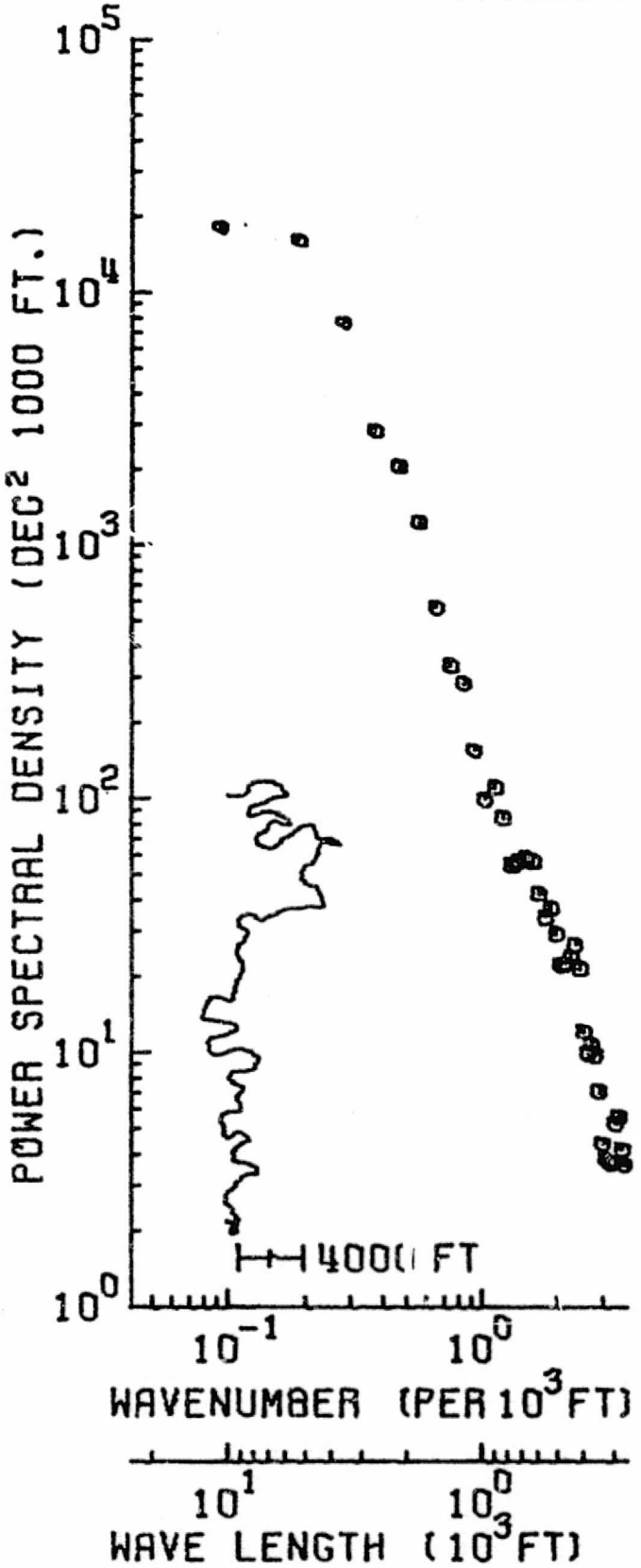

100 / 2700

PLT TAPE PSPLT1 F1 BLK 2 IN DISK KAUD3K P15096.HAJ.BADR.L
74 273 SEP 30 12:59:45.5

WHITE RIVER

STATION 4/0275 ASHLAND, WIS. 1948-1970

TP 4552, FIL 2, RECDS 682-937 PLOT 9 SET 1

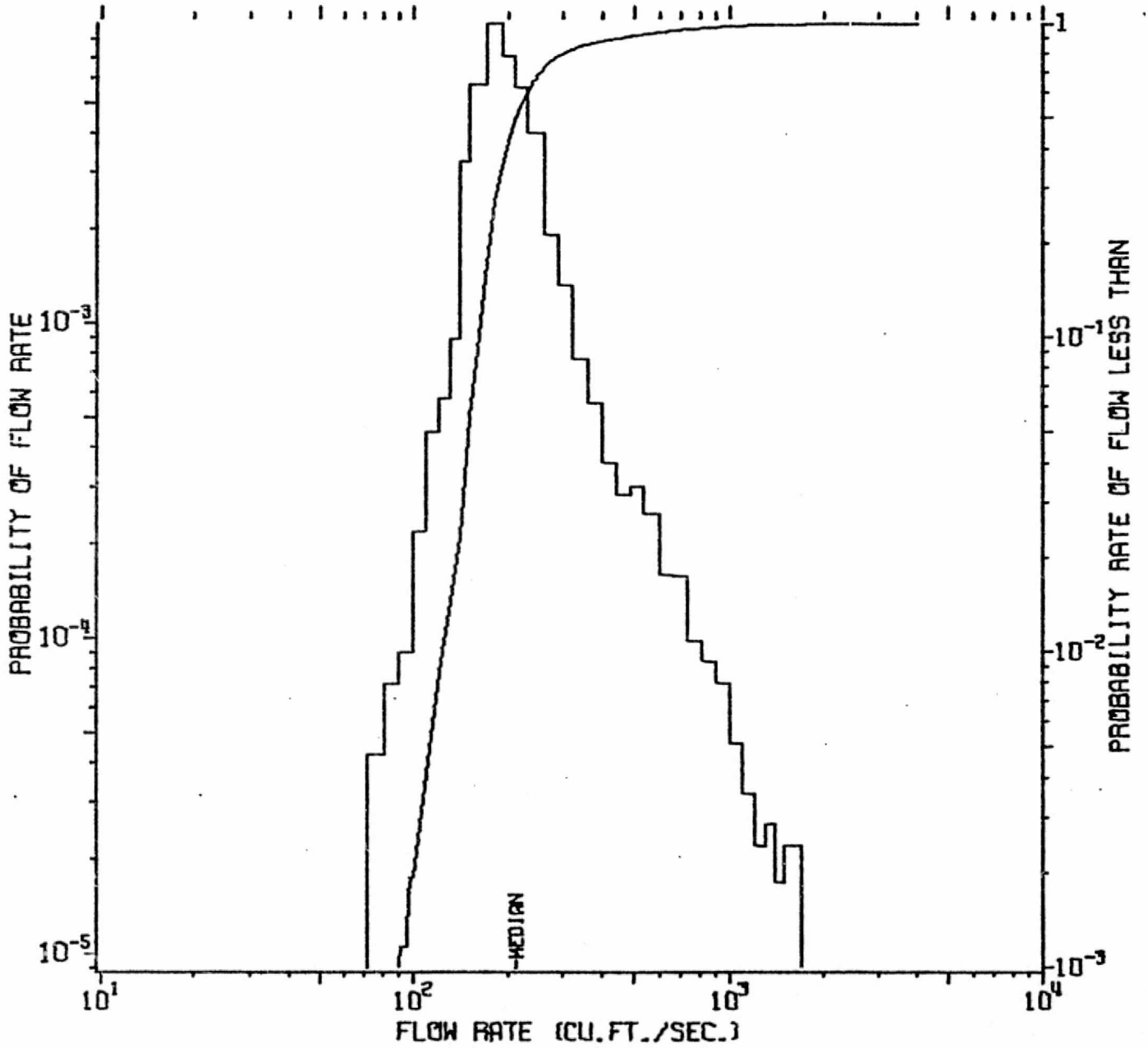

WHITE RIVER

1090 DATA PTS / 80 SPEC ESTS

5.8×10^4 FT REACH

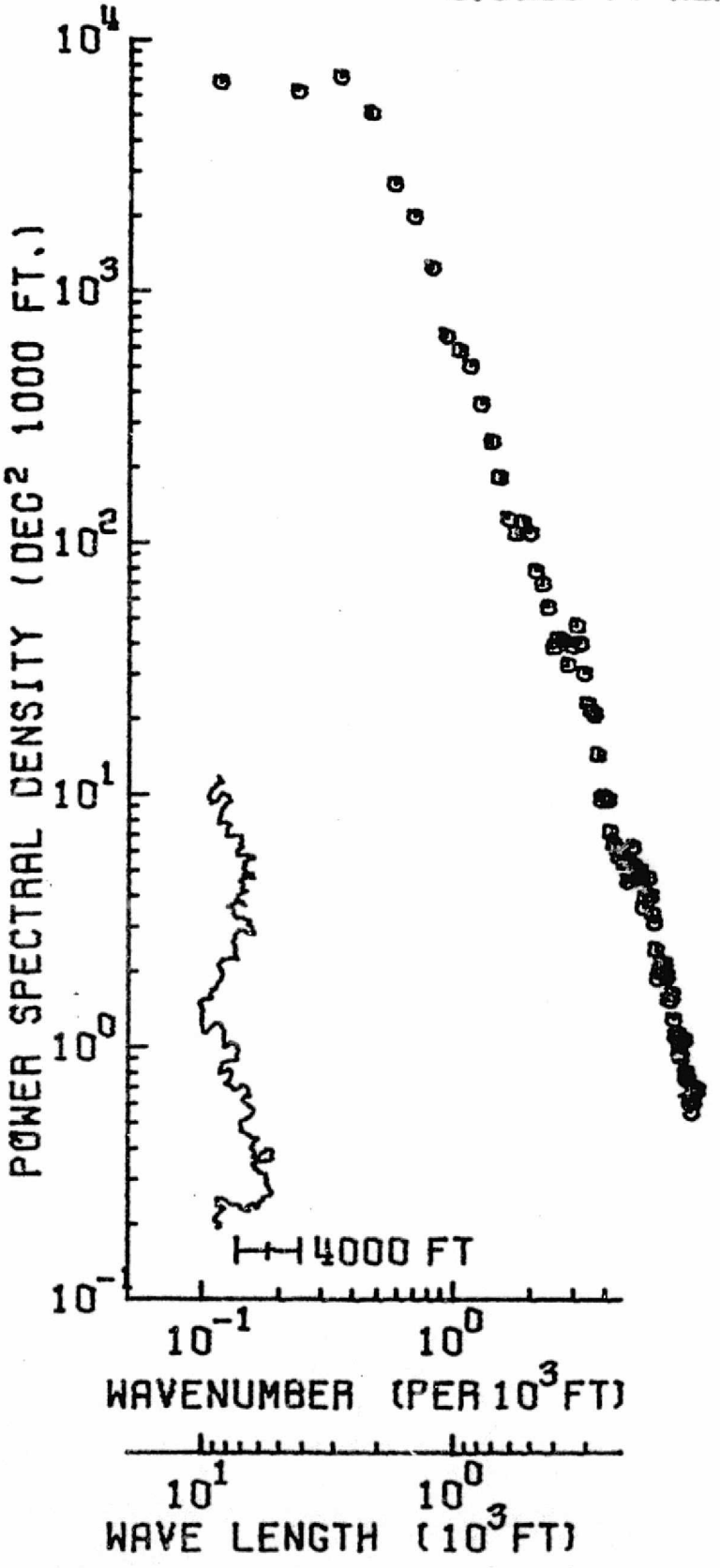

2000 / 4179

PLT TAPE P3PLT1 F4 BLK. 18 IN DISK KAUD3K PIS_MAJ_WHIK.L
74 283 OCT 10 00:27:18.9

WHITE RIVER

2089 DATA PTS / 125 SPEC ESTS

1.1×10^5 FT REACH

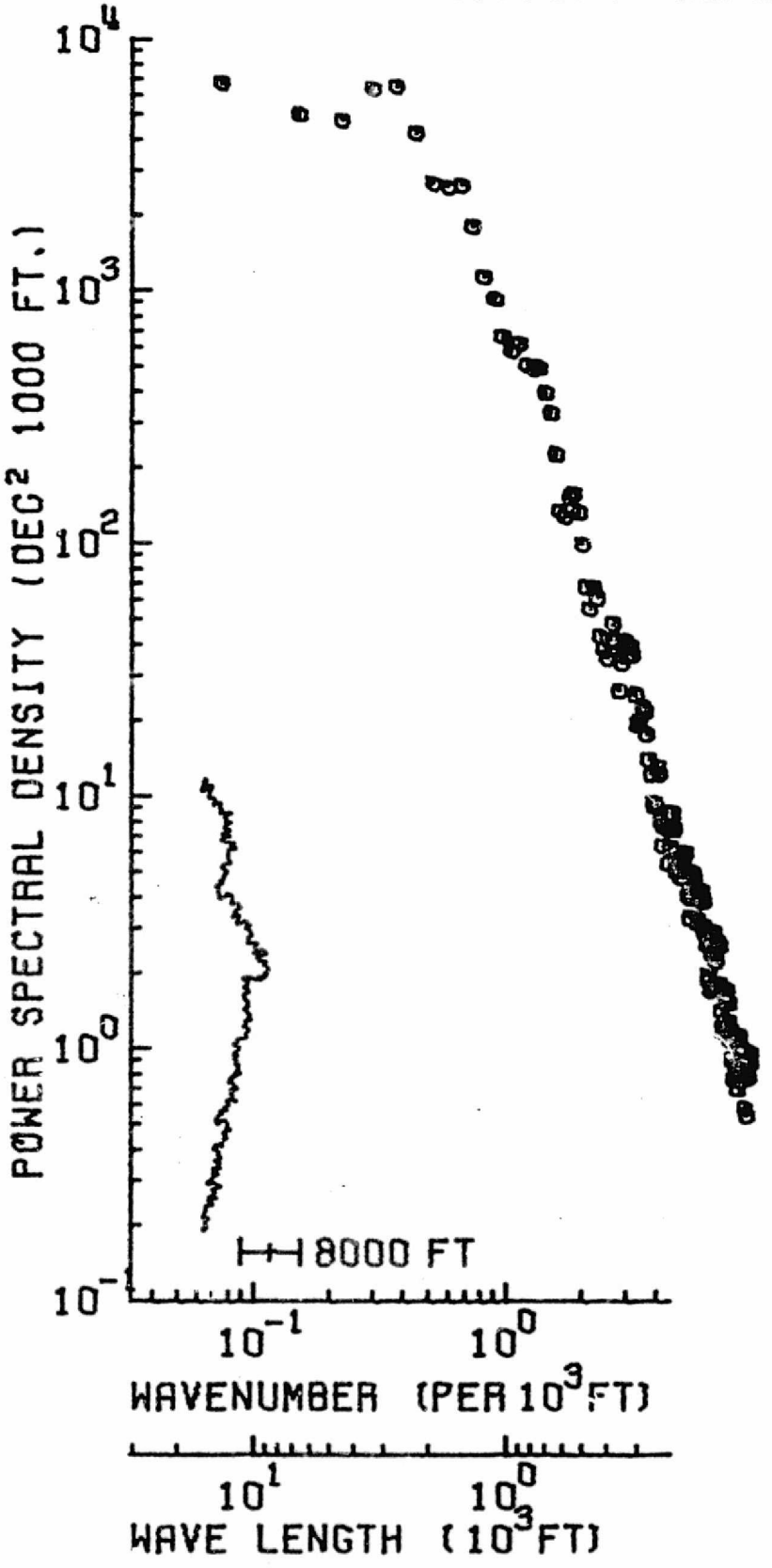

1 / 4179

PLT TAPE P3PLT1 F4 BLK. 19 IN DISK KAUDSK PIS.MAJ.WHIW.L
74 293 OCT 10 00:27:10.9

BOIS BRULE RIVER

STATION 4/0255 BRULE, WIS. 1942/10-1969/9

TP 4552, FIL 2, RECDS 1-324 PLOT 7 SET 1

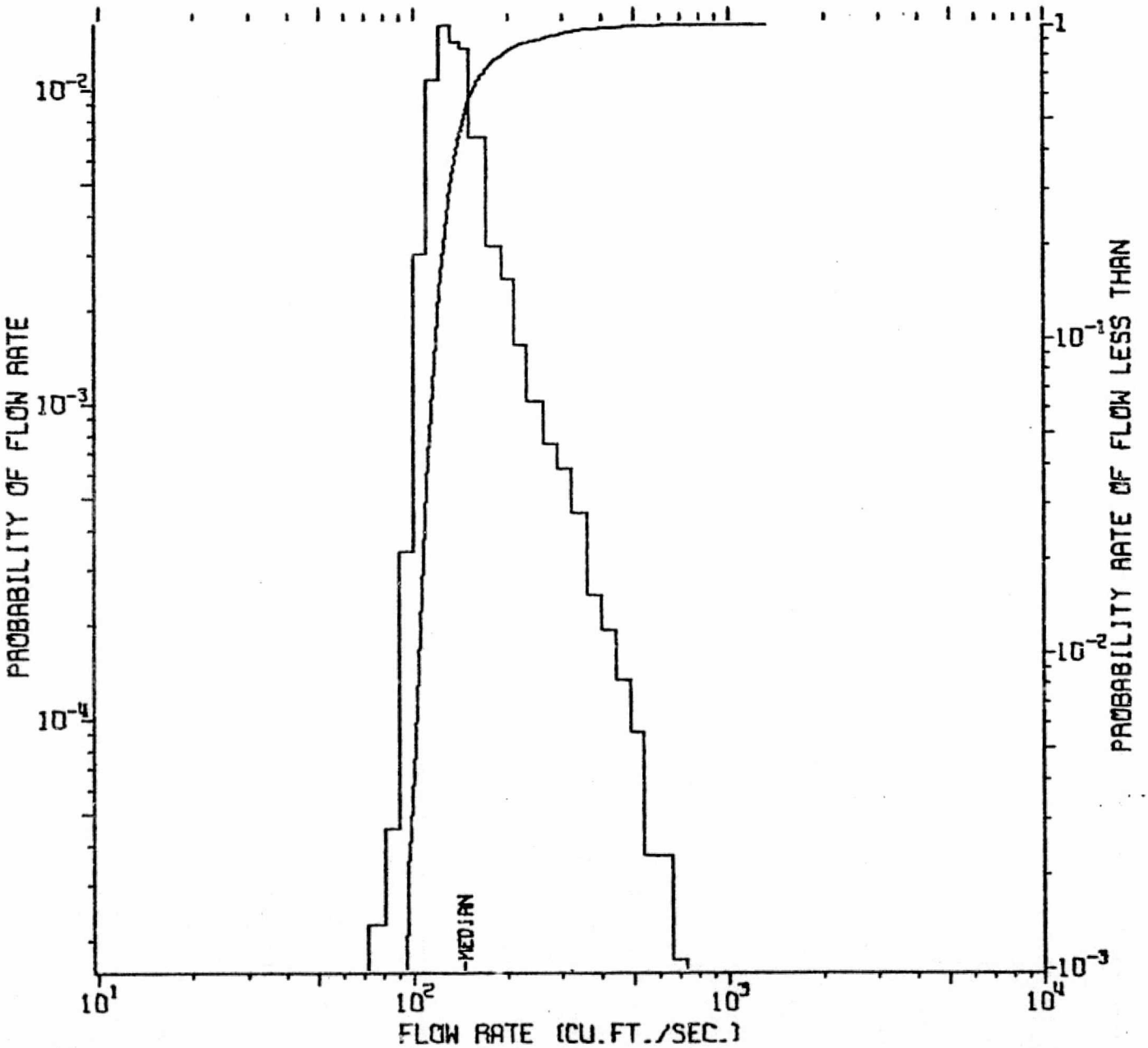

BOISE BRULE RIVER

399 DATA PTS / 40 SPEC ESTS

2.1×10^4 FT REACH

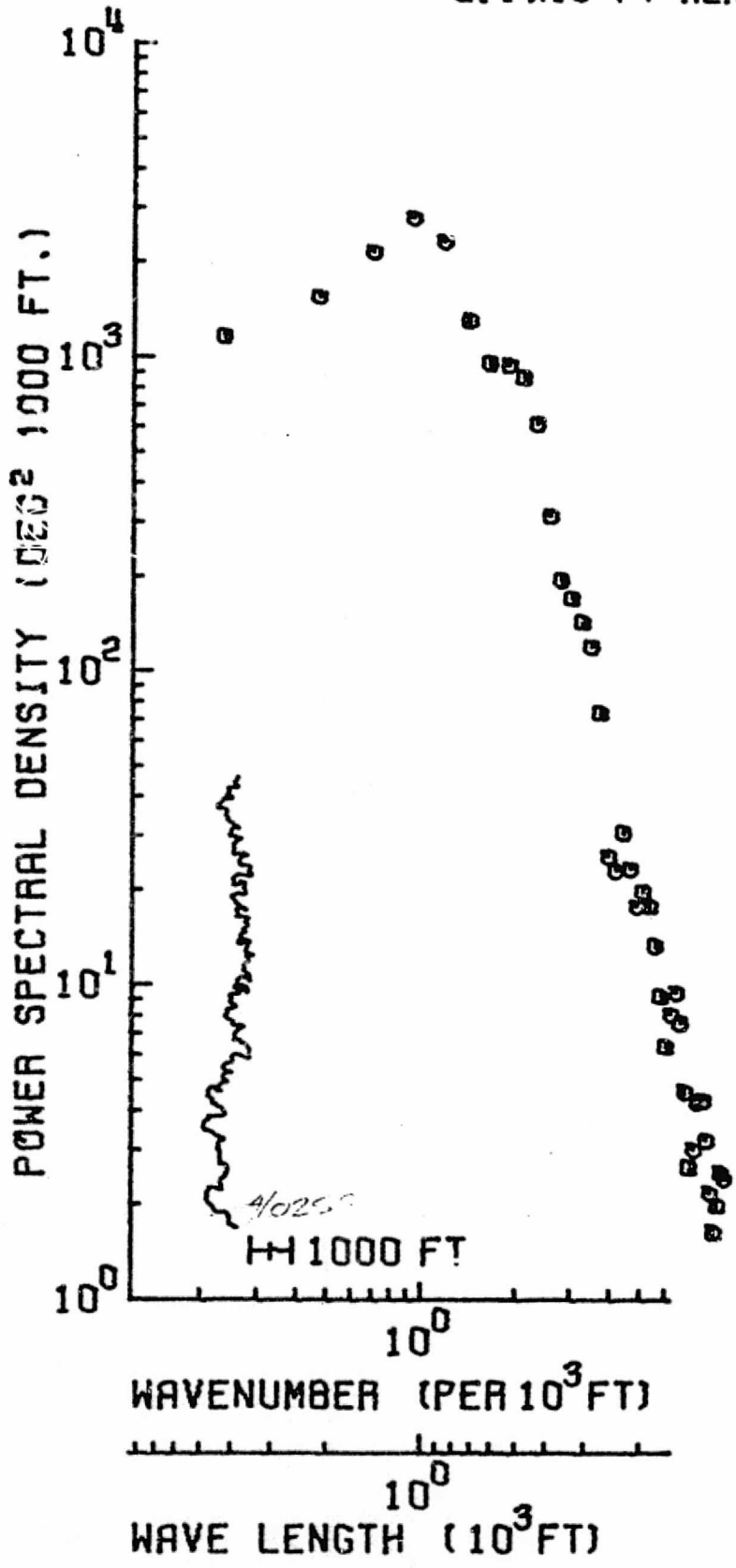

1 / 800

PLT TAPE PSPLT1 FY BLK 26 IN DISK KAUDSK PIS096.MAJ.BOIB.1
74 289 OCT 10 00:27:10.9

BOISE BRULE RIVER

1201 DATA PTS / 100 SPEC ESTS

1.3×10^5 FT REACH

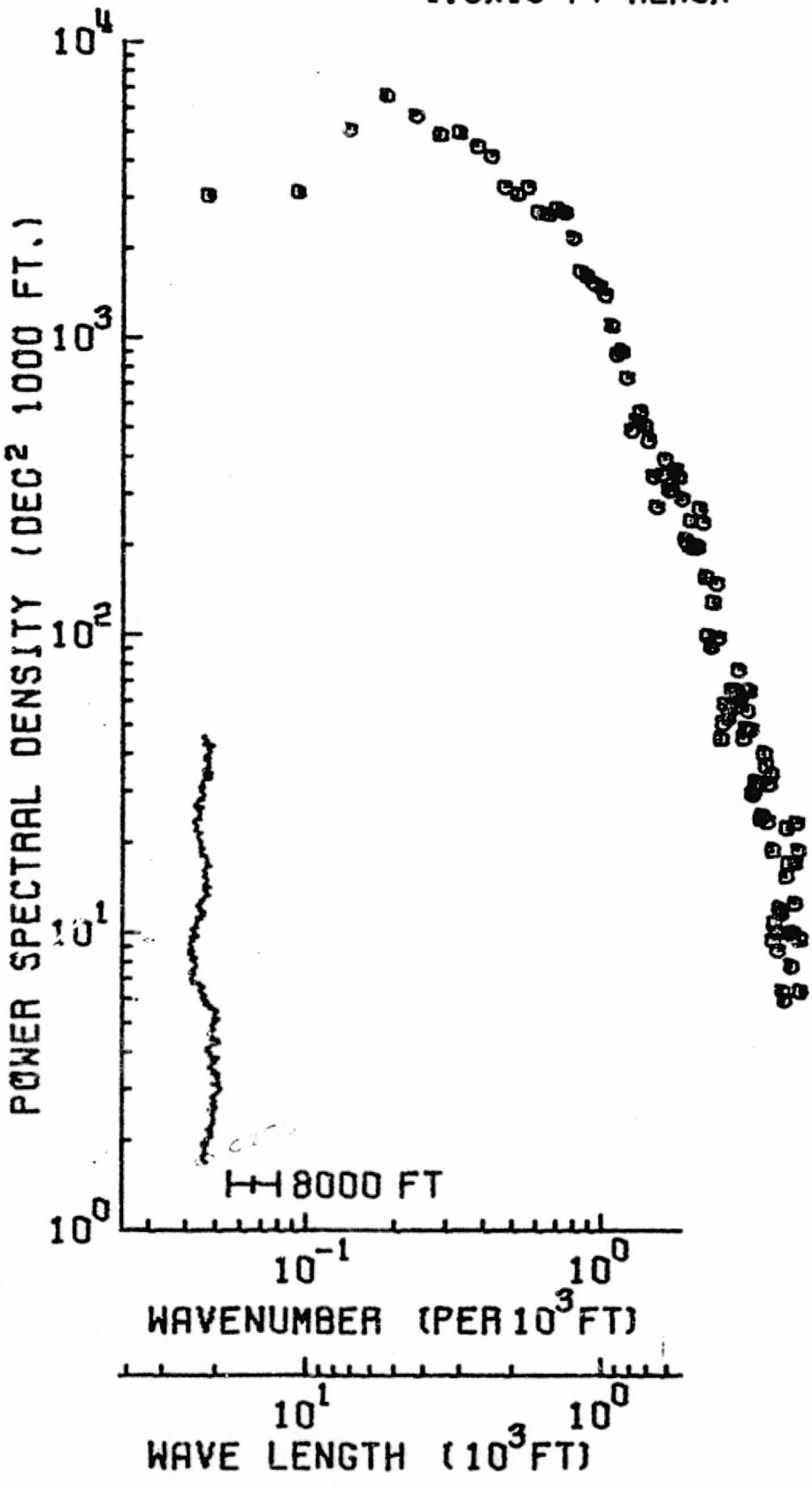

1 / 4807

PLT TAPE PSPLT1 F4 BLK 29 IN DISK KAUDSK PIS096.MAJ.BBIB.L
74 283 OCT 10 00:27:18.9

BOISE BRULE RIVER

1404 DATA PTS / 125 SPEC ESTS

7.5×10^4 FT REACH

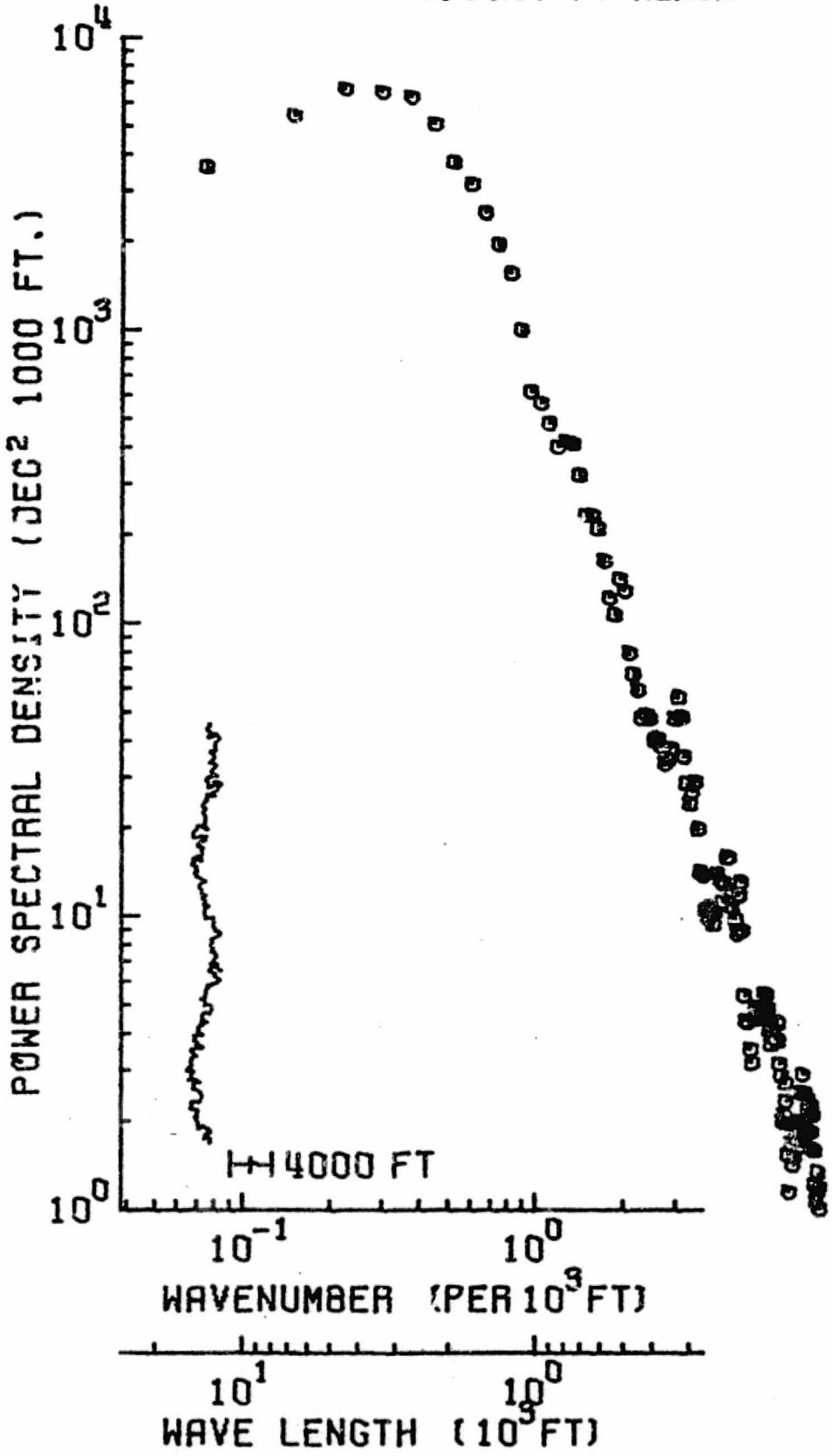

2000 / 4807

PLT TAPE PSPLT1 F4 BLK. 27 IN DISK KAUD3K PIS096.MAJ.BOIB.L
74 283 OCT 10 00:27:18.9

BOIS BRULE RIVER, WISC

500 DATA PTS / 83SPEC ESTS

2.9 X10^4 FT REACH

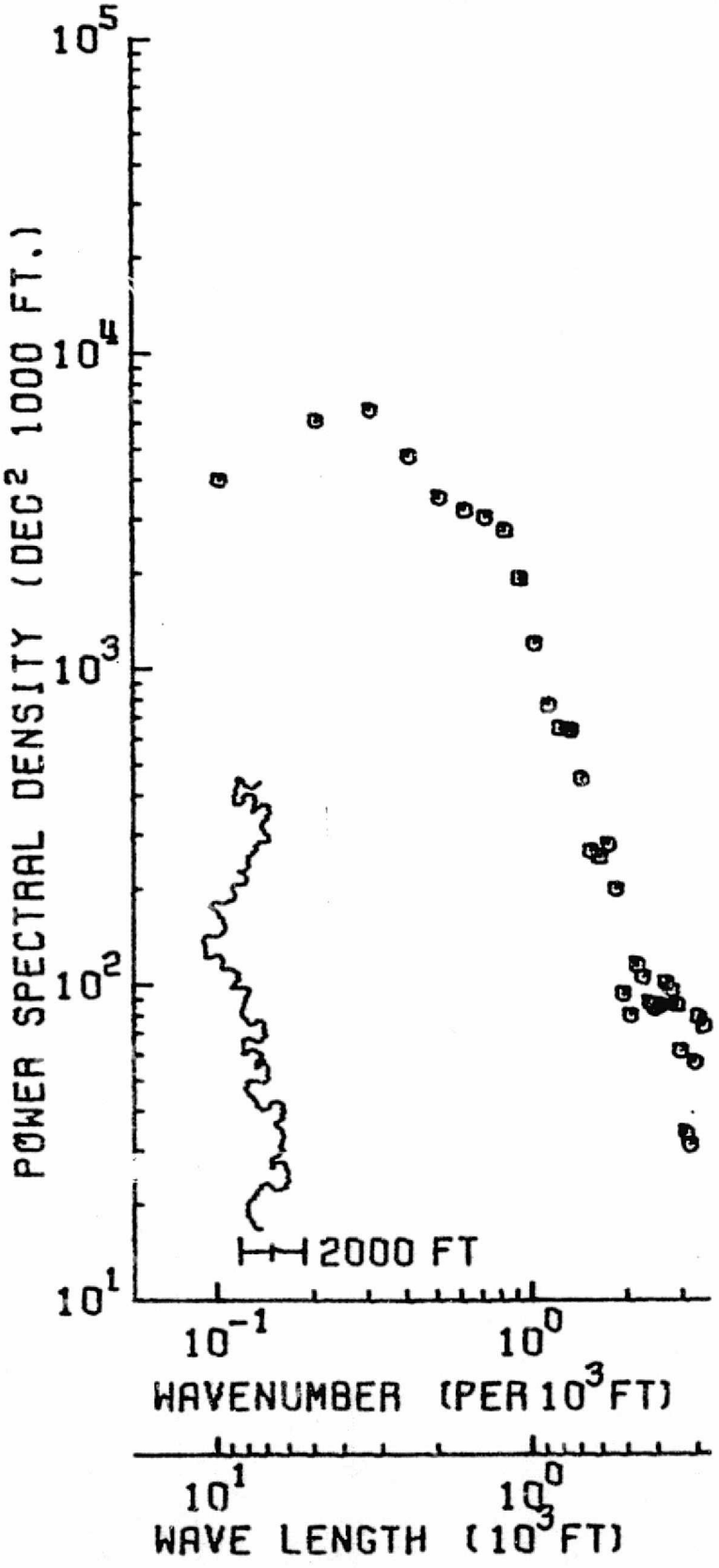

2400 / 3400

PLT IAPE ISTPLT F1 BLK 9 IN DISK KAUD3K PIS096.NAJ.BBIB3B

74 270 SEP 27 11:22:58.4 IN DISK KAUD3K PIS096.NAJ.BBIB3B.ANG2

RIFLE RIVER AT "THE RANCH"

STATION 4/1395 LAPTON, MICH. 1950/10-1970/9

TP 4552, FIL 2, RECDS 6308-6547 PLOT 27 SET 1

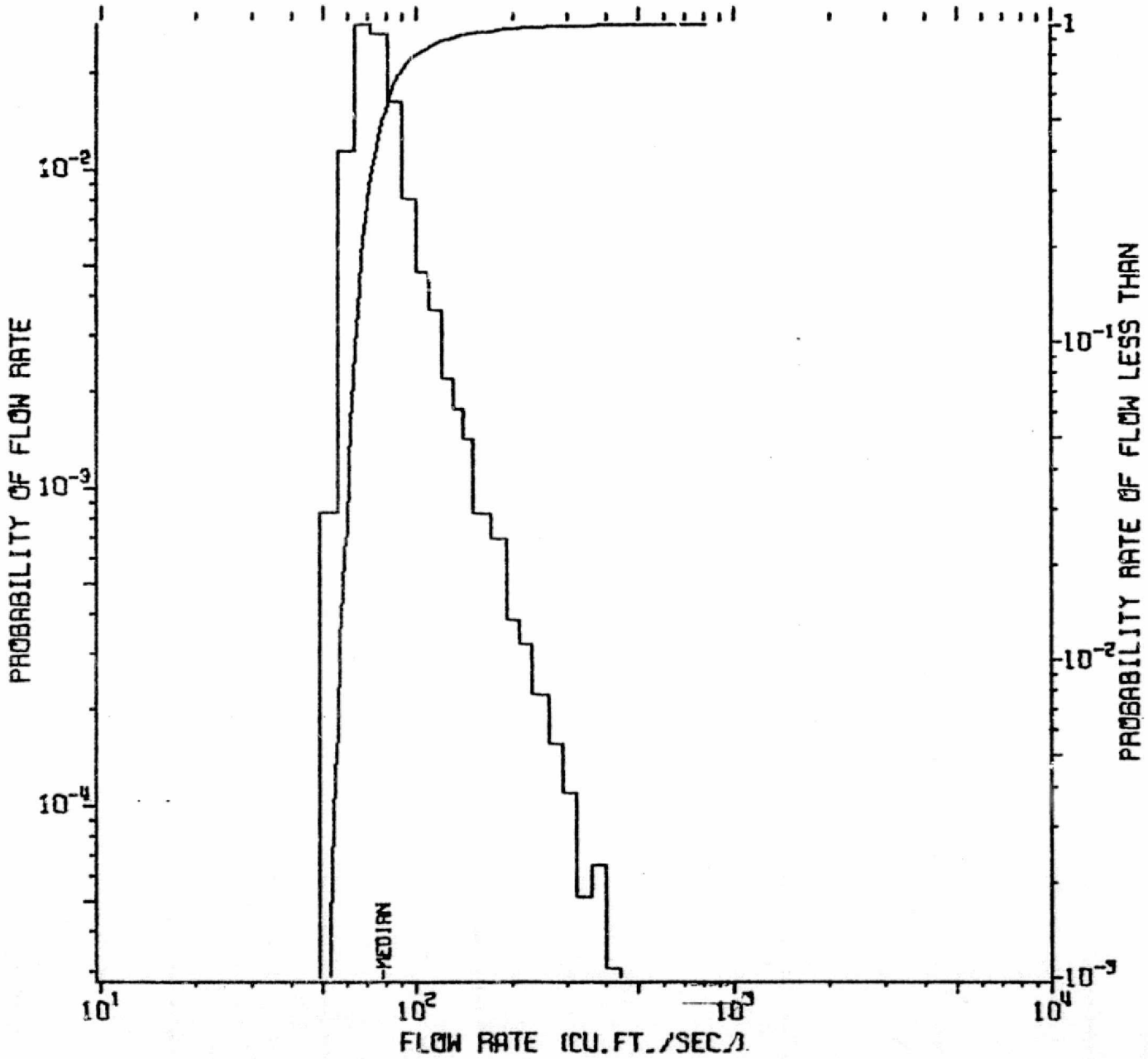

RIFLE RIVER

STATION 4/1405 SELKIRK, MICH. 1950/10-1970/9

TP 4552, FIL 2, RECDS 6548-6787 PLOT 28 SET 1

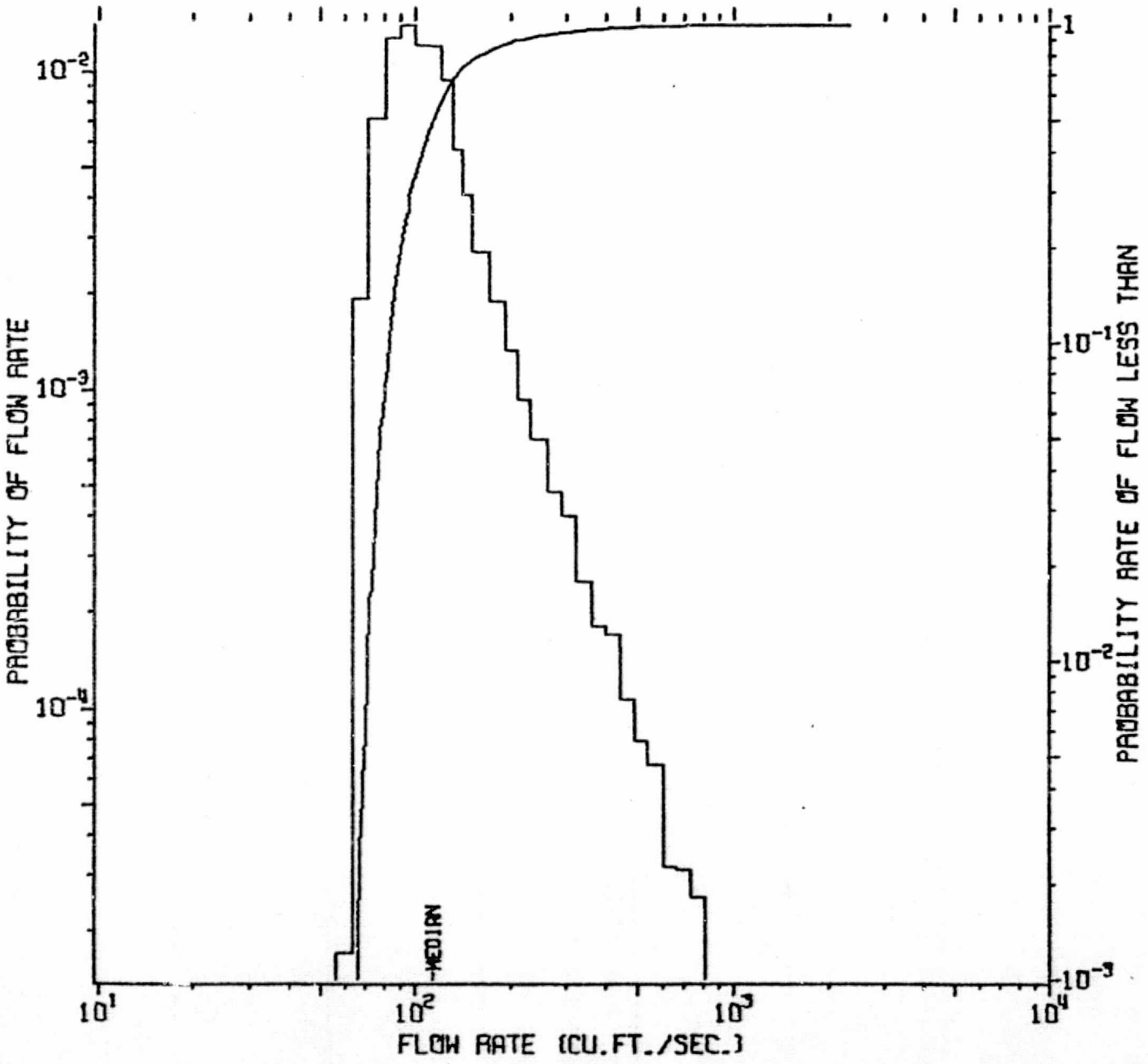

RIFLE RIVER AT HIGHWAY 70

STATION 4/1420 STERLING, MICH. 1936/10-1969/9

TP 4552, FIL 2, RECDS 6788-7183 PLOT 29 SET 1

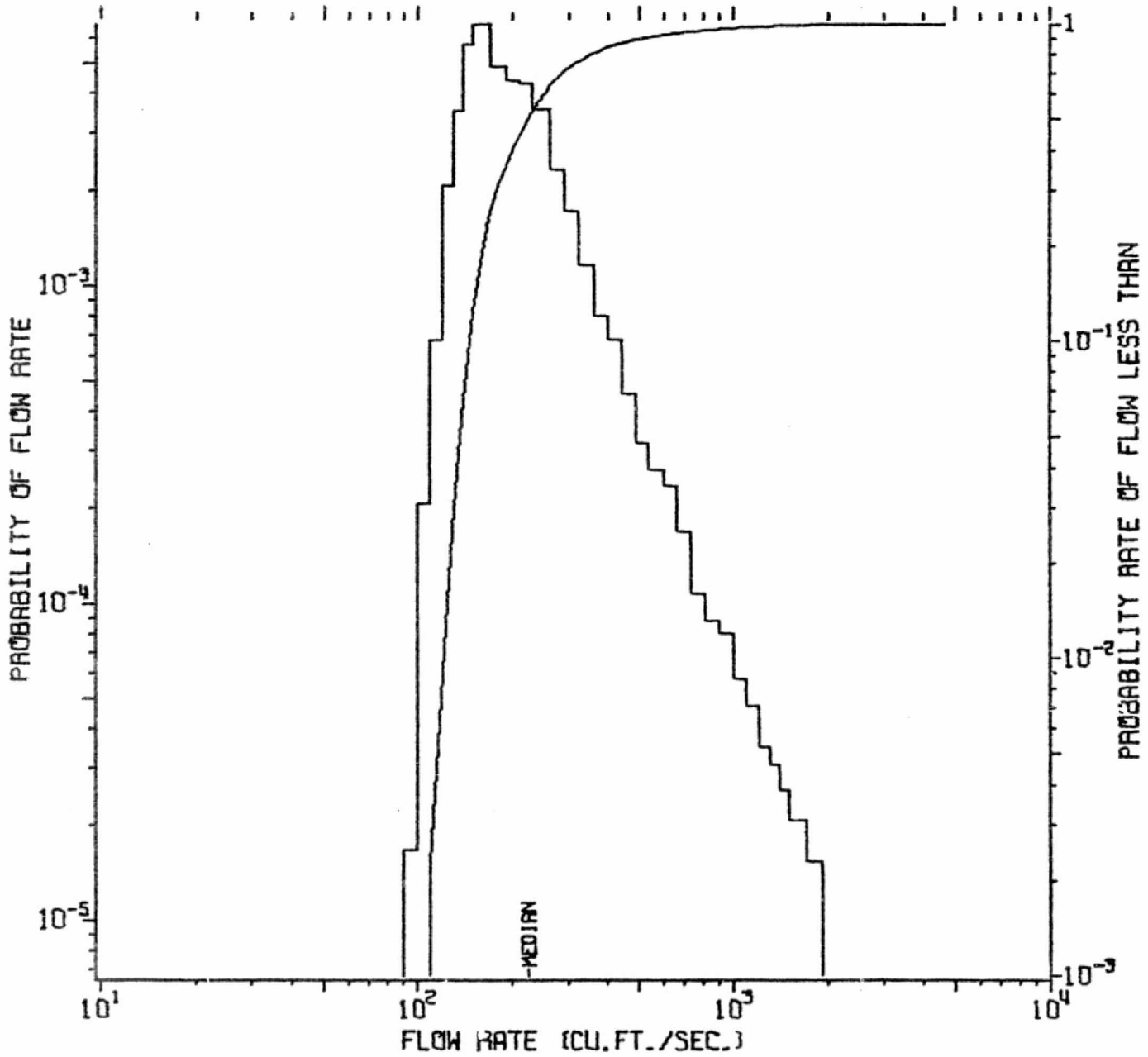

RIVER RIFD

858 DATA PTS / 80 SPEC ESTS

4.6×10^4 FT REACH

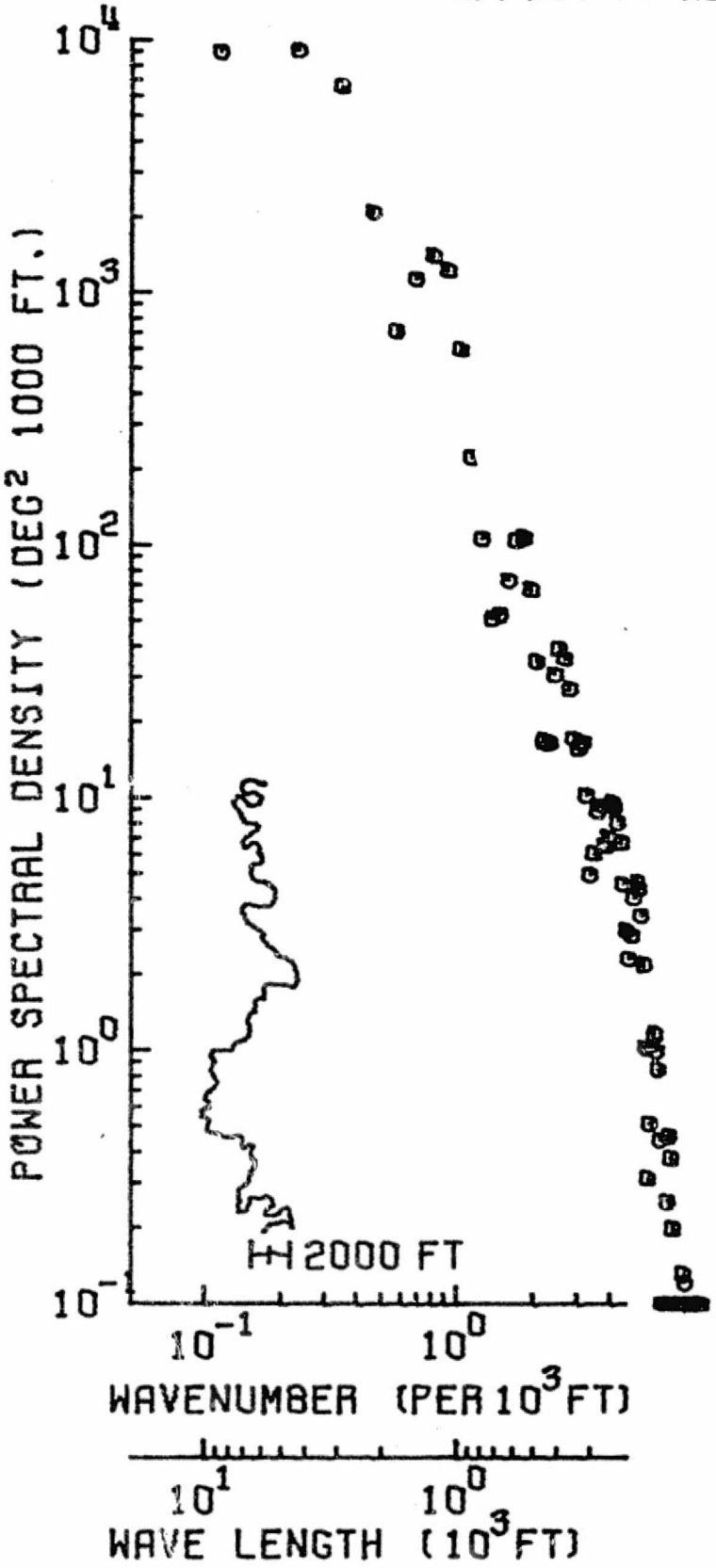

2750 / 4465

PLT IBGE PSPLT1 F30LK.1S IN DISK KAUDSK PIS096.MAJ.RIFD.L
74 282 OCT 9 04:06:19.7

RIVER RIFD

2232 DATA PTS / 180 SPEC ESTS

1.2 X 10^5 FT REACH

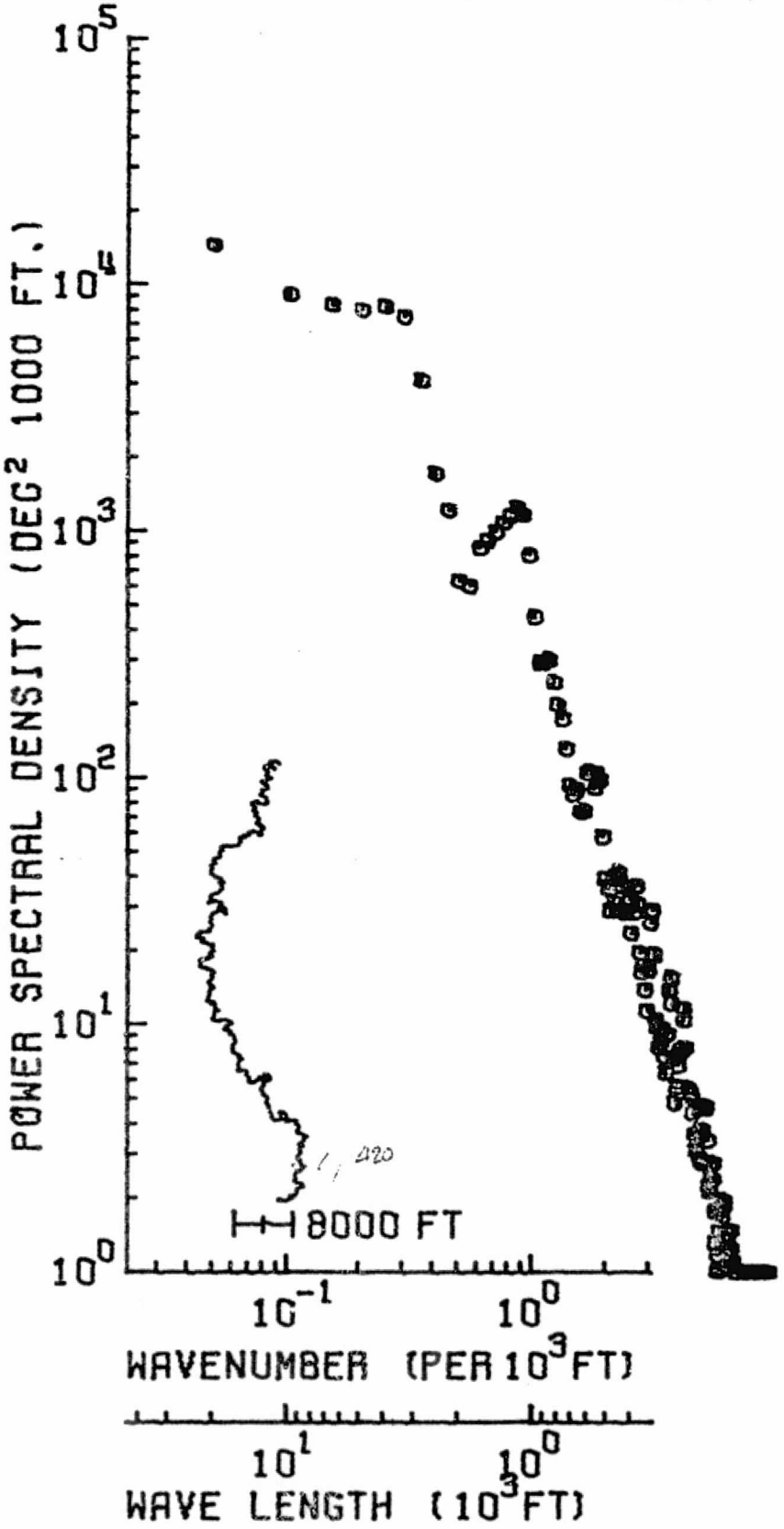

1 / 4465

PLT TAPE P3PLT1 F38LK.14 IN DISK KAUD3K PI5096.MAJ.RIFD.L
74 282 OCT 9 04:06:19.7

RIVER RIFM

332 DATA PTS / 50 SPEC ESTS

1.9×10^4 FT REACH

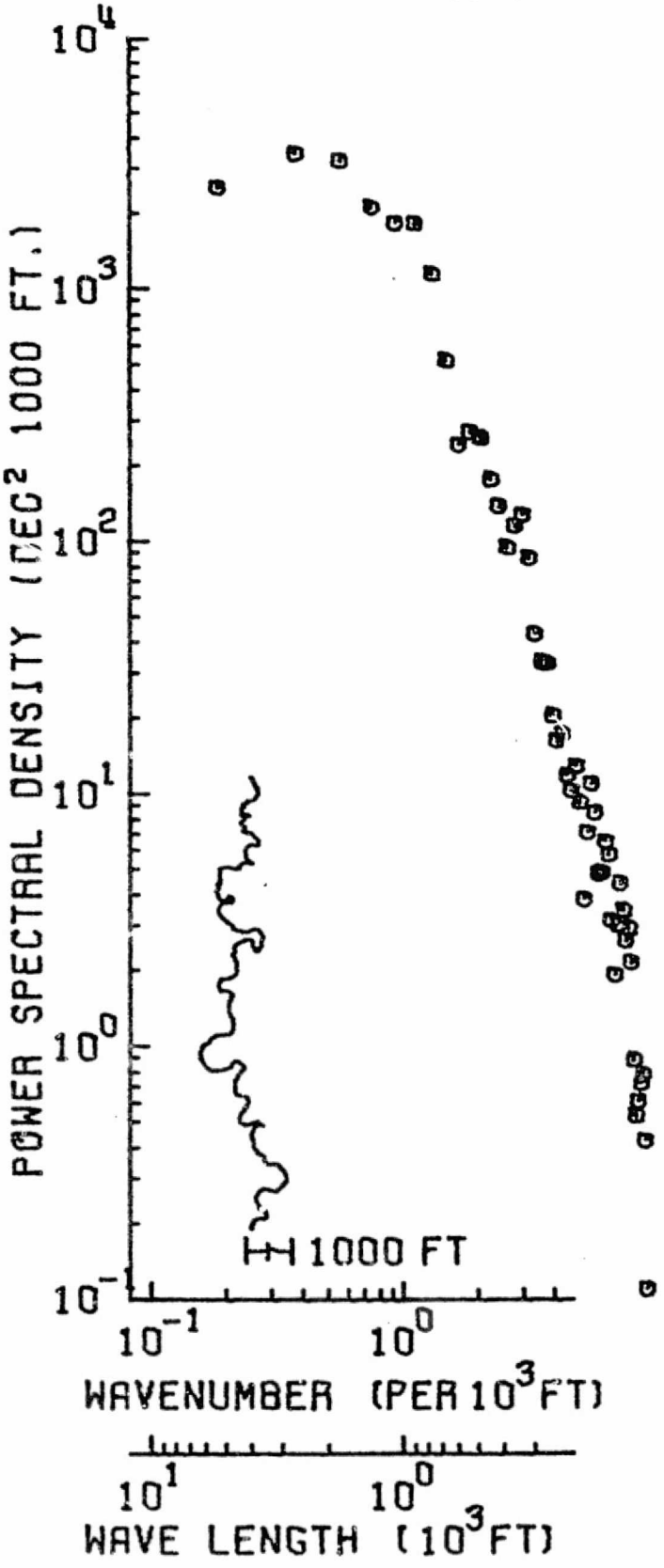

1 / 666

PLT TAPE PSPLT1 F2 BLK 11 IN DISK KAUD3K P15096.MAJ.RIFM.L

74 277 OCT 4 01:52:19.6

RIVER RIFU

1242 DATA PTS / 80 SPEC ESTS

3.3×10^4 FT REACH

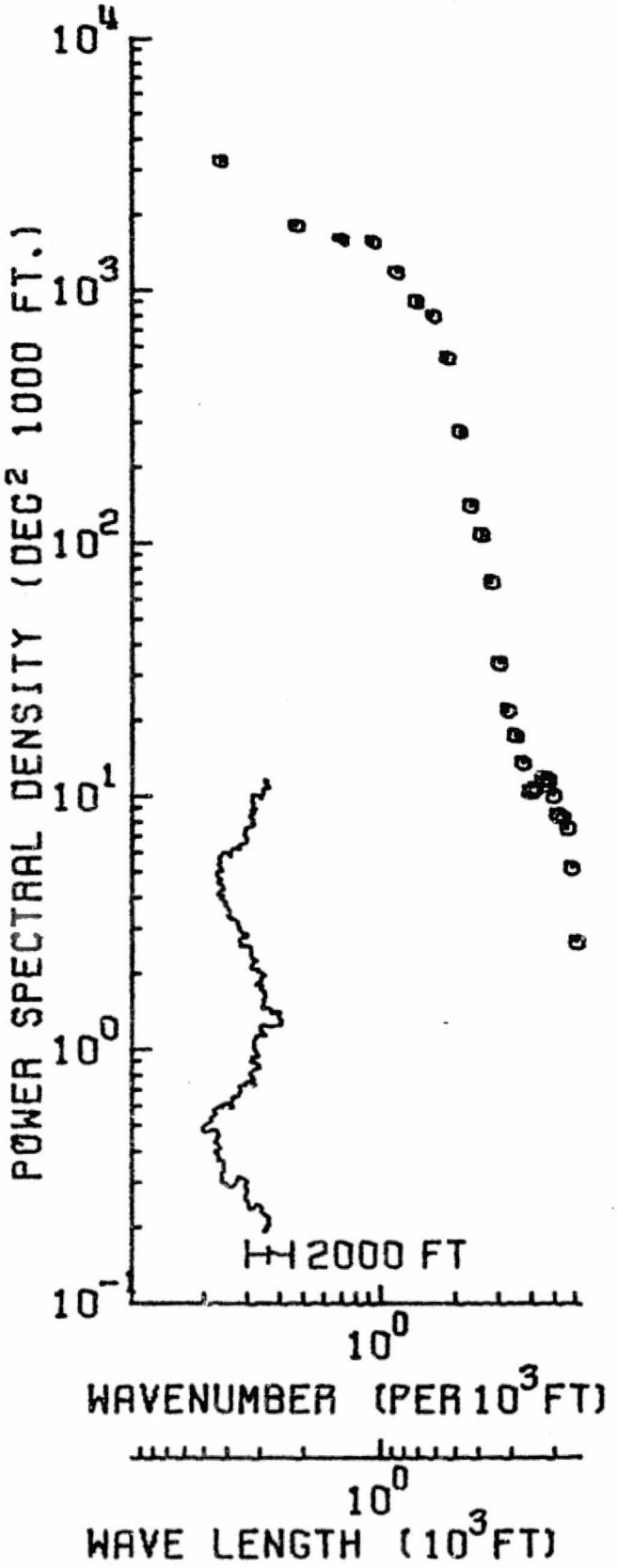

1 / 1243

PLT TAPE PSPLT1 FILE 5 IN DISK KAUDSK PIS096.MAJ.RIFU.L
74 273 SEP 30 12:58:45.5

JUMP RIVER

STATION 5/3620 SHELDON, WIS. 1915-1970

TP 4552, FIL 2, RECDS 7502-8151 PLOT 33 SET 1

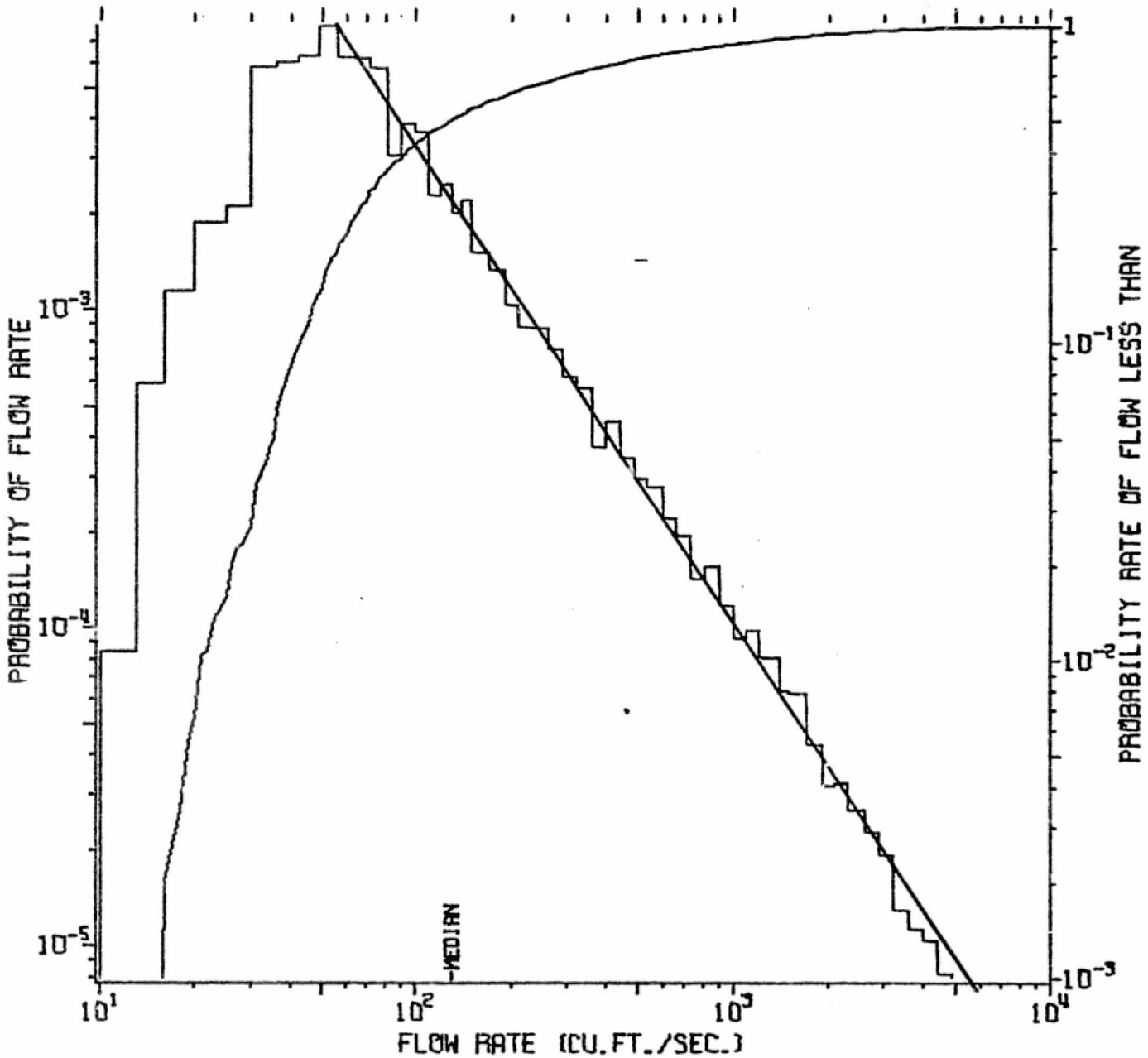

SOUTH FORK JUMP RIVER

STATION 5/3615 OGEMA, WIS. 1944/5-1954/9

TP 4552, FIL 2, RECDS 7377-7501 PLOT 32 SET 1

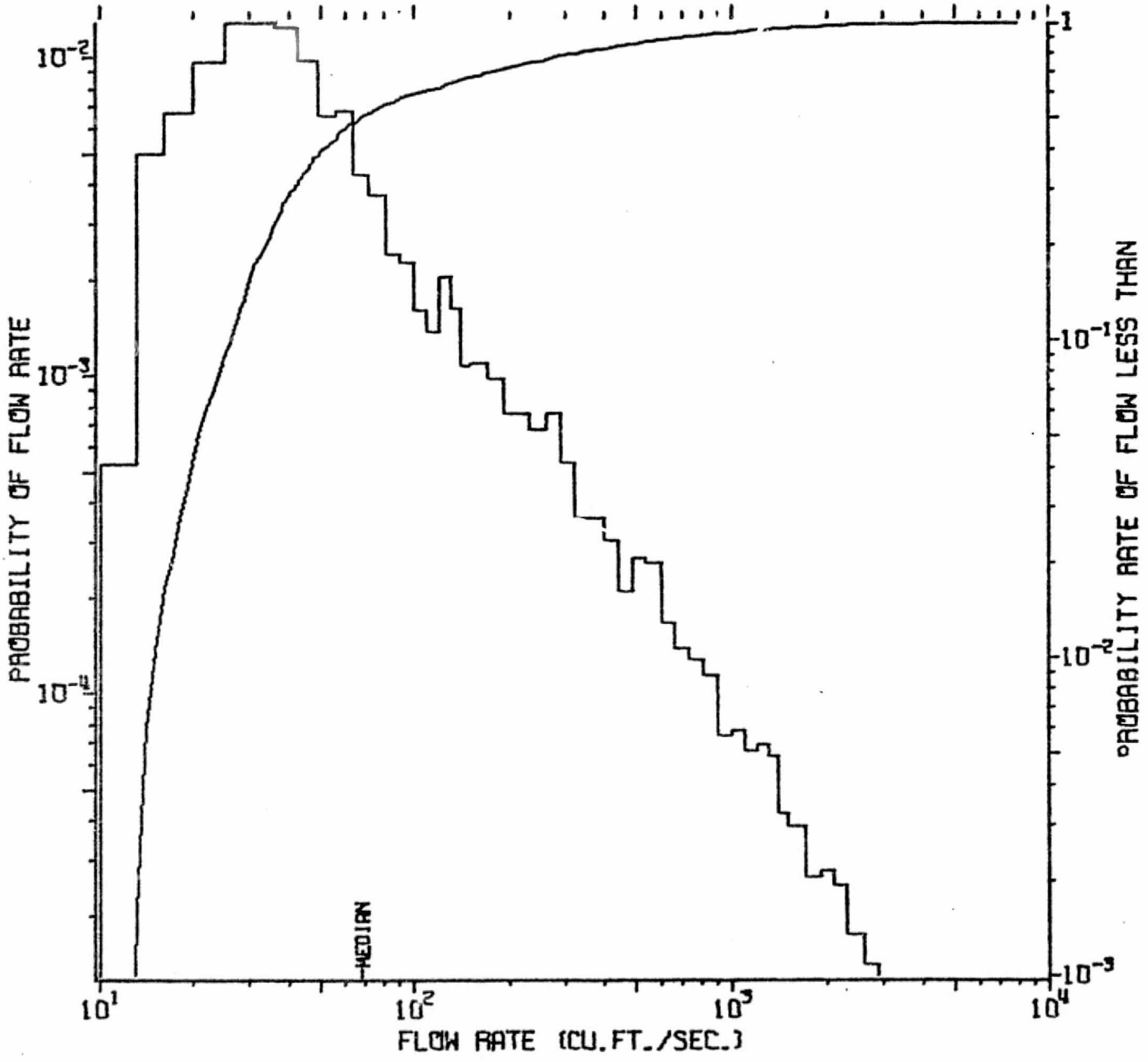

JUMP RIVER

1057 DATA PTS / 85 SPEC ESTS

1.8×10^5 FT REACH

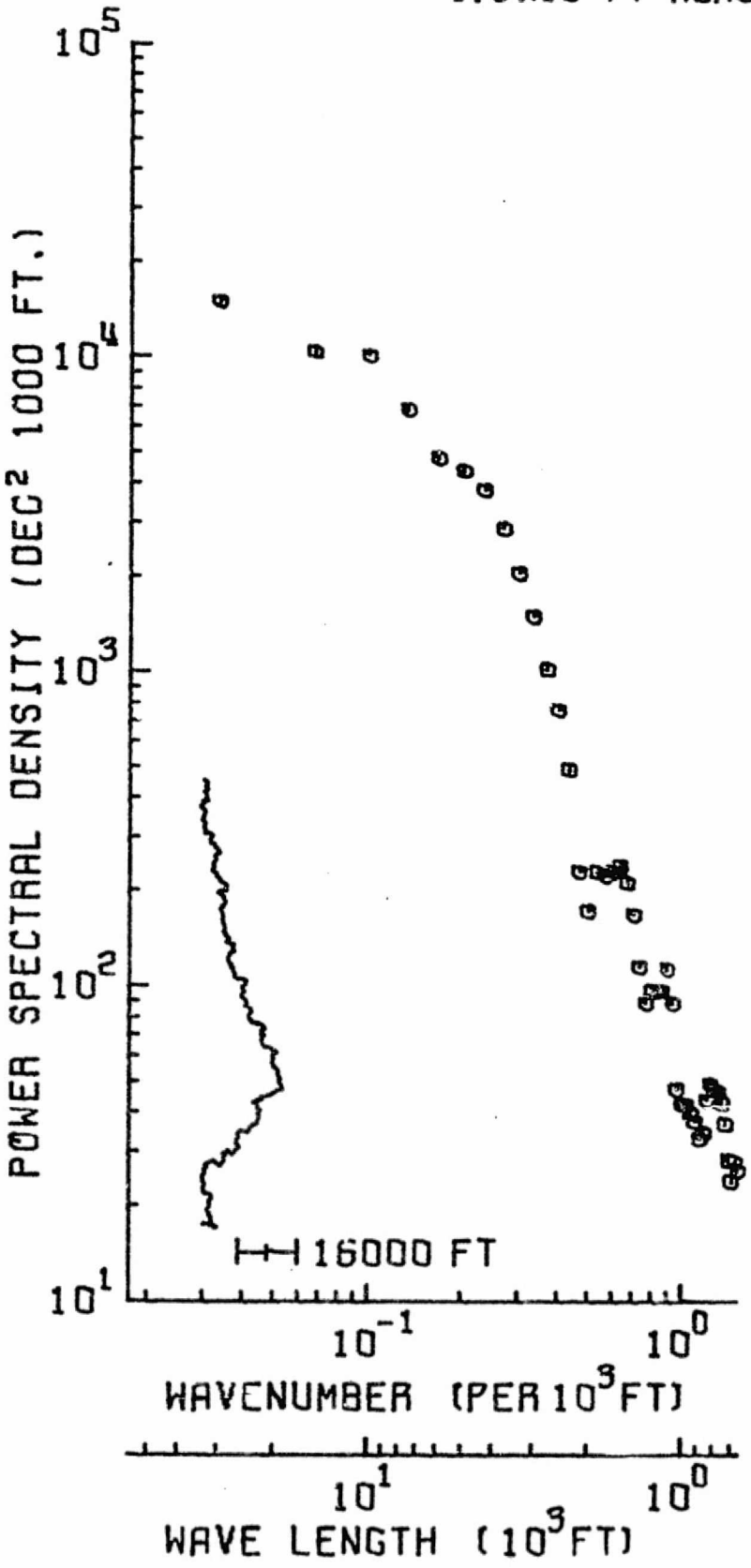

1 / 6345

PLT TAPE PSPLT1 F6 BLK SS IN DISK KAUD3K PIS096.MAJ.JUMP
74 295 OCT 22 03:49:10.1 IN DISK KAUD3K PIS096.MAJ.JUMP.ANG2